OPTIMIZATION OF ACTIVE CONTROL FOR A LOW-RISE BUILDING

A Thesis Submitted to
the Graduate School of
Izmir Institute of Technology
in Partial Fulfilment of the Requirements for the Degree of

MASTER OF SCIENCE

in Civil Engineering

by
Nabil BISHTAWI

July 2023
IZMIR

We approve the thesis of **Nabil BISHTAWI**

Examining Committee Members:

_____
Assoc. Prof. Dr. Gürsoy TURAN
Department of Civil Engineering, Izmir Institute of Technology

_____
Prof. Dr. Serhan Özdemir
Department of Mechanical Engineering, Izmir Institute of Technology

_____
Prof. Dr. Zeki KIRAL
Department of Mechanical Engineering, Dokuz Eylül University

14 July 2023

_____
Assoc. Prof. Dr. Gürsoy TURAN
Supervisor, Department of Civil Engineering, Izmir Institute of Technology

_____
Prof. Dr. Cemalettin DÖNMEZ
Head of the Civil Engineering Department

_____
Prof. Dr. Mehtap EANES
Dean of the Graduate School

ABSTRACT

OPTIMIZATION OF ACTIVE CONTROL FOR A LOW-RISE BUILDING

This study proposed optimization procedures to design an LQR controller for an active tuned mass damper on a 10-story structure. For the optimization, two multiobjective-function problems were formulated. The number of objective functions in both problems was equal to the number of stories, and they measured the ratio of controlled to uncontrolled drift. Optimizations of the ATMD have been realized by utilizing 28 near-field earthquake records with pulse ground motion. The performance of the resulting controller was assessed using five performance indices by utilizing 96 earthquakes comprised of near field with a pulse, near field without a pulse, and far-field records.

The first optimization problem has no bounds on the magnitude of the applied force. Frequency analysis has been used along with time domain analysis to assess and figure out the characteristics of the controlled structure. The results indicate that a high amount of active force is needed. Several methods were tested to find the most effective way to decrease the needed actuator’s force while keeping a good performance index similar to the original model.

In the second optimization problem, a limitation was considered for the applied force. In this problem, the time simulation and frequency analysis have been used as in the first one. The force limitation in this problem triggers a bang-bang action issue. Several low-pass FIR filters have been tested against the issue, resulting in a better understanding of the originating reason for the bang-bang action and the filters' effect on the controller.

To decrease the number of sensors used for the feedback system Kalman filter has been used. The output of Kalman filter was the same as the original system. The robustness of the controller was assessed by changing the characteristics of the uncontrolled structure and comparing it with the original model. It turns out that the optimized LQR-ATMD is robust.

ÖZET

ALÇAK KATLI BİR BİNANIN AKTİF KONTROLÜNÜN OPTİMİZASYONU

Bu çalışma, 10 katlı bir yapı üzerinde aktif ayarlanmış bir kütle sönümleyici için bir LQR kontrolörü tasarlamak için optimizasyon prosedürleri önermiştir. Optimizasyon için iki çok amaçlı fonksiyon problemi formüle edilmiştir. Her iki problemde de amaç fonksiyonlarının sayısı kat sayısına eşittir ve kontrollü kaymanın kontrolsüze oranı ölçüldü. ATMD'nin optimizasyonları, 28 yakın saha darbe tipi deprem yer hareketi kaydı kullanılarak gerçekleştirilmiştir. Ortaya çıkan kontrolörün performansı, darbeli yakın alan, darbesiz yakın alan ve uzak alan kayıtlarından oluşan 96 deprem kullanılarak beş performans indeksi kullanılarak değerlendirildi.

İlk optimizasyon probleminin uygulanan kuvvetin büyüklüğü üzerinde bir sınırı yoktur. Kontrol edilen yapının özelliklerini değerlendirmek ve anlamak için zaman alanı analizi kullanılarak frekans analizi kullanılmıştır. Sonuçlar, yüksek miktarda aktif kuvvete ihtiyaç duyulduğunu göstermektedir. İyi performans endeksini korurken gerekli aktüatörün kuvvetini azaltmanın en etkili yolunu bulmak için orijinal modele benzer çeşitli yöntemler test edildi.

İkinci optimizasyon probleminde uygulanan kuvvet için bir sınırlama düşünülmüştür. Bu problemde ilk problemde olduğu gibi zaman simülasyonu ve frekans analizi kullanılmıştır. Bu problemdeki kuvvet sınırlaması, bir bang-bang eylemi sorununu tetikler. Birkaç düşük geçişli FIR filtresi bu soruna karşı test edildi ve bu da bang-bang eyleminin kaynağının ve filtrelerin denetleyici üzerindeki etkisinin daha iyi anlaşılmasını sağladı.

Geri besleme sisteminde kullanılan sensör sayısını azaltmak için Kalman filtresi kullanılmıştır. Kalman filtresinin çıktısı orijinal sistemle aynıydı. Denetleyicinin sağlamlığı, kontrolsüz yapının özellikleri değiştirilerek ve orijinal modelle karşılaştırılarak değerlendirildi. Optimize edilmiş LQR-ATMD'nin sağlam olduğu ortaya çıktı.

TABLE OF CONTENTS

LIST OF FIGURES

Figure **Page**

LIST OF TABLES

CHAPTER 1

INTRODUCTION

Natural disasters cost thousands of lives each year rather than the direct and indirect economic costs, but the cause of those deaths is not directly because of the disaster itself; it is the consequences like in the earthquake case, the falling apart structure and ruined infrastructures are the leading cause of deaths. Modern structural design philosophy tries to minimize the risk of any structural failure by making structural members withstand the vibration caused by earthquakes. However, this method is a multi-process, and to make it work, we need a good design and strict supervision during the building phases, even though it contains much uncertainty. Because of that, engineers came up with structural control systems to mitigate earthquake-induced vibration and other sources.

Figure 1.1 shows the frequency of natural events like earthquakes, storms, and floods between 1998-2017. Earthquakes are the least frequent event, yet it causes 56% of the overall deaths, and 1% of earthquake events contribute more than any other events to economic losses have the same percentage, making earthquakes the most deadly and destructive among natural events.

Control systems work as anti-vibration devices to avoid resonance, decrease the structural response, and terminate the transient vibrations (El Ouni et al., 2022). Control systems are categorized into Passive, Semi-active, Active, and hybrid systems based on their need to outsource power.

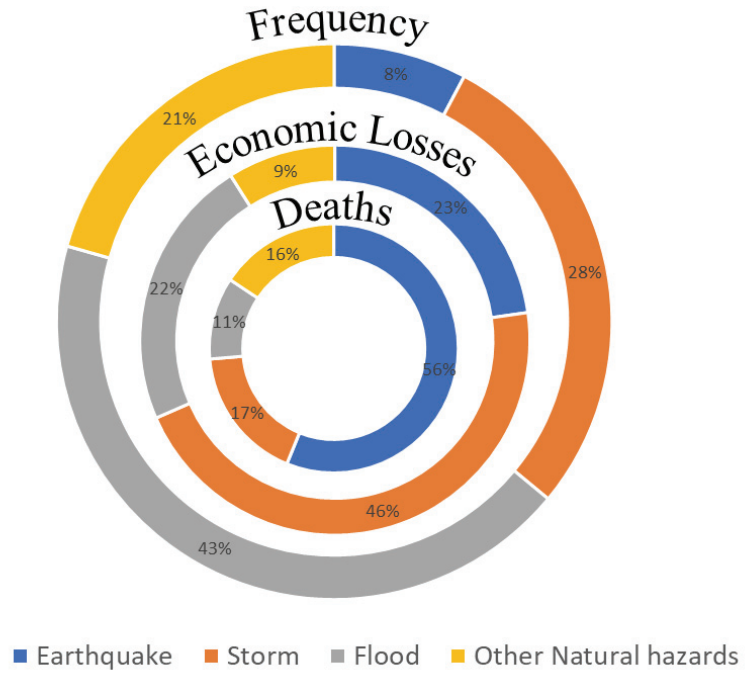

Figure 1.1 Displaying several natural hazards' frequencies and their effects.

Passive systems aim to enhance the structural response by decreasing the input energy to the controlled structure by using either base isolation or energy dissipation devices. Isolation devices consist of multiple layers of a material that are flexible in the horizontal direction and rigid in the vertical direction (Housner et al., 1997a) usually installed between the foundation and the soil to increase the fundamental period, which causes fewer energy transitions from soil to the structure during earthquakes (Clemente, 2017), the most effective are lead-rubber bearing system, high-damping bearing system, and friction-pendulum spherical sliding bearings (Spencer & Nagarajaiah, 2003a). Energy dissipation devices contain multiple families like hysteretic devices, viscoelastic devices, re-centring devices, and phase transformation devices as well as dynamic vibration absorbers such as tuned mass damper (TMD), which is a set of extra mass, damper and stiffness elements deployed first in the 1900s to control the vibration at a specified frequency (F. Yang et al., 2022). The goal is to Suppress the effective modes which are responsible for most of the motion. This is applicable by tuning the TMD to the most effective mode or, in the case of a multiple-tuned mass damper (MTMD), tuning each mass and stiffness element for a particular mode. Extensive research has been conducted on TMD in the past. Bekdas and Nigdeli (Bekdaş & Nigdeli, 2013)

investigated the effective TMD mass ratio, Krenk (Krenk, 2005) studied the relation between damping ratio and optimum tuning, Tsai and Lin (Tsai & Lin, 1993) presented tuning under harmonic base excitation, Sadek et. Al , Krenk and Hogsberg, Warburton and Hoang et Al. (Hoang et al., 2008; Krenk & Høgsberg, 2008; SADEK et al., 1997; Warburton, 1982) presented a closed-form solution to design TMD.

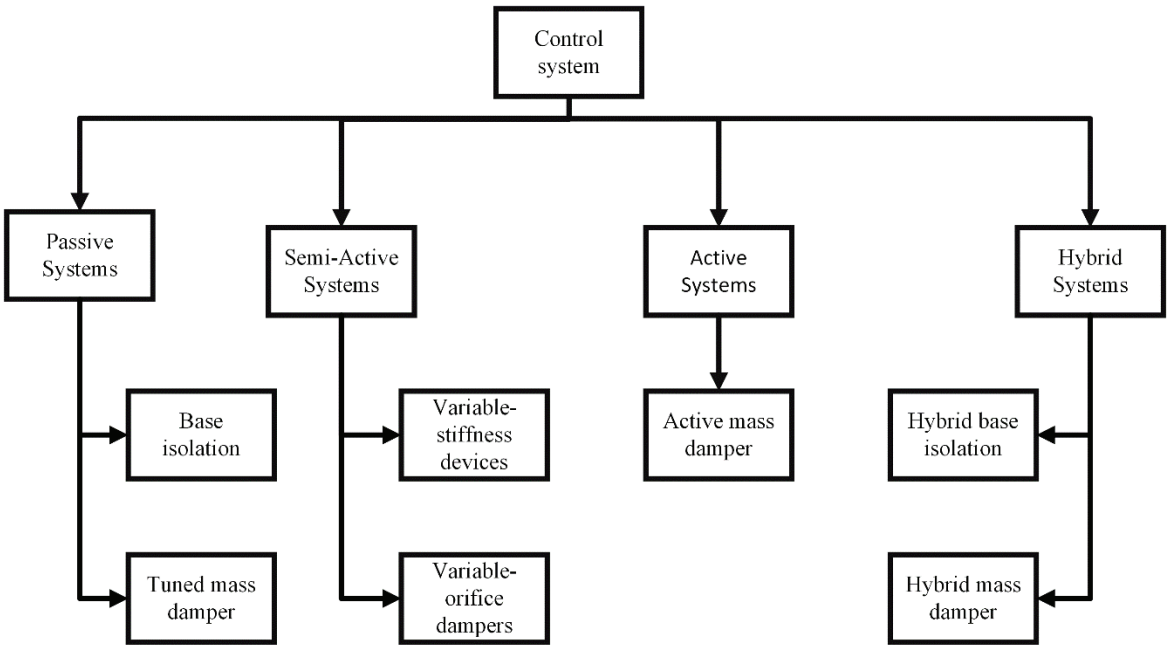

Figure 1.2 Control system families and number of applications for each family.

Active systems make use of the current state of structure to achieve a better state by applying forces. These Forces are provided to the structure by an actuator powered by an external source and governed by feedback law. The feedback law yields the required force based on the real-time sensors' readings and predefined factors regarding the readings. The active mass driver (AMD) is an active system consisting of an actuator and mass. The active mass driver is also known as an active mass damper. The damper term came from the fact that the AMD effect is similar to the effect of increasing the damping of the structure (Cao et al., 1998a). Feedback signals in AMD can be displacement, velocity, acceleration, or a combination of any of them. A number of methods have been proposed to design the AMD. For instance, Linear quadratic regulator (LQR) which considered as full state feedback (Cao et al., 1998b), linear quadratic gaussian (LQG) uses acceleration signal (Wu & Yang, 2000), model reference sliding model control (MRSMC) with unscented Kalman filter (UKF) (Li et al., 2019), and fuzzy controller (Battaini et al., 1998).

The semi-active system is a combination of both passive and active systems. It contains a feedback algorithm which keeps track of the structure's response or excitation. The feedback modifies the characteristics of the control device, not adding force (Symans & Constantinou, 1999). Adjusting control device characteristics aims to enhance the structure's global stability and be more reliable in seismic events since a small battery can make it work (Symans & Constantinou, 1999). Variable-orifice dampers, variable-stiffness devices, smart-tuned mass dampers and variable-friction dampers are examples of the semi-active system (Spencer & Nagarajaiah, 2003b).

The hybrid system uses both passive and active devices or semiactive and passive devices. Its importance relies on overcoming limitations that active, passive and semi-active systems might face. Active tuned mass damper (ATMD) and hybrid base isolation are examples of hybrid systems. ATMD combines TMD and AMD, where the mass is connected to an actuator, stiffness, and damping elements. ATMD is also called a hybrid mass damper (HMD), especially in mechanical research. ATMD aims to improve performance, cut back on energy use and minimize the moving mass's stroke (Chesné et al., 2019). Kayabekir et al. proposed a PID-ATMD design by optimizing the displacement of the top story and limiting the stroke capacity (Kayabekir et al., 2020). Samali and Al-Dawod implemented ATMD on a five-story benchmark using a fuzzy controller (Samali & Al-Dawod, 2003). Huo et al. proposed H-infinity (H_∞) controller (Huo et al., 2008), .Bani-Hani proposed a neural network model to design the ATMD system (Bani-Hani, 2007). You et al. l proposed an LQG controller to decrease the effect of wind load on tall buildings (You et al., 2014). Kayabekir et al. studied the uncertainty in structural rigidity on the ATMD efficiency (Kayabek.Ir et al., 2022). The hybrid base isolation comprised of a passive base isolation and active control actuator aims to increase the effect of passive base isolation (Housner et al., 1997b). Cancellara and Angelis studied the effect of three hybrid base isolation models on a reinforced concrete structure under bidirectional ground motion (Cancellara & De Angelis, 2016).

The mathematical model for uncontrolled structure, TMD-controlled structure and ATMD models, along with the state model, were developed in the second chapter.

In chapter 3, the LQR concept and its equation were presented, along with the LQR usage and LQR equation in both displacement and drift coordinates were explained.

In chapter 4, the optimization problems were formulated, and both of driving excitation and performance indices were introduced. Two multiobjective functions problems were defined both utilize the same objectives' function. The first problem is free from any constraints, while the second one has a bounding on the magnitude of the active force.

In chapter 5, the results for each problem were presented separately and compared with uncontrolled and TMD-controlled structures. Each problem's result shaded light on a number of issues. A suggestion has been made to solve the issues, and its results were presented.

In chapter 6, a conclusion about the study, along with future work, were presented.

CHAPTER 2

MATHEMATICAL MODEL

The mathematical model of the uncontrolled structure and its characteristics will be presented in Section 1. A mathematical model for the Tuned mass damper (TMD) controlled structure will be developed in section 2. A model for an active-controlled structure using an active tuned mass damper (ATMD) will be introduced in section 3. The state space model will be presented in section 4.

2.1. Uncontrolled Structure Model

A 10-story structure shear-type building was chosen, modelled as a spring mass damper system as shown in Figure 2.1.The mass of each floor is 50 tons, and the stiffness is (1.5×10^4)kN/m for the first four floors, (1.05×10^4)kN/m for the following three floors and (7.35×10^3)kN/m for the last three floors with 2% damping for all modes. The governing equation of the uncontrolled structure is presented in (2.1). The characteristics of the structure are presented in Table 2.1.

$$M\ddot{x}(t)+C\dot{x}(t)+Kx(t)=-\Gamma\ddot{u}_g(t) \qquad (2.1)$$

Where x is the displacement, Γ is a column vector used to transform the ground acceleration into force for each degree of freedom, $\ddot{u}_g$ is the earthquake acceleration. M, C and K are the mass damping and stiffness of the system.

Table 2.1 Characteristics of the uncontrolled structure

Mode	Natural frequency (rad/sec)	Damping ratio (%)	Mode	Natural frequency (rad/sec)	Damping ratio (%)
1	2.38	0.02	6	20.97	0.02
2	6.38	0.02	7	22.92	0.02
3	10.41	0.02	8	26.26	0.02
4	14.54	0.02	9	28.61	0.02
5	17.86	0.02	10	32.91	0.02

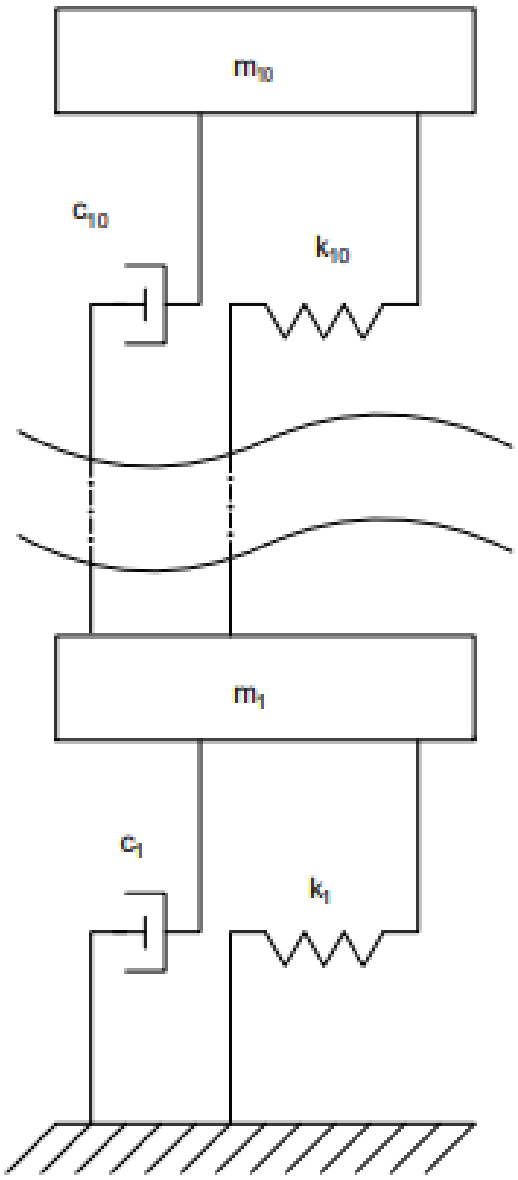

Figure 2.1 Uncontrolled structure model

2.2. TMD Mathematical Model

TMD represent a new degree of freedom. Because of that, the governing equation in (2.1) will stay intact while the matrices will be expanded to include the dynamic effect of the TMD, and it is imposed on the top story. The expanded governing equation for the TMD model is shown in (2.5).

$$M_{TMD} = \begin{bmatrix} m_{TMD} & & & & & & \\ & m_n & & & & & \\ & & m_{n-1} & & & & \\ & & & \ddots & & & \\ & & & & m_2 & & \\ & & & & & m_1 \end{bmatrix}_{(n+1)x(n+1)} \tag{2.2}$$

$$K_{TMD} = \begin{bmatrix} k_{TMD} & -k_{TMD} & & & & & \\ -k_{TMD} & k_{TMD}+k_n & -k_n & & & & \\ & -k_n & k_n+k_{n-1} & -k_{n-1} & & & \\ & & & \ddots & & & \\ & & & -k_3 & k_3+k_2 & -k_2 & \\ & & & & -k_2 & k_1+k_2 \end{bmatrix}_{(n+1)(n+1)} \tag{2.3}$$

$$C_{TMD} = \begin{bmatrix} c_{TMD} & -c_{TMD} & & & & & \\ -c_{TMD} & c_{TMD}+c_n & -c_n & & & & \\ & -c_n & c_n+c_{n-1} & -c_{n-1} & & & \\ & & & \ddots & & & \\ & & & -c_3 & c_3+c_2 & -c_2 & \\ & & & & -c_2 & c_1+c_2 \end{bmatrix}_{(n+1)x(n+1)} \tag{2.4}$$

$$M_{TMD}\ddot{x}(t)+C_{TMD}\dot{x}(t)+K_{TMD}x(t)=-\Gamma_{TMD}\ddot{u}_g(t) \tag{2.5}$$

Sadek et al. proposed a TMD design by choosing the optimum values for damping ratios and frequency tuning to decrease earthquake load response(SADEK et al., 1997).

$$\mu=\frac{m_{TMD}}{\phi_1^T[M]\phi_1} \tag{2.6}$$

$$\xi=\Phi\left[\frac{\beta}{1+\mu}+\sqrt{\frac{\mu}{1+\mu}}\right] \tag{2.7}$$

$$\omega_{TMD}=f\,\omega_1 \tag{2.8}$$

$$c_{TMD}=2\,\xi\,m_{TMD}\,\omega_{TMD} \tag{2.9}$$

Here, μ is the mass ratio, m_{TMD} is the TMD's mass, ϕ_1 is the first mode shape normalized to have a unit participation factor, ξ is the TMD's damping ratio, β is the structure's first mode damping ratio, Φ is the amplitude of the normalized mode shape at the location of TMD, f is the tuning ratio, ω_1 is the uncontrolled structure first mode natural frequency and ω_{TMD} is the TMD's natural frequency.

Table 2.2 Characteristics of the added TMD.

μ	f	ξ	m_{TMD} (ton)	k_{TMD} (kN/m)	c_{TMD}(kN.sec/m)
0.02	0.97	0.21	7.992	42.764	7.91

Table 2.3 Characteristics of the TMD-controlled structure.

Mode	Natural frequency (rad/sec)	Damping ratio (%)	Mode	Natural frequency (rad/sec)	Damping ratio (%)
1	2.319	0.0902	6	20.975	0.0203
2	2.370	0.1452	7	22.917	0.0201
3	6.389	0.0235	8	26.265	0.0200
4	10.414	0.0214	9	28.614	0.0200
5	14.541	0.0211	10	32.914	0.0200
6	17.862	0.0204			

The Characteristics of the added TMD are presented in Table 2.2. It is established before that TMD adds a new degree of freedom which means an increase in the number of modes by the number of added TMD. The concept of TMD is based on decreasing the structure's response due to a specific mode. For example, Sadek et al. use the TMD to countereffect the first mode by using the first mode frequency in tuning the TMD frequency, which is shown in (2.8). The characteristics of TMD-controlled structure are presented in Table 2.3. The extra mode added by TMD is around the first mode, and it will be called the first mode twin. The twin concept here indicates which mode the TMD

is tuned to decrease. For example, if the TMD uses the second mode instead of the first mode, it will be called the second mode twin.

2.3. ATMD

In this thesis, the ATMD will adopt mass, stiffness and damping ratio characteristics from the TMD design, which is determined based on Sadek et al. equations. The system model will change as a result of the ATMD force. In contrast to the TMD, the ATMD effect is represented in the governing equation by an additional term that includes the active force. The ATMD governing equation is presented in (2.10).

$$M_{TMD}\ddot{x}(t)+C_{TMD}\dot{x}(t)+K_{TMD}x(t)=-\Gamma\ddot{u}_g(t)- ru_f(t) \tag{2.10}$$

$$r = \begin{bmatrix} 1 \\ -1 \\ 0 \\ \vdots \\ 0 \end{bmatrix}_{(n+1)x1} \tag{2.11}$$

Where F(t) is the applied active force, and r is the position vector for the applied force. Note that the active force is applied in two locations, and those locations are the last story and the added mass. The forces' directions are opposite to each other. It is impossible to supply a force to the last story alone. However, in numerical analysis, applying a single force is possible, and it is called a skyhook. The skyhook algorithm does not give the real response. However, it is used to judge whether or not the proposed system is worth further investigating.

The feedback variables and associated gain values, which are discussed in the following chapters, determine the magnitude of the active force.

2.4. State Space Model

Frequency analysis can give insight into stability and system dynamics using a bode plot, eigenvalues and eigenvectors analysis. Adopting the state space model can facilitate implementing the frequency analysis and also play a key role in designing the controller, especially in the Linear quadratic regulator (LQR) controller type.

The state model is comprised of two equations and three types of variables. Variables are state, input, and output variables. Equations are state (or dynamic) and output equations, presented in (2.12) and (2.13), respectively.

$$\dot{z}(t)=Az(t)+\sum_{i=0}^{h} B_i u_i(t) \tag{2.12}$$

$$y(t)=C_S z(t)+\sum_{i=0}^{h} D_i u_i(t) \tag{2.13}$$

$$A=\begin{bmatrix} [0]_{mxm} & [1]_{mxm} \\ -[M^{-1}K]_{mxm} & -[M^{-1}C]_{mxm} \end{bmatrix}_{2mx2m} \tag{2.14}$$

The state equation is a combination of two parts. The first part represents the relationship between state variables, and the second represents the relation between state variables and inputs. While relationships among state variables are predefined by one matrix called a system matrix and symbolized as A, relationships between inputs and state variables are governed by a matrix for each input and symbolized by B_i.

The bode plot depends on A, B, C, and D in (2.12) and (2.13). The analyst decides on the output of the state model using the output equation. The output can be any linear combination of the system's states and the inputs.

- A change with the system change.
- B is obtained from the earthquake-excited governing equation. The excited equation is presented in (2.1) for the uncontrolled system, (2.5) for the TMD-controlled structure, and (2.10) for the ATMD-controlled structure.
- C represents the output and is always for the first degree of freedom displacement.
- D is always zero.

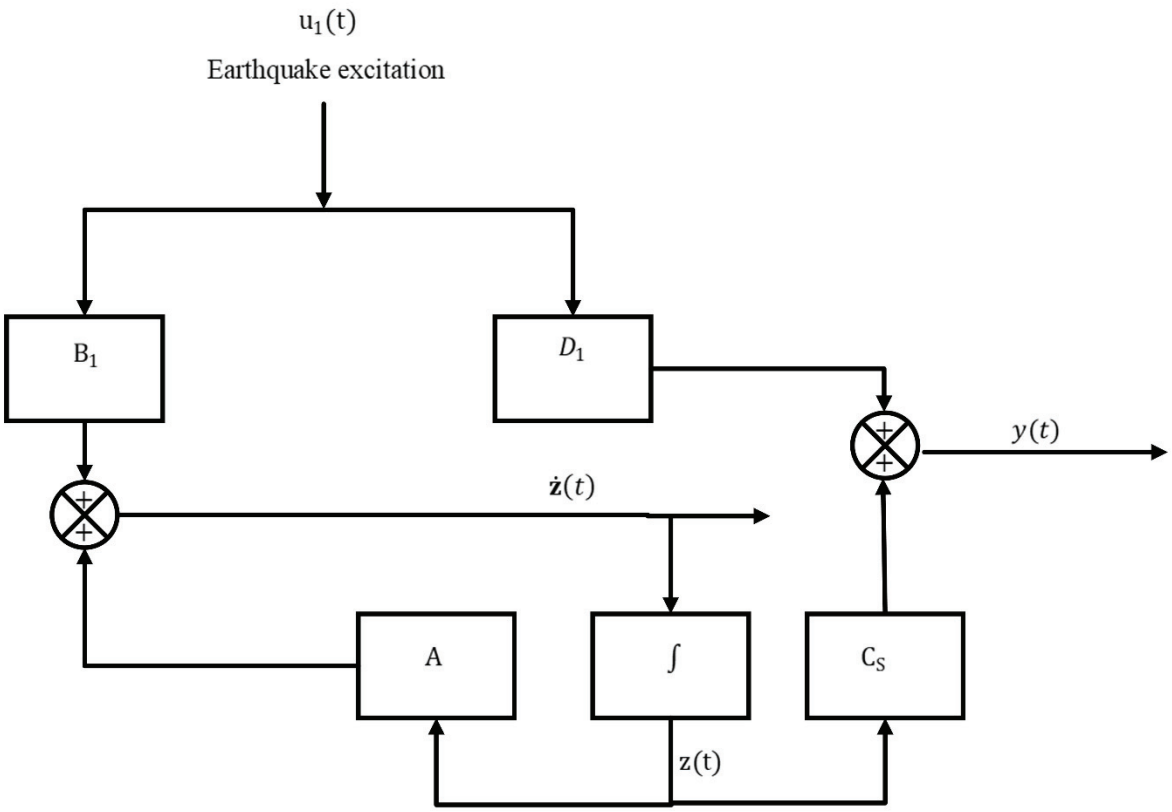

Figure 2.2 State model for uncontrol system under earthquake excitation.

CHAPTER 3

ACTIVE TUNED MASS DAMPER DESIGN

The active tuned mass damper (ATMD) system is comprised of auxiliary mass connected to the structure with damping, stiffness, and an actuator. The physical difference between the tuned mass damper (TMD) and ATMD is the existence of the actuator in order to enhance the performance. TMD targets one mode only, while ATMD may be programmed to control as many modes as are desired, which is why it performs better.

ATMD delivers a control force to the structure, and its amount is determined based on the design algorithm. In this chapter, LQR is adopted to design the feedback system, and it is presented with two models. The first model is a displacement model, and the second is a drift model.

3.1. Linear Quadratic Regulator (LQR)

The linear quadratic regulator is a full-state feedback control method and a key method in optimal control theory. Its importance came from its ability in balancing between energy needs and performance requirements using a quadratic objective function (Wang et al., 2010).

$$J=\frac{1}{2}\int_0^\infty (z^T Q z+u_f{}^T R u_f)dt \tag{3.1}$$

Here, J is the objective function, Q and R are the design parameters, which serve as cost function. They regulate the state vector and input control force relation (Vinodh Kumar & Jerome, 2013). Obtaining optimum gain values that ensure response enhancing, minimizing control energy, and stable eigenvalues for the system are the goals of using LQR (Y. Yang, 2012).

In terms of civil structures, full-state feedback uses displacements and velocities of each structural degree of freedom in the feedback law. The state's model is developed based on the chosen state variables in the feedback design. Equation (3.3) shows the state model with external disturbance included, while equation (3.4) shows the undisturbed state model.

$$z(t)=\begin{bmatrix}x(t)\\ \dot{x}(t)\end{bmatrix} \tag{3.2}$$

$$\dot{z}(t)=Az(t)+B_d u_d(t)+B_f u_f(t) \tag{3.3}$$

$$\dot{z}(t)=Az(t)+B_f u_f(t) \tag{3.4}$$

A minimization for the cost function in (3.1) can be obtained by the Riccati equation (or order reduced-matrix Riccati equation).

$$A^T P+PA-PB_f R^{-1} B_f{}^T P+Q=0 \tag{3.5}$$

$$u_f(t)=-G\, z(t) \tag{3.6}$$

Order reduced-matrix Riccati equation and the proposed control law are presented in (3.5) to (3.6). The Riccati equation can stabilize the closed-loop presented in (3.7) by providing suitable gain values if a specific condition is met. The condition is to have a positive-definite matrix (P). In the case of condition violation, there are no stabilizing gain values for the given input into the Riccati equation.

$$\dot{z}(t)=Az(t)-B_f Gz(t) \tag{3.7}$$

$$G=R^{-1}B_f^T P \tag{3.8}$$

$$G=[G_{x,n}\quad G_{x,n-1}\quad \cdots\quad G_{x,1}\quad G_{\dot{x},n}\quad G_{\dot{x},n-1}\quad \cdots\quad G_{\dot{x},1}] \tag{3.9}$$

Here, $G_{x,n}$ and $G_{\dot{x},n}$ represent displacement gain value for the nth degree of freedom and velocity gain value for the nth degree of freedom, respectively.

Reduced-matrix Riccati equation solution yields the optimum gain factor for the chosen Q & R. However, it does not mean it is the global optimum for the system. Getting the global optimum requires choosing the best pair of Q & R, which is usually iterative (Vinodh Kumar & Jerome, 2013).

There are requirements for the Reduced-matrix Riccati equation to give stable eigenvalues for the closed-loop system:

- Q is a positive-definite Hermitian matrix (or positive-semidefinite).
- R is a positive-definite Hermitian matrix.
- P is a positive-definite matrix.

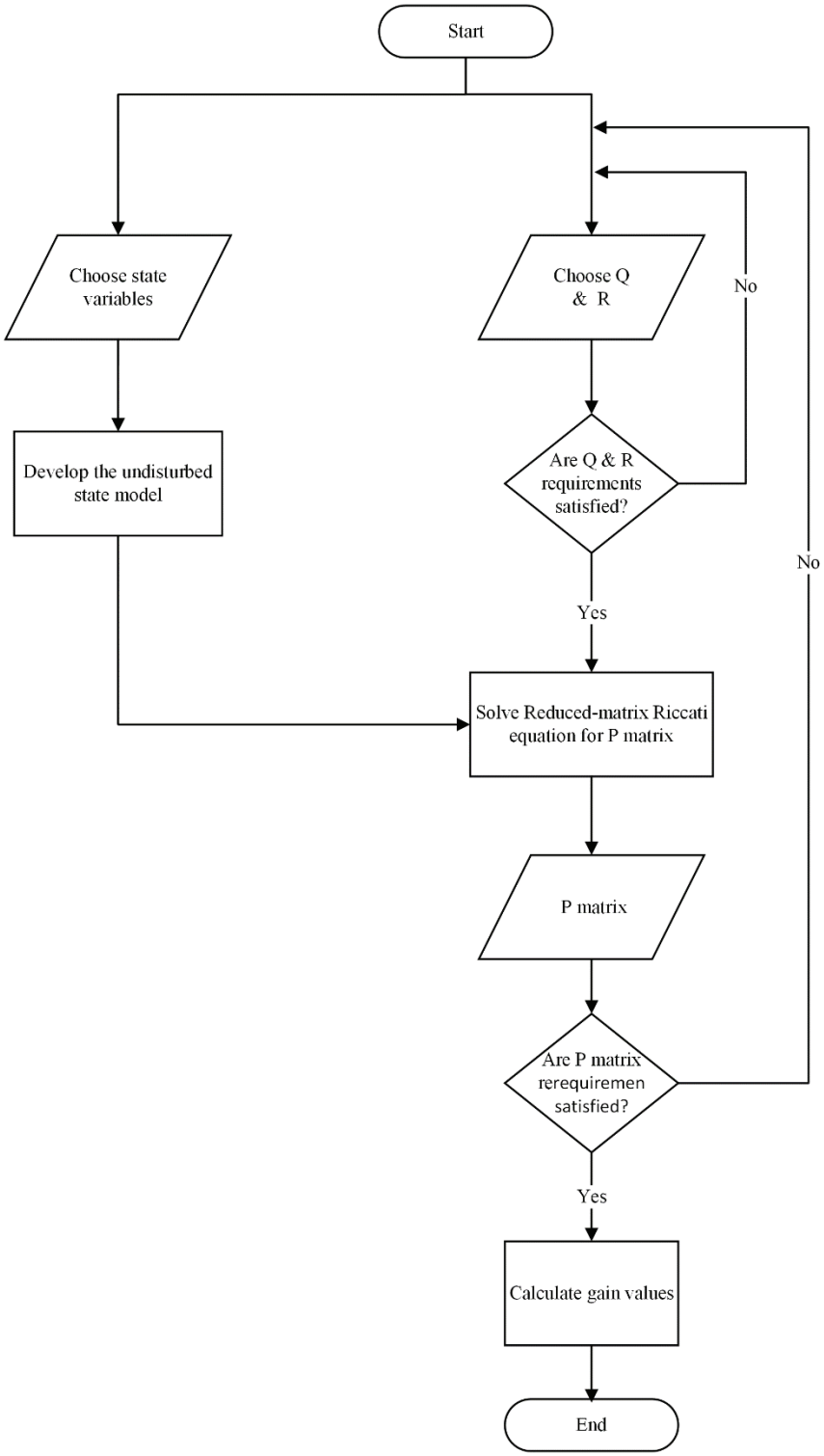

Figure 3.1 Linear quadratic regulator design steps

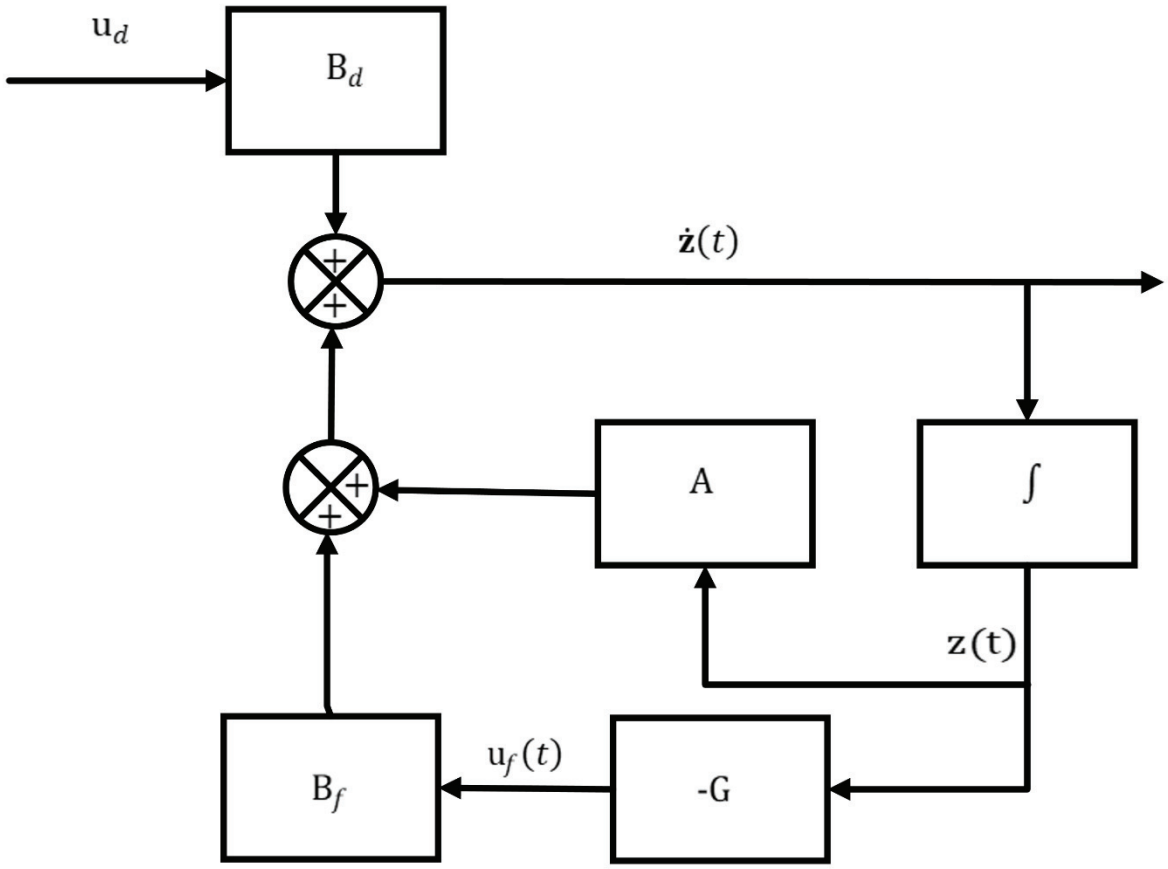

Figure 3.2 State model for control system under excitation

3.2. Design Domain

The linear quadratic regulator is not bounded to any specific domain. As long as the requirements for all LQRs' inputs, like Q and R are met, LQR will yield gain values under that domain, such as frequency and time domains.

The time domain is adopted in this study. However, the design will be conducted under the drift coordinate, not the displacement coordinate. Displacement in structural analysis refers to the relative displacement, not absolute, which is not much informative quantity of the structure. On the other hand, drift is a more informative quantity. Drift gives a more meaningful perspective on the demands on structural elements. For example, large drift values may indicate yielding in that particular story. Overall, drift analysis makes structural issues like a soft story more straightforward to spot, thus it is critical to evaluate the structure's performance.

The displacement can be represented as a linear transformation from the drift coordinate. Velocity and acceleration may be transformed in a similar manner. The new quantities will be called drift, velocity-drift and acceleration-drift and will be symbolized as $\bar{x}$, $\dot{\bar{x}}$ and $\ddot{\bar{x}}$, respectively.

$$x = T\,\bar{x} \tag{3.10}$$

$$\dot{x} = T\,\dot{\bar{x}} \tag{3.11}$$

$$\ddot{x} = T\,\ddot{\bar{x}} \tag{3.12}$$

$$T=\begin{bmatrix} 1 & 1 & \cdots & 1 \\ & 1 & \cdots & 1 \\ & & \ddots & \vdots \\ & & & 1 \end{bmatrix} \tag{3.13}$$

Here, T is the linear transformation matrix from drift coordinates to displacement. The first row of T sums up the drift value of the TMD and all of the structural drift values. The first story displacement is simply equal to the drift of the first story.

Reflecting this transformation to equation (2.10) which is the equation of motion under active control, will yield (3.14).

$$M_{TMD}T\,\ddot{\bar{x}}(t)+C_{TMD}T\,\dot{\bar{x}}(t)+K_{TMD}\,T\,\bar{x}(t) = -\Gamma\ddot{u}_g(t)- rF(t) \tag{3.14}$$

The structure's mass, stiffness, and damping matrices in the standard form regulate the relation between displacement coordinate quantities displacement, velocity and acceleration of the system with disturbances. However, we can reflect the linear transformation matrix (T) in equation (3.14) on the structure's matrices to have a more compacted form of the equation of motion. The newly transformed matrices presented in (3.15) to (3.17) regulate the relation between drift quantities and disturbances. They will be named the drift-based mass, damping, and stiffness matrices.

$$\overline{M_{TMD}}=M_{TMD}T \tag{3.15}$$

$$\overline{C_{TMD}}=C_{TMD}T \tag{3.16}$$

$$\overline{K_{TMD}}=K_{TMD}\,T \tag{3.17}$$

Here, $\overline{M_{TMD}}$, $\overline{C_{TMD}}$ and $\overline{K_{TMD}}$ are drift-based matrices for mass, damping and stiffness of TMD-controlled structure, respectively.

Utilizing the new drift-based matrices in (3.15), (3.16) and (3.17) will yield the equation of motion of active control structure in the drift coordinates displayed in (3.18). It is worth noting that disturbances will not be affected by any transformation.

$$\overline{M_{TMD}}\,\ddot{\bar{x}}(t)+\overline{C_{TMD}}\,\dot{\bar{x}}(t)+\overline{K_{TMD}}\,\bar{x}(t)=-\Gamma\ddot{u}_g(t)-rF(t) \qquad (3.18)$$

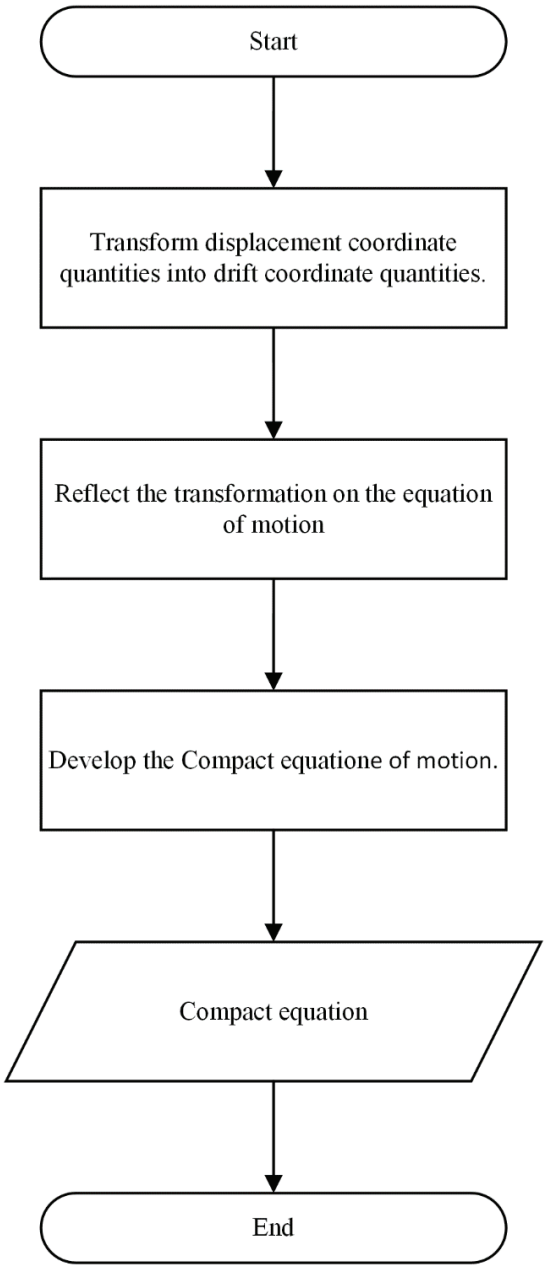

Figure 3.3 Domain transformation steps

3.3. Drift State Space Model

In previous sections, the state space model was developed for displacement coordinate, and its relation to LQR equations was clarified, but since the drift equation of motion was derived, the state space model displacement-based must be updated to a drift-based model.

The quadratic objective function in equation (3.1) depends on the displacement quantities, which should be altered. The drift objective function, control law and state variables are displayed in (3.19), (3.20), and (3.21).

$$\bar{J}=\frac{1}{2}\int_0^{\infty}\left(\bar{z}^T\bar{Q}\bar{z}+u_f{}^T R u_f\right)dt \tag{3.19}$$

Here, $\bar{J}$ is the objective function, and $\bar{Q}$ have the same meaning as Q, but it represents the relationship with drift quantities, not displacement quantities.

$$\bar{z}(t)=\begin{bmatrix}\bar{x}(t)\\ \dot{\bar{x}}(t)\end{bmatrix} \tag{3.20}$$

$$u_f(t)=-\bar{G}\bar{z}(t) \tag{3.21}$$

Here, $\bar{z}$ and $\bar{G}$, are drift-based state variables, and drift-based gain values, respectively.

State equation in the drift state model will only change the parts related to system dynamics and state variables, but not the disturbances, the active force, or their location vector. Equations (3.22) and (3.23) present the drift-based state model with external disturbance included and the undisturbed model, respectively.

$$\dot{\bar{z}}(t)=\bar{A}\bar{z}(t)+B_d u_d(t)+B_f u_f(t) \tag{3.22}$$

$$\dot{\bar{z}}(t)=\bar{A}\bar{z}(t)+B_f u_f(t) \tag{3.23}$$

$$\bar{A}=\begin{bmatrix} [0]_{mxm} & [1]_{mxm} \\ -[(\overline{M_{TMD}})^{-1}\overline{K_{TMD}}]_{mxm} & -[(\overline{M_{TMD}})^{-1}\overline{C_{TMD}}]_{mxm} \end{bmatrix}_{2mx2m} \quad (3.24)$$

Here, $\bar{A}$ is the system matrix for the drift model.

The Order reduced-matrix Riccati equation for the drift-based model in (3.25) is also covered by the same positive-definite matrix criteria for matrix ($\bar{P}$). If the condition is satisfied, the required gain vector for a stabilized closed loop is presented in (3.26).

$$\bar{A}^T\bar{P}+\bar{P}\bar{A}-\bar{P}B_f R^{-1}B_f{}^T\bar{P}+Q=0 \quad (3.25)$$

$$\bar{G}=R^{-1}B_f^T P \quad (3.26)$$

$$\bar{G}=\begin{bmatrix}\bar{G}_{\bar{x},n} & \bar{G}_{\bar{x},n-1} & \cdots & \bar{G}_{\bar{x},1} & \bar{G}_{\dot{\bar{x}},n} & \bar{G}_{\dot{\bar{x}},n-1} & \cdots & \bar{G}_{\dot{\bar{x}},1}\end{bmatrix} \quad (3.27)$$

Here, $\bar{G}_{\bar{x},n}$ and $\bar{G}_{\dot{\bar{x}},n}$ represent drift gain value for the nth degree of freedom and velocity-drift gain value for the nth degree of freedom, respectively.

The relation between drift-base gain values and displacement gain values is presented in (3.28). The relationship enables the design in drift coordinates and implementation to be in the displacement coordinates. Drift is a more informative quantity, while displacement is easier to implement.

$$G_{1x2n}=\bar{G}_{1x2n}\begin{bmatrix}[T^{-1}]_{n\,x\,n} & [0]_{n\,x\,n} \\ [0]_{n\,x\,n} & [T^{-1}]_{n\,x\,n}\end{bmatrix}_{2n\,x\,2n} \quad (3.28)$$

It is worth saying that the structure's characteristics, like eigenvalues, will not differ from one coordinate system to another.

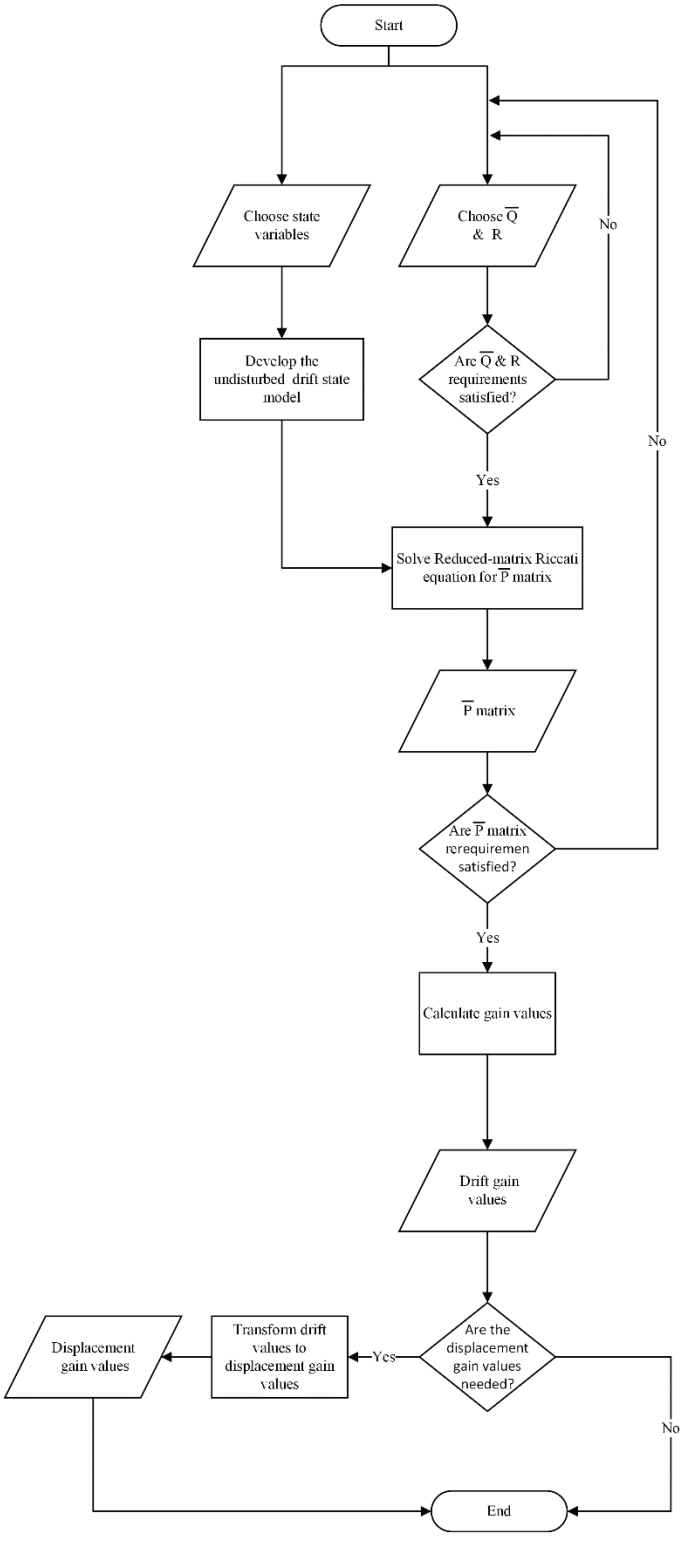

Figure 3.4 Steps for obtaining gain values in displacement and drift coordinates

CHAPTER 4

OPTIMIZATION

In chapter 3, it is stated that Q & R are determined based on iterative manners. This iterative procedure is transformed into an optimization problem. A multiobjective function was proposed to maximize the effect of the LQR controller on the whole structure. Non-dominated Sorting Genetic Algorithm (NSGA-II) is used to search for the global optimum solution in this chapter.

4.1. Nondominated Sorting Genetic Algorithm (NSGA-II)

Multiobjective optimization problems (MOOPs) mean having multiple conflicted objective functions. Conflicted objectives mean a single solution for minimizing all objectives does not exist. However, a set of solutions exist, each minimizing one objective function. One of the methods of choosing a good solution is using the pareto concept.

The pareto optimal solution is comprised of a non-dominated solutions set. A solution x^* said to be a non-dominated solution in case of minimization if the following two conditions are satisfied:

1. The objective values of x^* are equal or lower than any other solution space solution. The condition is symbolized in equation (4.1), where i and x present the number of the objective function and any solution in the solution set, respectively.

$$f_i(x) \geq f_i(x^*) \quad [\forall i \ \& \ \forall x] \tag{4.1}$$

2. The objective values of x^* are lower than any other solution space solution in one objective at least. The condition is symbolized in equation (4.4).

$$f_i(\mathrm{x}) > f_i(\mathrm{x}^*) \tag{4.2}$$

The dominancy concept used in literature by the previously mentioned words, non-dominated and dominated solution, are equivalent to dominant and non-dominant solutions, respectively. The non-dominated solution or dominant solution are better than dominated solution. Figure 4.1 and Table 4.1 present example for dominancy classification and pareto frontier graph.

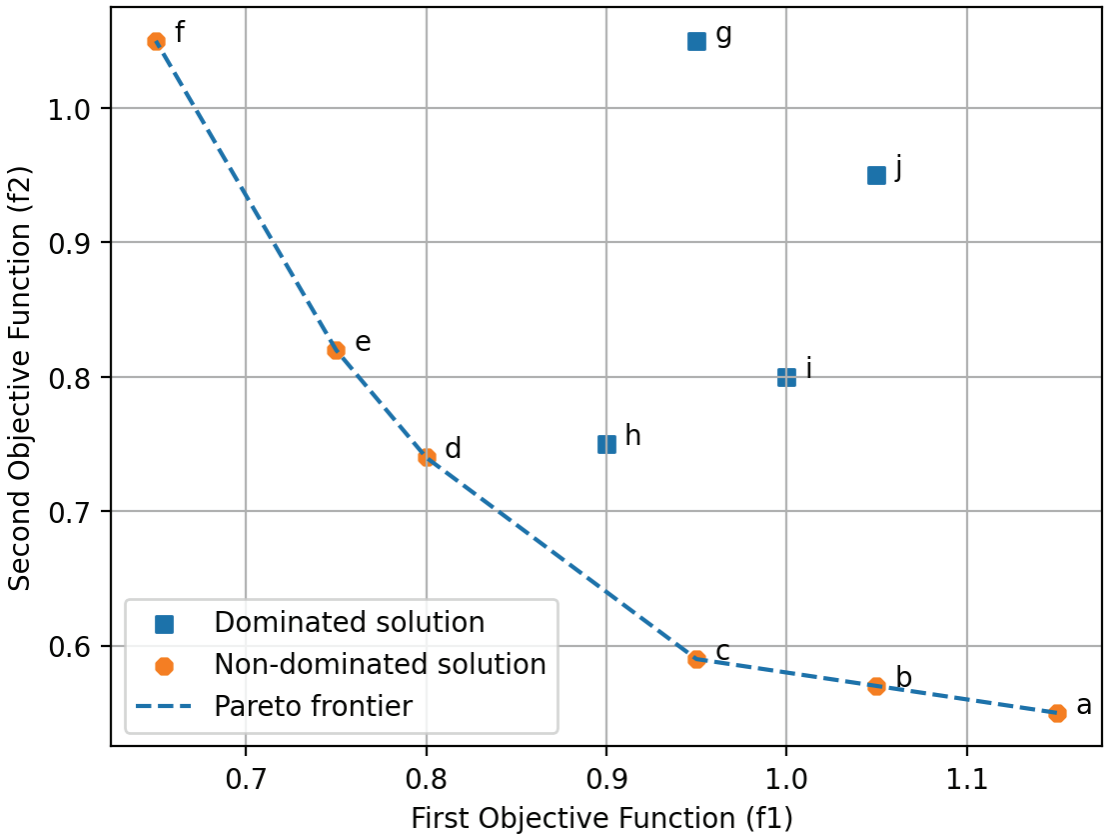

Figure 4.1 Pareto frontier

Table 4.1 Dominancy classification

Point	Dominated point	Non-dominated / Dominated
a	None	Non-dominated
b	j	Non-dominated
c	g j i	Non-dominated
d	g j i h	Non-dominated
e	g j	Non-dominated
f	g	Non-dominated
g	None	Dominated
h	g j i	Dominated
i	j	Dominated
j	None	Dominated

Non-dominated sorting genetic algorithm II (NSGA-II) is one of the multiobjective evolutionary algorithms (MOEAs). NSGA-II uses the pareto concept to obtain the solution. NSGA-II comes with $O(MN^2)$ complexity where M and N is the number of the objective function and the number of solution in one iteration (generation), respectively. The time complexity is a characteristic of the algorithm, used to differentiate the time required for different algorithms to be executed, regardless of the solver(computer) speed. The lower the time complexity, the faster the algorithm. For example, the time complexity for NSGA is $O(MN^3)$ while NSGA-II $O(MN^2)$, which makes it faster. This thesis uses NSGA-II to solve the optimization problem. Deb et. al provides a complete explanation in (Deb et al., 2002).

The NSGA-II's last generation will contain many solutions. Those solutions will contain dominated and non-dominated solutions. A Trade-off between objective functions is expected. A simple procedure is used to choose one solution from the generation. The procedure is presented in Figure 4.2 and explained in the following steps:

1. Classify solutions into non-dominated and dominated solutions.
2. Exclude the dominated solutions.
3. Exclude any unfeasible solution. A solution is said to be unfeasible if an objective for that solution has a value higher than one.

4. Reduce the multiobjectives for each solution into one value. The reduced value equals the maximum objective value among other values.
5. Rank the solution based on the reduced value and choose the lowest one.

4.2. Problem Definition

The structure under the excitation effect will witness drifts along the height, and those drift values are unequal. A non-proper ATMD design can decrease the last story's drift substantially and increase the lower story substantially. At the same time, a proper control design can decrease the drift on all stories. This maximization depends on the active force limit and the proper LQR design parameters.

Multiple cases are studied in this thesis. Each case has its objective function. However, all of them are built upon the objective function presented in (4.3).

$$\min \left[\frac{\bar{x}_{\text{Active controlled}}}{\min[\bar{x}_{\text{uncontrolled}}, \bar{x}_{\text{TMD controlled}}]} \right]_n \tag{4.3}$$

Here n is the number of stories of the uncontrolled structure.

4.3. Earthquake

Ground motion is classified into near-field and far-field records. Near fields are also classified for pulse-type motion and non-pulse, where pulses can be easily identified in the velocity record. Pulse-type motion creates more demands on the structure, making it more critical than other records (Bray & Rodriguez-Marek, 2004).

In this study, two sets of earthquakes are used. The first set comprised a near-field pulse-type motion and was used for design optimization. The second set comprises far-field and non-pulse-type near-field records, which are used to evaluate the design's robustness. Earthquake types and peak ground acceleration are presented in Table 4.2, while full details are presented in Table A.

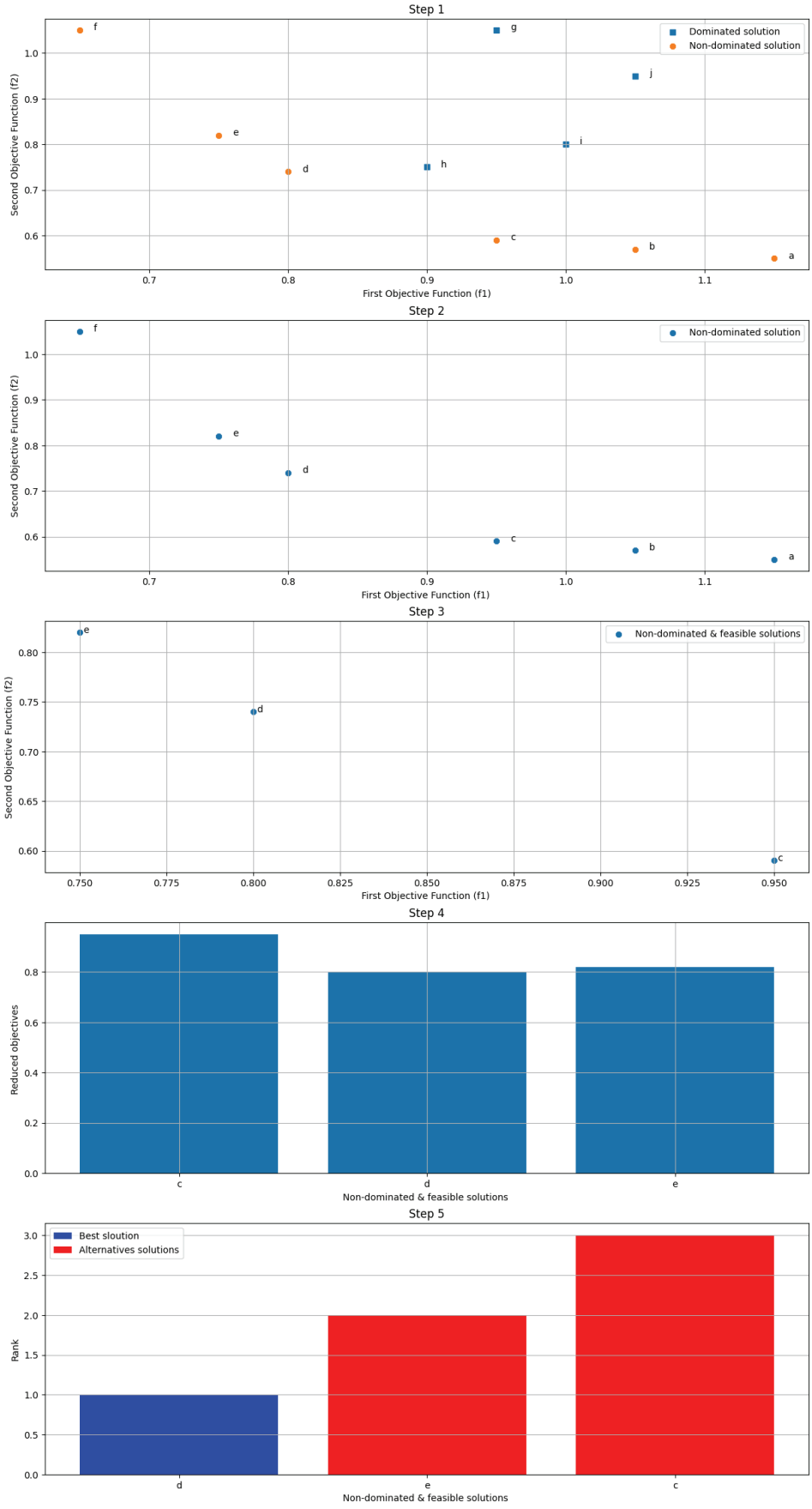

Figure 4.2 Determining the best solution procedures

Table 4.2 Summary of earthquakes

Event Number	Type	PGA (g)	Event Number	Type	PGA (g)	Event Number	Type	PGA (g)
1	Near field- with pulse	0.87	34	Near field- without pulse	0.32	67	Far field	0.36
2	Near field- with pulse	0.47	35	Near field- without pulse	0.70	68	Far field	0.32
3	Near field- with pulse	0.60	36	Near field- without pulse	0.86	69	Far field	0.47
4	Near field- with pulse	0.84	37	Near field- without pulse	0.50	70	Far field	0.51
5	Near field- with pulse	0.23	38	Near field- without pulse	0.32	71	Far field	0.74
6	Near field- with pulse	0.17	39	Near field- without pulse	1.01	72	Far field	0.81
7	Near field- with pulse	0.79	40	Near field- without pulse	0.43	73	Far field	0.51
8	Near field- with pulse	0.58	41	Near field- without pulse	0.60	74	Far field	0.50
9	Near field- with pulse	0.30	42	Near field- without pulse	0.78	75	Far field	0.24
10	Near field- with pulse	0.17	43	Near field- without pulse	0.27	76	Far field	0.35
11	Near field- with pulse	0.40	44	Near field- without pulse	0.25	77	Far field	0.37
12	Near field- with pulse	0.51	45	Near field- without pulse	0.33	78	Far field	0.38
13	Near field- with pulse	0.45	46	Near field- without pulse	0.30	79	Far field	0.27
14	Near field- with pulse	0.45	47	Near field- without pulse	1.11	80	Far field	0.33
15	Near field- with pulse	0.16	48	Near field- without pulse	1.20	81	Far field	0.22
16	Near field- with pulse	0.27	49	Near field- without pulse	0.52	82	Far field	0.19
17	Near field- with pulse	0.23	50	Near field- without pulse	0.36	83	Far field	0.36
18	Near field- with pulse	0.32	51	Near field- without pulse	0.46	84	Far field	0.26
19	Near field- with pulse	0.43	52	Near field- without pulse	0.50	85	Far field	0.47
20	Near field- with pulse	0.38	53	Near field- without pulse	0.64	86	Far field	0.29
21	Near field- with pulse	0.51	54	Near field- without pulse	0.48	87	Far field	0.51
22	Near field- with pulse	0.33	55	Near field- without pulse	1.49	88	Far field	0.44
23	Near field- with pulse	0.50	56	Near field- without pulse	1.04	89	Far field	0.56
24	Near field- with pulse	0.39	57	Far field	0.48	90	Far field	0.37
25	Near field- with pulse	0.59	58	Far field	0.46	91	Far field	0.28
26	Near field- with pulse	0.66	59	Far field	0.23	92	Far field	0.42
27	Near field- with pulse	0.73	60	Far field	0.23	93	Far field	0.24
28	Near field- with pulse	0.79	61	Far field	0.21	94	Far field	0.15
29	Near field- without pulse	0.75	62	Far field	0.13	95	Far field	0.40
30	Near field- without pulse	0.93	63	Far field	0.31	96	Far field	0.47
31	Near field- without pulse	0.34	64	Far field	0.36			
32	Near field- without pulse	0.46	65	Far field	0.34			
33	Near field- without pulse	0.23	66	Far field	0.40			

4.4. Linear Case

In this case, each story's degree of freedom has its own objective function which is presented in (4.4). Objective functions have no constraints nor force limitations. Force could be as high as required. The calculation steps for the objective function are presented in Figure 4.3 and will be explained shortly.

The drift space model is adopted, the Q matrix is the optimization variable, while the R-value is set for a specified value. Q is set to be a positive diagonal to maintain the condition of the Riccati equation. The Q values represent the velocity-drift states whose lies in the lower diagonal are set to be ones, while the drift states values are set for optimization. The search domain is set to $[1,10^5]$. A summary of optimization is presented in Table 4.3

Table 4.3 Optimization details for the linear case

R	10^{-9}
$\bar{Q}$	$\text{diag}(\bar{q}_{11},\bar{q}_{10},\bar{q}_{9},.....\bar{q}_{1},1,1,....1)$
$\bar{q}_x$ domain	$[1,10^5]$

$$F_n=\left[\frac{\bar{x}_{\text{Active controlled}}}{\min[\bar{x}_{\text{uncontrolled}},\bar{x}_{\text{TMD controlled}}]}\right]_n \tag{4.4}$$

Figure 4.3 (a &b) presents the first step in objective function calculation. This step involves the responses of both the uncontrolled structure and the TMD-controlled structure, and it includes the following components:

1. Analyze the uncontrolled structure and TMD-controlled structure under earthquakes.
2. Keep the maximum drift as in the first step for uncontrolled and TMD-controlled structures in a different matrix.
3. Compare each element in both matrices and keep the critical one (smaller).

The second step, which is presented in Figure 4.3 (c), is related to the response of the actively controlled structure, and it is comprised of the following:

1. Analyze the structure under earthquakes and unlimited LQR force.

2. Store the maximum drift for each degree of freedom for each earthquake in one matrix.

Figure 4.3 (d) shows the third step. This step is just an element-wise division of the matrix from the second step by the matrix resulting in the first step. The final step is averaging the resulting matrix from the previous step along the rows shown in Figure 4.3 (e). The steps from the second to the last are iterative along the optimization, while the first step is not.

4.5. Nonlinear Case

The only difference between this case and the linear case is that a force limited-drift-LQR model was adopted. Limited means that if the calculated force by LQR exceeds the specified limited force, the limited force will be applied instead of the calculated. The force limitation changes the linear feedback into nonlinear feedback because the relationships and the applied force are nonlinear.

Table 4.4 Optimization details for the nonlinear case

R	10^{-9}
Q	$\text{diag}(\bar{q}_{11},\bar{q}_{10},\bar{q}_{9},.....\bar{q}_{1},1,1,....1)$
$\bar{q}_x$ domain	$[1,10^9]$
Force limit	245 kN (5% of the structure's weight)

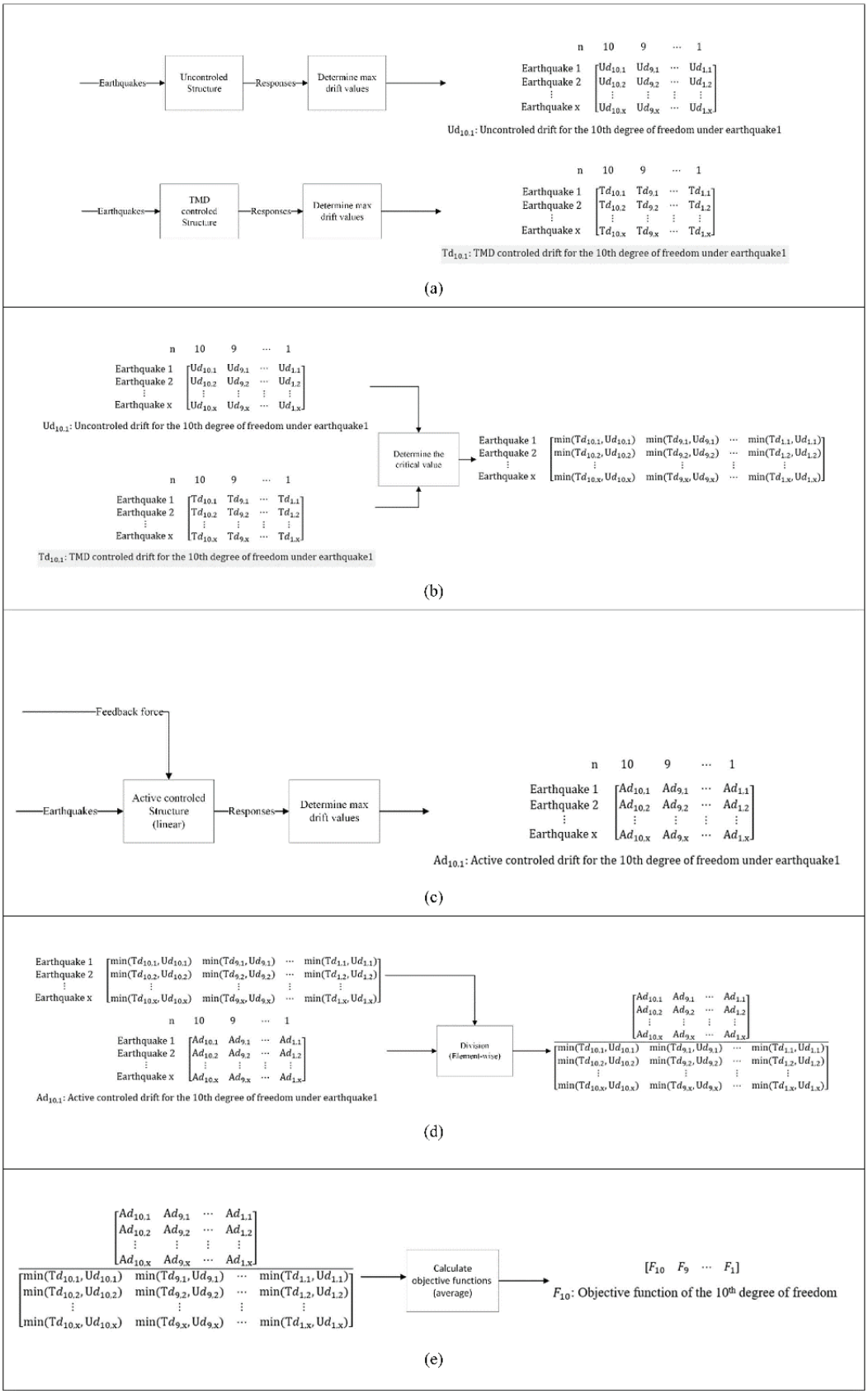

Figure 4.3 Linear case steps

4.6. Performance Indices

The designer assumes that an active control system decreases the structure's response. However, the assumption must be verified because a faulty design can worsen the response. Assessing the effectiveness of the proposed design is measured by the performance index. The performance index reflects how effective the control design is on the structure's response. Five performance indices are proposed in this study to assess the control system efficiency (Ohtori et al., 2004).

The first performance index measures the reduction in base shear between controlled and uncontrolled structures, presented in (4.5).

$$J_1 = \max_{EQx} \left\{ \frac{\max_{t} \left| \sum_{i=1}^{n} m_i \ \ddot{x}_{TMD,i} \right|}{|F_b|} \right\} \tag{4.5}$$

Here, m_i is the i'th story mass of controlled structure, and F_b is base shear of uncontrolled structure, respectively.

The second performance presented in (4.6) measures the reduction in acceleration.

$$J_2 = \max_{EQx} \left\{ \frac{\max_{t,i} \left| \ddot{x}_{AMD,i} \right|}{\max_{t,i} |\ddot{x}_i|} \right\} \tag{4.6}$$

Here, $|\,.\,|$ denotes the absolute value.

The third index presented in (4.7), measures the normalized relative displacement of controlled to uncontrolled structures.

$$J_3 = \max_{EQx} \left\{ \frac{\max_{i} \|x_{AMD,i}\|}{\max_{i} \|x_i\|} \right\} \tag{4.7}$$

Here, $\|\cdot\|$ denotes the root mean square (RMS) of the quantity.

The fourth index presented in (4.8) measures the change in maximum drift between control and uncontrolled structure.

$$J_4 = \max_{EQx} \left\{ \frac{\max_{t,i} \left| \overline{x_{AMD,i}} \right|}{\text{drift}} \right\} \tag{4.8}$$

The fifth index presented in (4.9), relates the maximum control force to the structure's weight.

$$J_5 = \max_{EQx} \left\{ \frac{\max_{t} \left| u_f \right|}{w} \right\} \tag{4.9}$$

The performance indices presented in (4.5) to (4.9) are non-dimensional quantities. In the indices, the lower the value, the better the design.

Table 4.5 Summary of evaluation criteria

Base Shear $J_1 = \max_{EQx} \left\{ \frac{\max_{t} \left\lvert \sum_{i=1}^{n} m_i \ddot{x}_{TMD,i} \right\rvert}{\lvert F_b \rvert} \right\}$	Acceleration $J_2 = \max_{EQx} \left\{ \frac{\max_{t,i} \left\lvert \ddot{x}_{AMD,i} \right\rvert}{\max_{t,i} \lvert \ddot{x}_i \rvert} \right\}$
Normed Floor Displacement $J_3 = \max_{EQx} \left\{ \frac{\max_{i} \lVert x_{AMD,i} \rVert}{\max_{i} \lVert x_i \rVert} \right\}$	Drift $J_4 = \max_{EQx} \left\{ \frac{\max_{t,i} \left\lvert \overline{x_{AMD,i}} \right\rvert}{\text{drift}} \right\}$
Control Force $J_5 = \max_{EQx} \left\{ \frac{\max_{t} \left\lvert u_f \right\rvert}{w} \right\}$	

CHAPTER 5

RESULTS

This chapter presents the result of optimization cases containing findings and problems. Several proposed methods were presented. The effectiveness of each model was presented using time history for multiple quantities. Characteristics of each linear system, like modal damping, natural frequencies, and earthquake bode plot, are presented. In the case of a nonlinear system, a linearized characteristic was presented for comparison reasons.

5.1. Linear Case

The optimization of targeted Q's components is presented in Table 5.1, and associated drift gains are presented in Table 5.2. Table 5.3 introduces the transformed displacement gain values from drift gain values using (3.28). The system's characteristics, such as damping, natural frequencies, and bode plot, are identified.

The characteristics of the uncontrolled, TMD-controlled, and ATMD-controlled systems are presented in Figure 5.1. Several observations can be detected in Figure 5.1 :

1. The twin mode of both TMD and ATMD is for the first mode. Twin mode means the added mode by the extra mass on top is tuned for the first mode and has a frequency close to the first mode.
2. The first mode and its twin natural frequencies changed slightly between ATMD and TMD. At the same time, there is a noticeable change in the damping ratios with ATMD.
3. The TMD affects only the first mode. This affection explains why the bode plot of the TMD approximately coincides with the uncontrolled bode plot after the first mode region.

4. ATMD increases the damping and changes the natural frequency. This effect dimmish as the frequency increases. In this case, the effects extend till the seventh mode.

Table 5.1 Linear case optimization variable result

q_{11}	1
q_{10}	14903
q_9	99979
q_8	96745
q_7	4071
q_6	1321
q_5	288
q_4	859
q_3	74
q_2	193
q_1	87

Table 5.2 Linear case drift-coordinate gain values

$\bar{x}_{11}$	10448.67	$\ddot{\bar{x}}_{11}$	44950.78
$\bar{x}_{10}$	-6939171.31	$\ddot{\bar{x}}_{10}$	-472825.26
$\bar{x}_9$	46304.81	$\ddot{\bar{x}}_9$	-388677.06
$\bar{x}_8$	-3053987.54	$\ddot{\bar{x}}_8$	-276563.79
$\bar{x}_7$	-2032319.15	$\ddot{\bar{x}}_7$	-50415.48
$\bar{x}_6$	-791488.60	$\ddot{\bar{x}}_6$	62031.40
$\bar{x}_5$	-1909911	$\ddot{\bar{x}}_5$	148261.32
$\bar{x}_4$	-1317616.15	$\ddot{\bar{x}}_4$	268104.95
$\bar{x}_3$	86106.59	$\ddot{\bar{x}}_3$	340494.27
$\bar{x}_2$	565367.96	$\ddot{\bar{x}}_2$	331162.20
$\bar{x}_1$	122452.41	$\ddot{\bar{x}}_1$	292287.34

Table 5.3 Linear case displacement-coordinate gain values

x_{11}	10448.67	$\dot{x}_{11}$	44950.78
x_{10}	-6949619.98	$\dot{x}_{10}$	-517776.05
x_9	6985476.12	$\dot{x}_9$	84148.19
x_8	-3100292.35	$\dot{x}_8$	112113.27
x_7	1021668.39	$\dot{x}_7$	226148.31
x_6	1240830.54	$\dot{x}_6$	112446.89
x_5	-1118422.39	$\dot{x}_5$	86229.91
x_4	592294.84	$\dot{x}_4$	119843.63
x_3	1403722.75	$\dot{x}_3$	72389.31
x_2	479261.36	$\dot{x}_2$	-9332.06
x_1	-442915.54	$\dot{x}_1$	-38874.85

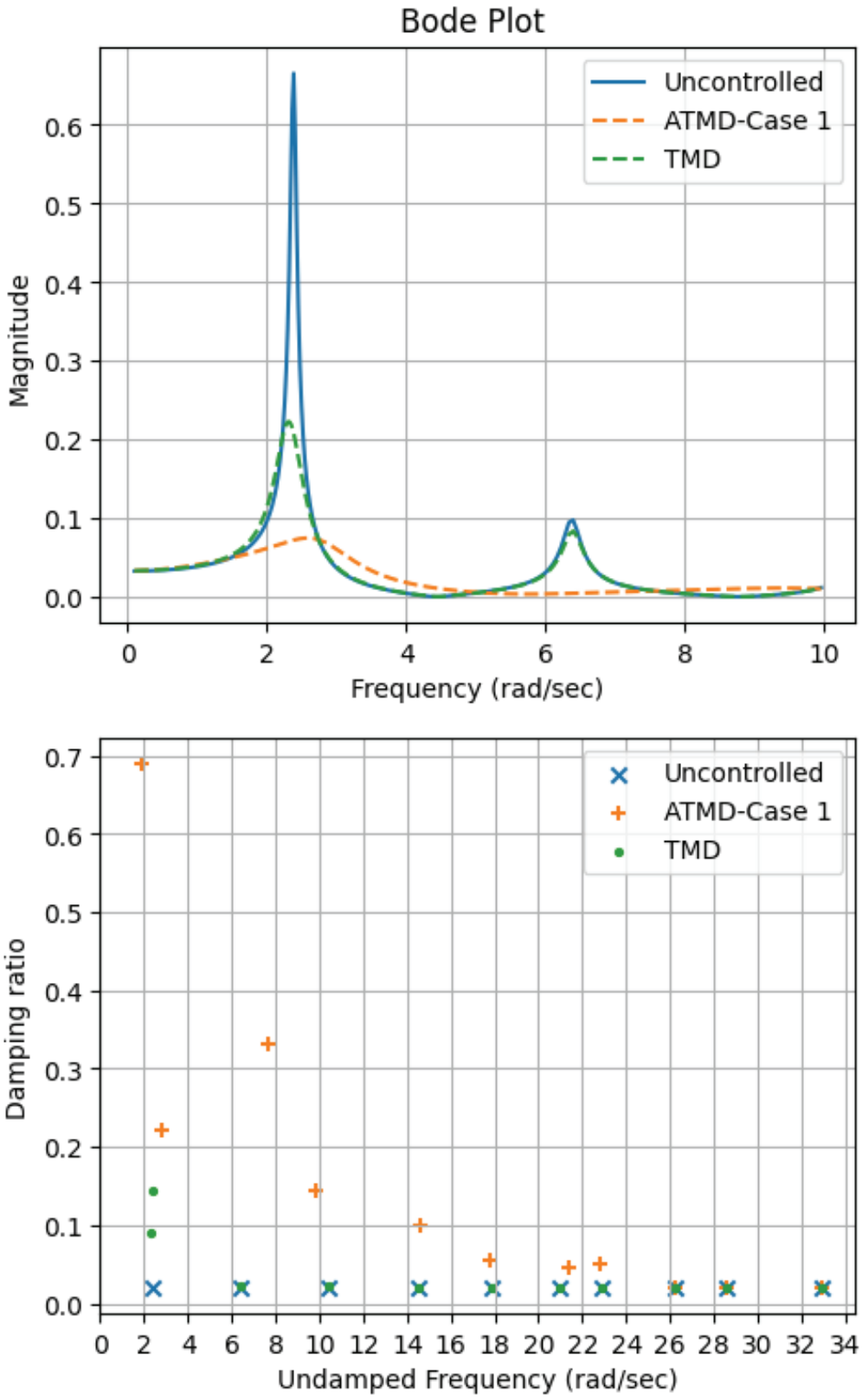

Figure 5.1 Charcetersitcs of ATMD, TMD and uncontrolled structure

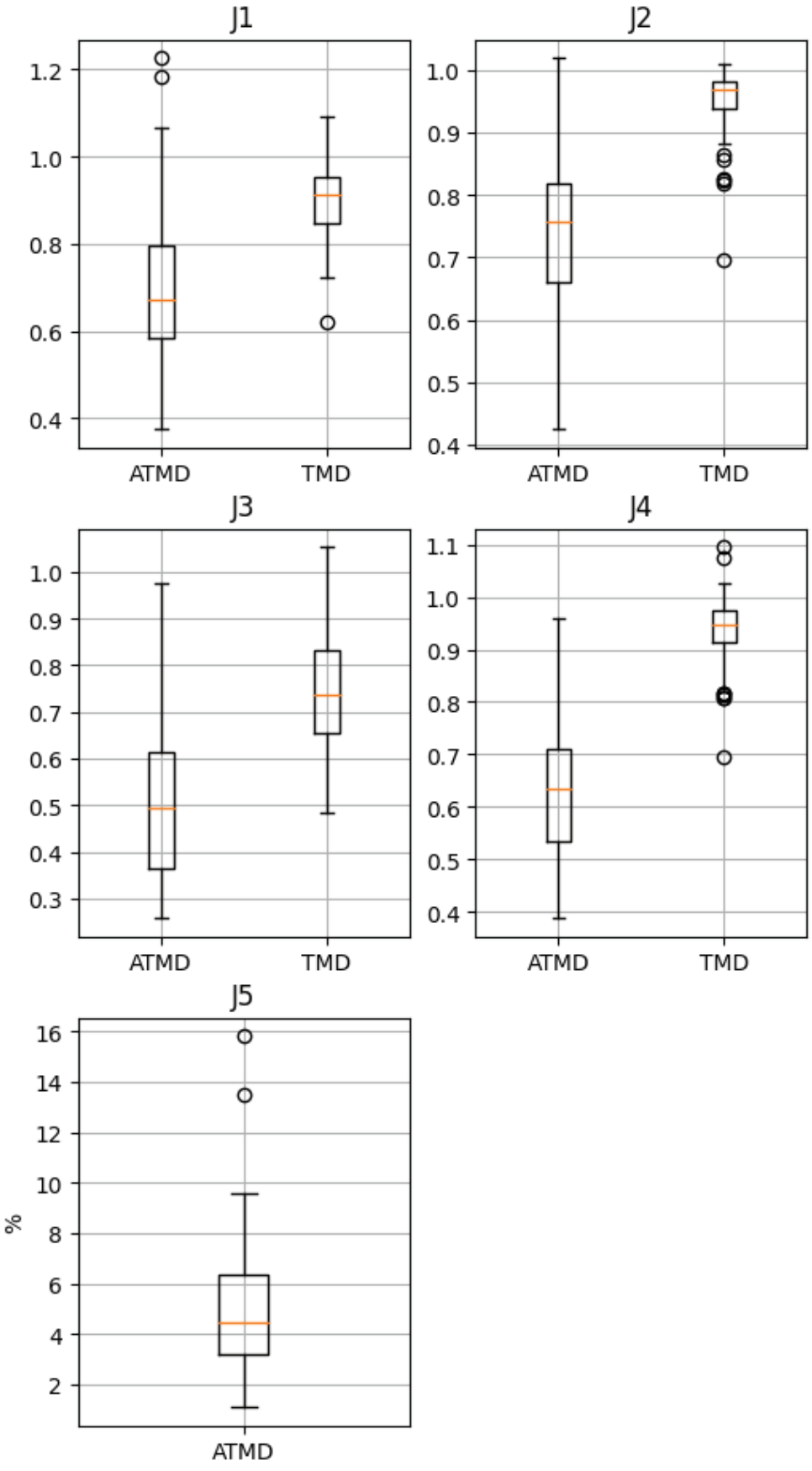

Figure 5.2 Performance indices of ATMD and TMD controlled structure

Figure 5.2 presents the ATMD and TMD performance indices under all provided earthquakes. Index J5 points to a problem of high required force. J3 & J4 indicate that ATMD outperforms TMD in decreasing normalized displacement and drift. However, J1 & J2 indicate that both TMD and ATMD are inefficient in decreasing the structure's acceleration and base shear as in decreasing the drift. Random samples for drift, displacement, acceleration, and inertial force time histories are presented in Figure 5.3, Figure 5.4, Figure 5.5, and Figure 5.6, respectively.

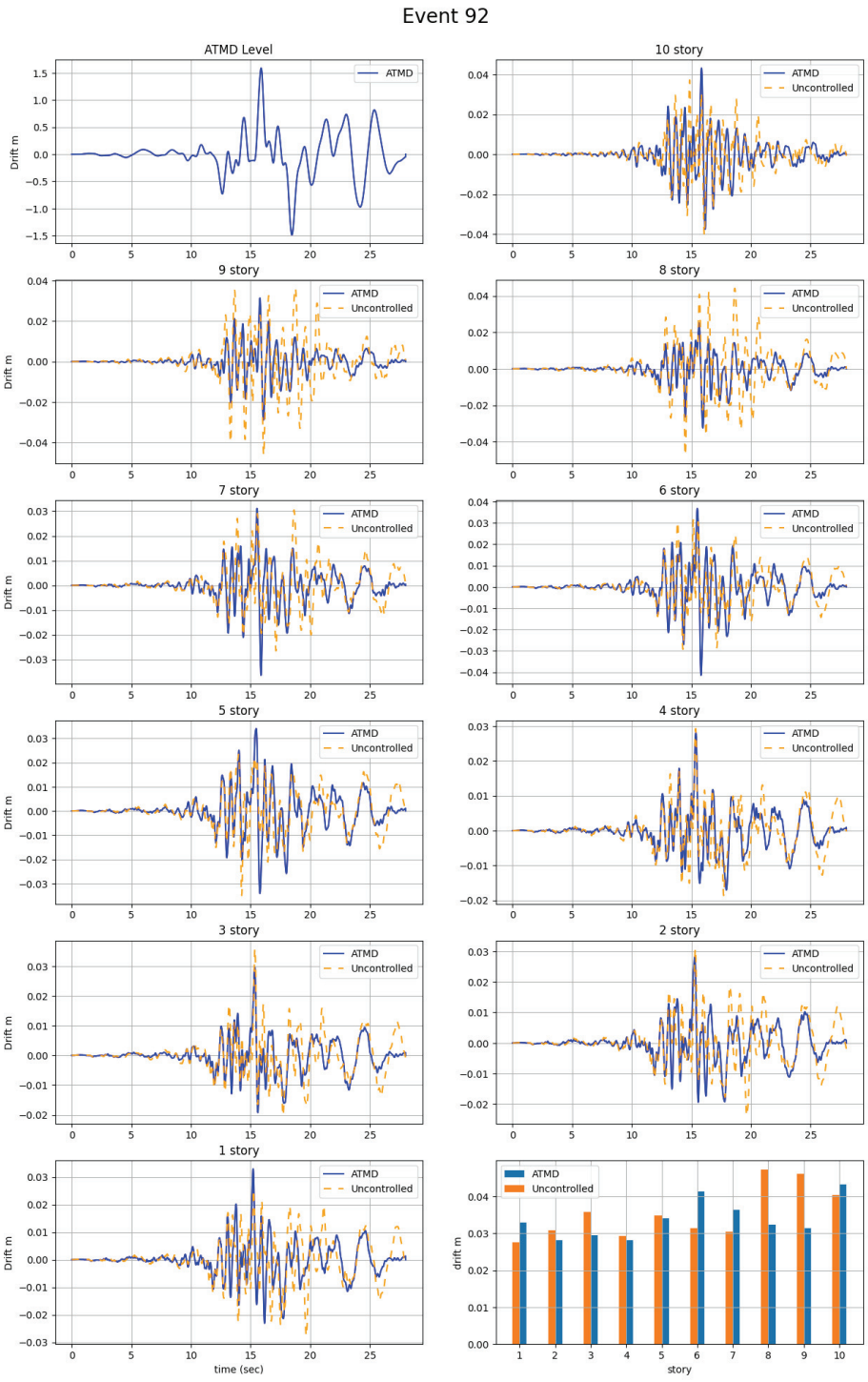

Figure 5.3 Drift of each story under event 92

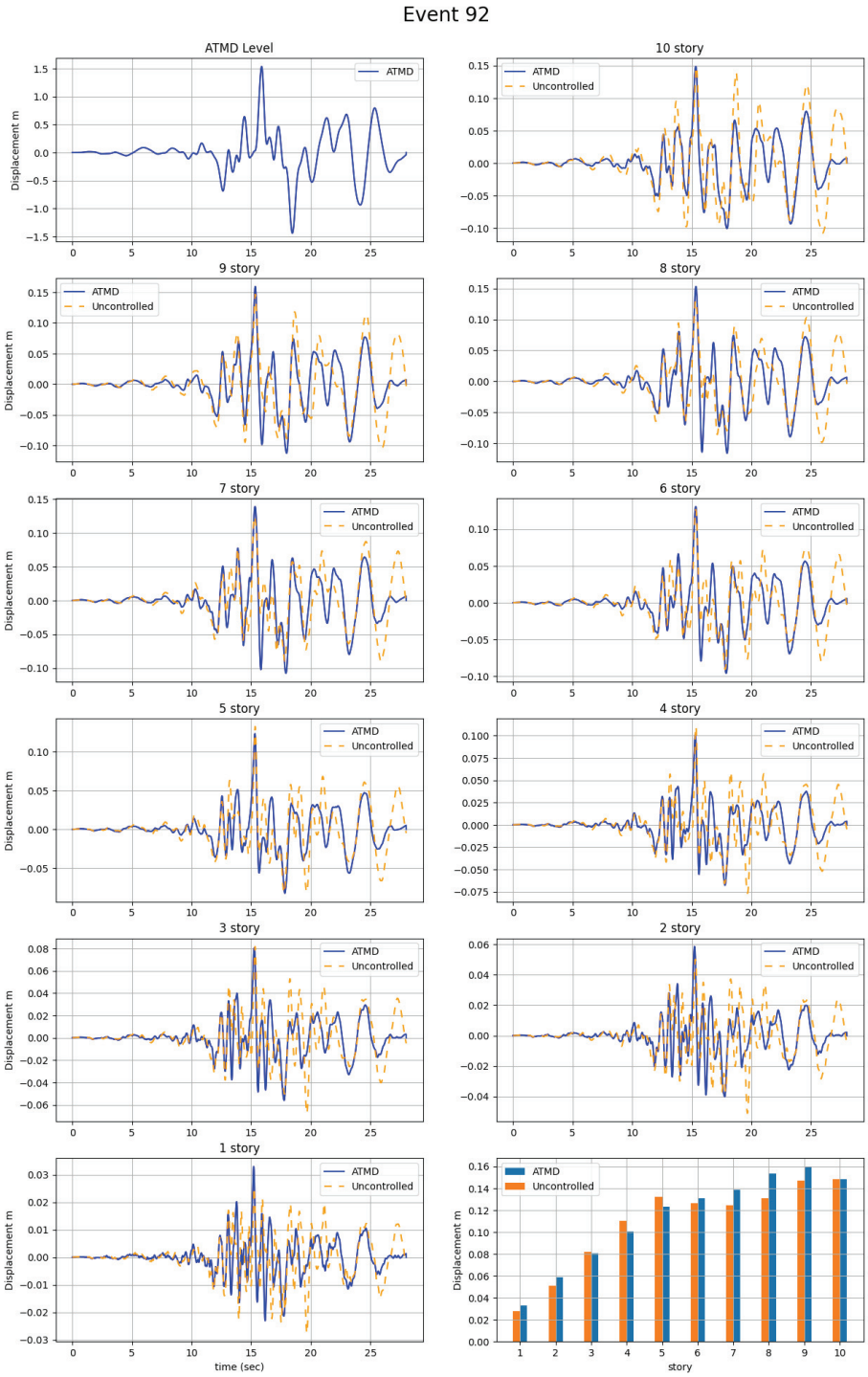

Figure 5.4 Displacement of each story under event 92

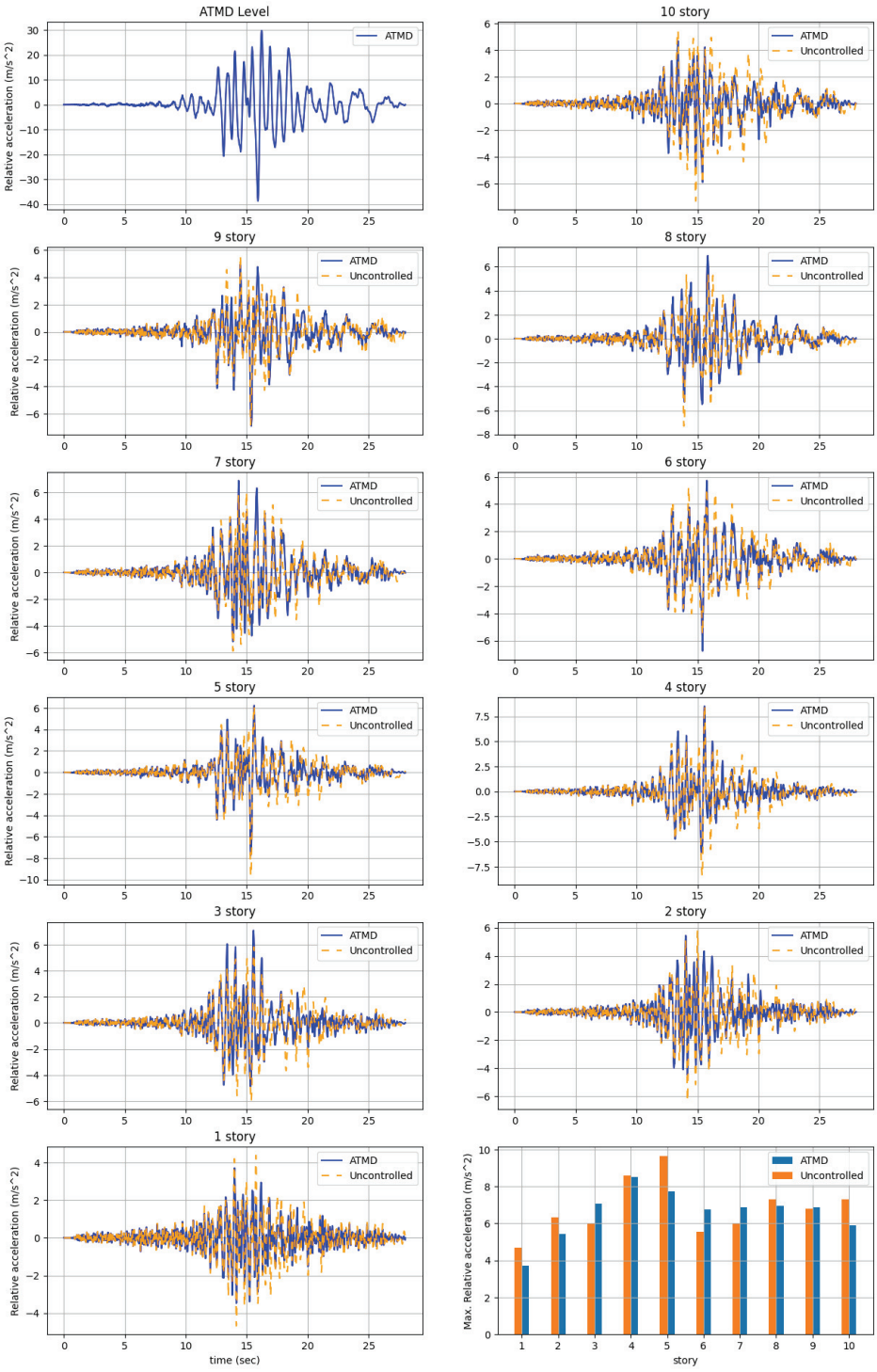

Figure 5.5 Acceleration of each story under event 92

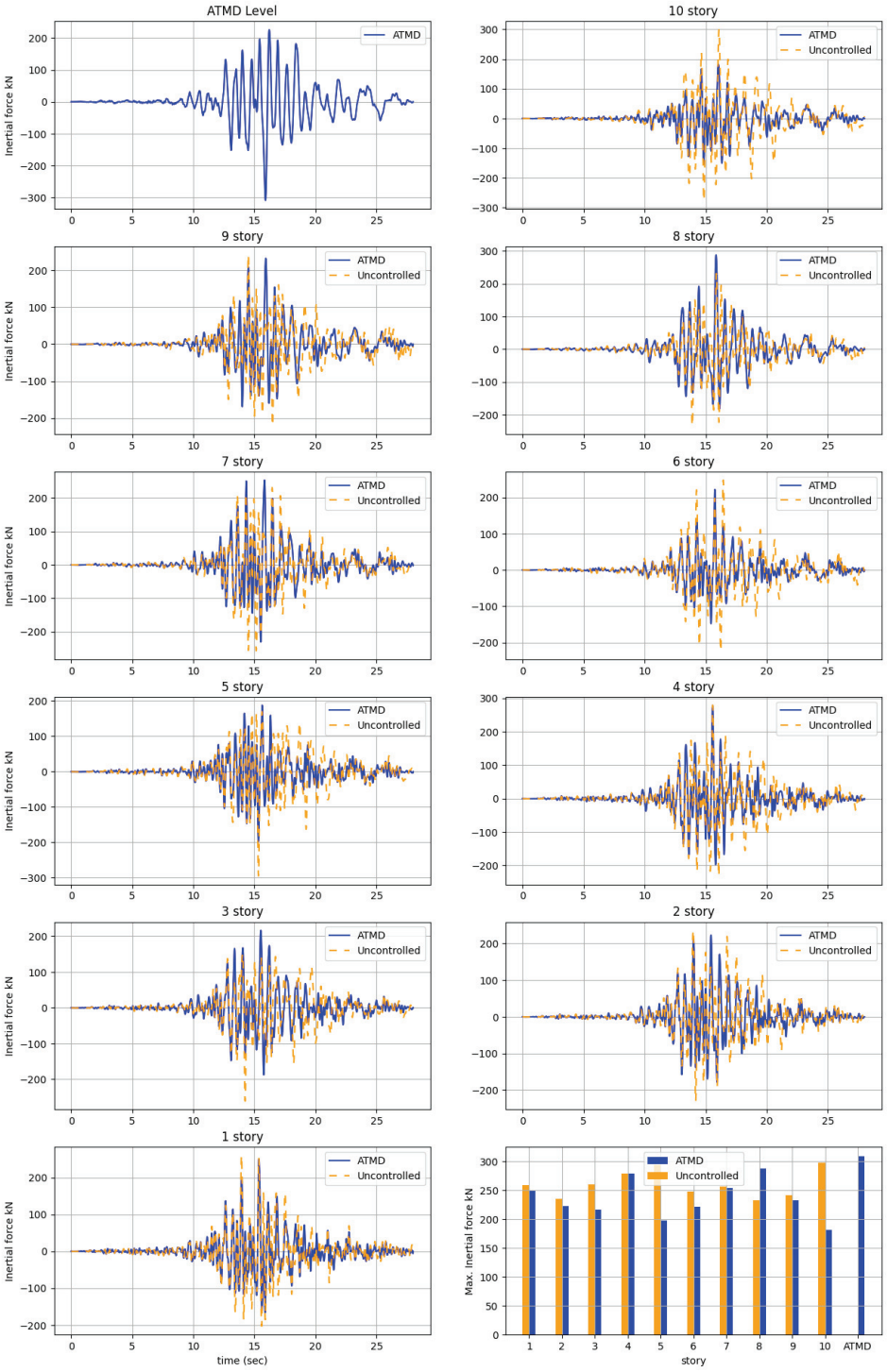

Figure 5.6 Inertial force of each story under event 92

Figure 5.6 presents the inertial forces for each floor, and it is pretty clear that ATMD decreases the maximum inertial forces of most floors. However, the base shear time history presented in Figure 5.7 shows that ATMD structure suffers from a higher base shear than uncontrolled structure in a number of records. However, only one among those records belongs to the 28 optimization records. Figure 5.8 presents the relation among indices, and the force index has no relation with the base shear index, while its relation with other indices looks not crucial. In contrast, J1 to J4 indices have a fuzzy relation, and it looks like the drift index is the master. However, Before naming the main reason behind the high base shear, further investigation must be carried out with new quantities like the stroke distance and acceleration of each story.

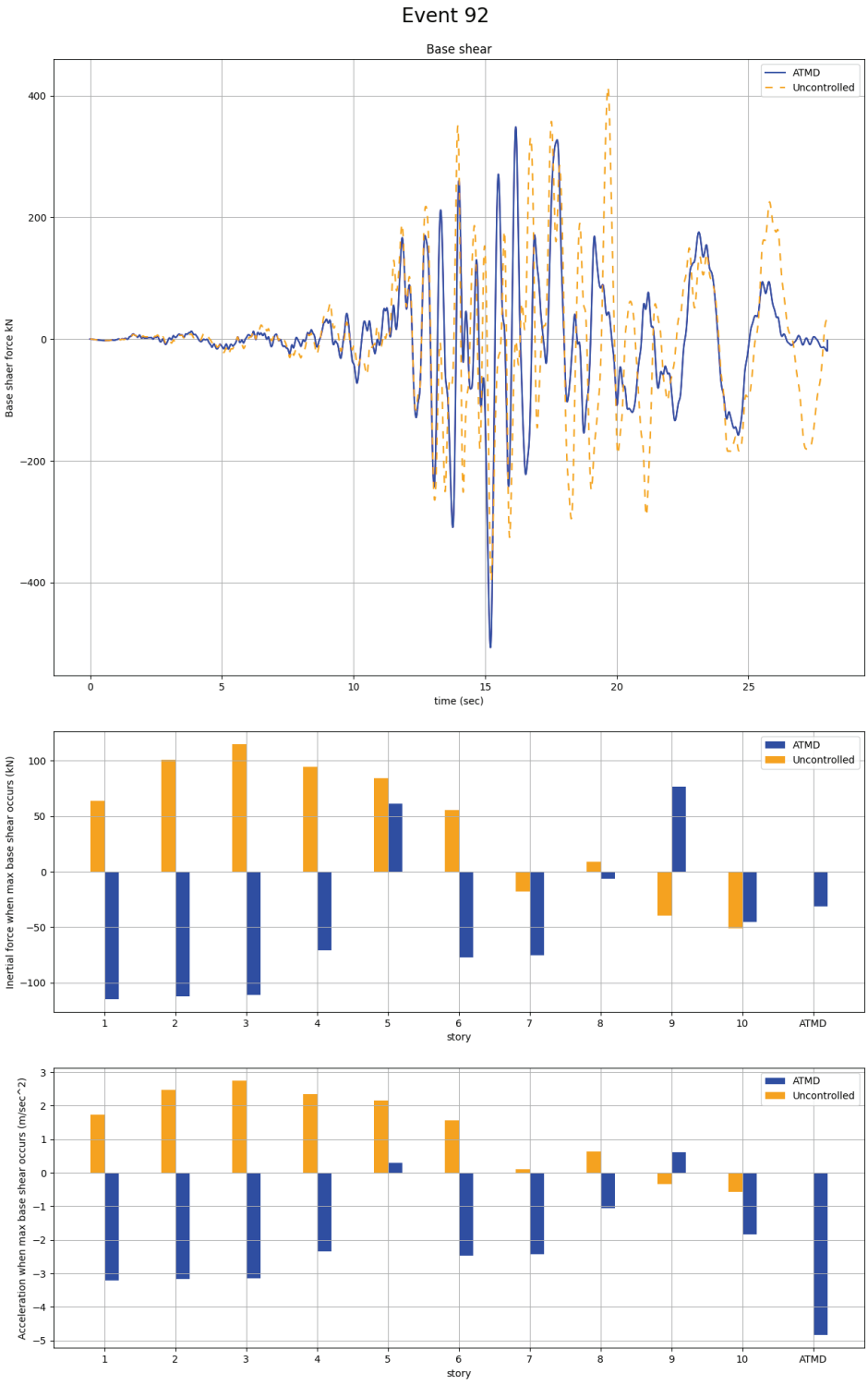

Figure 5.7 Base shaer time history for ATMD and uncontrolled structure

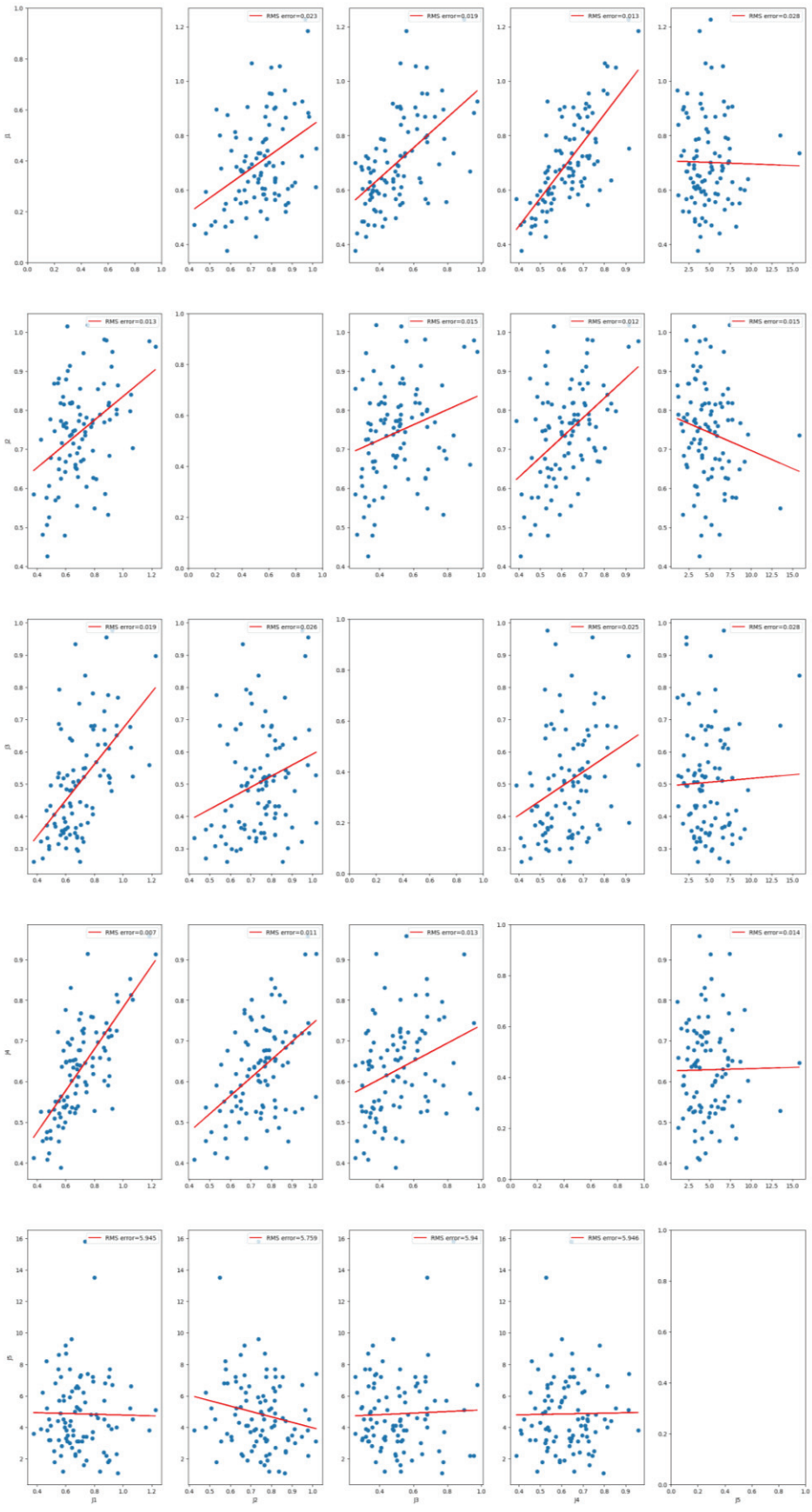

Figure 5.8 Linear regression of the relation among performance indices

In this case, the high required force by LQR-ATMD can go beyond the acceptable 5% range of the structural weight. Such a high demand cannot be applied in a real situation. A change in the value of the gains is proposed to decrease the demand in this linear case.

The reduced damping model is proposed to decrease the force demand. This method relocates the poles generated by the LQR by changing only the damping ratio and getting the new poles' gain values. Figure 5.9 show poles locations of LQR-ATMD under gain values in Table 5.2 and Table 5.3 and present the new poles obtained by reducing the modal damping ratios to their half value in the first two modes. Original and reduced gains values are presented in Table 5.4 and Table 5.5, respectively.

Table 5.4 Linear case drift-coordinate gain values for normal and reduced ATMD

#	ATMD	Reduced ATMD	#	ATMD	Reduced ATMD
$\bar{x}_{11}$	10448.67	10448.67	$\dot{\bar{x}}_{11}$	44950.78	17804.66
$\bar{x}_{10}$	-6939171.31	-2484214.62	$\dot{\bar{x}}_{10}$	-472825.26	-254110.04
$\bar{x}_{9}$	46304.81	871100.16	$\dot{\bar{x}}_{9}$	-388677.06	-26539.49
$\bar{x}_{8}$	-3053987.54	-2468359.94	$\dot{\bar{x}}_{8}$	-276563.79	-142406.52
$\bar{x}_{7}$	-2032319.15	-1954019.28	$\dot{\bar{x}}_{7}$	-50415.48	17923.88
$\bar{x}_{6}$	-791488.60	-423399.09	$\dot{\bar{x}}_{6}$	62031.40	129087.27
$\bar{x}_{5}$	-1909911	-1219461.06	$\dot{\bar{x}}_{5}$	148261.32	128200.44
$\bar{x}_{4}$	-1317616.15	-1070967.65	$\dot{\bar{x}}_{4}$	268104.95	153397.79
$\bar{x}_{3}$	86106.59	213496.08	$\dot{\bar{x}}_{3}$	340494.27	195155.08
$\bar{x}_{2}$	565367.96	1411572.53	$\dot{\bar{x}}_{2}$	331162.20	216264.68
$\bar{x}_{1}$	122452.41	1836069.08	$\dot{\bar{x}}_{1}$	292287.34	214655.10

Table 5.5 Linear case displacement-coordinate gain values for normal and reduced ATMD

#	ATMD	Reduced ATMD	#	ATMD	Reduced ATMD
x_{11}	10448.67	10448.67	$\dot{x}_{11}$	44950.78	17804.66
x_{10}	-6949619.98	-2494663.30	$\dot{x}_{10}$	-517776.05	-271914.71
x_{9}	6985476.12	3355314.79	$\dot{x}_{9}$	84148.19	227570.55
x_{8}	-3100292.35	-3339460.11	$\dot{x}_{8}$	112113.27	-115867.03
x_{7}	1021668.39	514340.66	$\dot{x}_{7}$	226148.31	160330.41
x_{6}	1240830.54	1530620.19	$\dot{x}_{6}$	112446.89	111163.38
x_{5}	-1118422.39	-796061.97	$\dot{x}_{5}$	86229.91	-886.82
x_{4}	592294.84	148493.40	$\dot{x}_{4}$	119843.63	25197.35
x_{3}	1403722.75	1284463.74	$\dot{x}_{3}$	72389.31	41757.28
x_{2}	479261.36	1198076.44	$\dot{x}_{2}$	-9332.06	21109.60
x_{1}	-442915.54	424496.54	$\dot{x}_{1}$	-38874.85	-1609.57

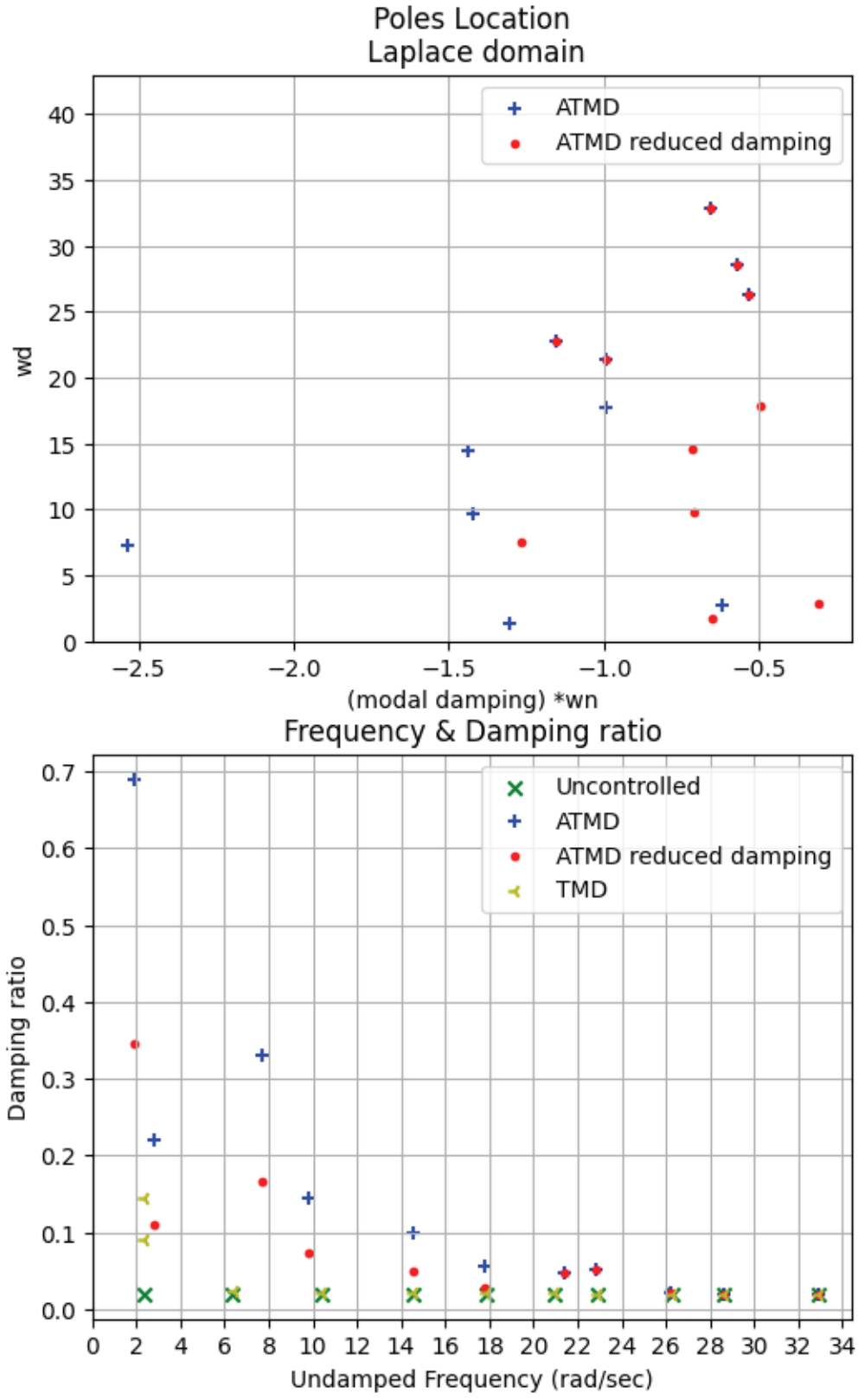

Figure 5.9 Poles location and associated details for different controlled system

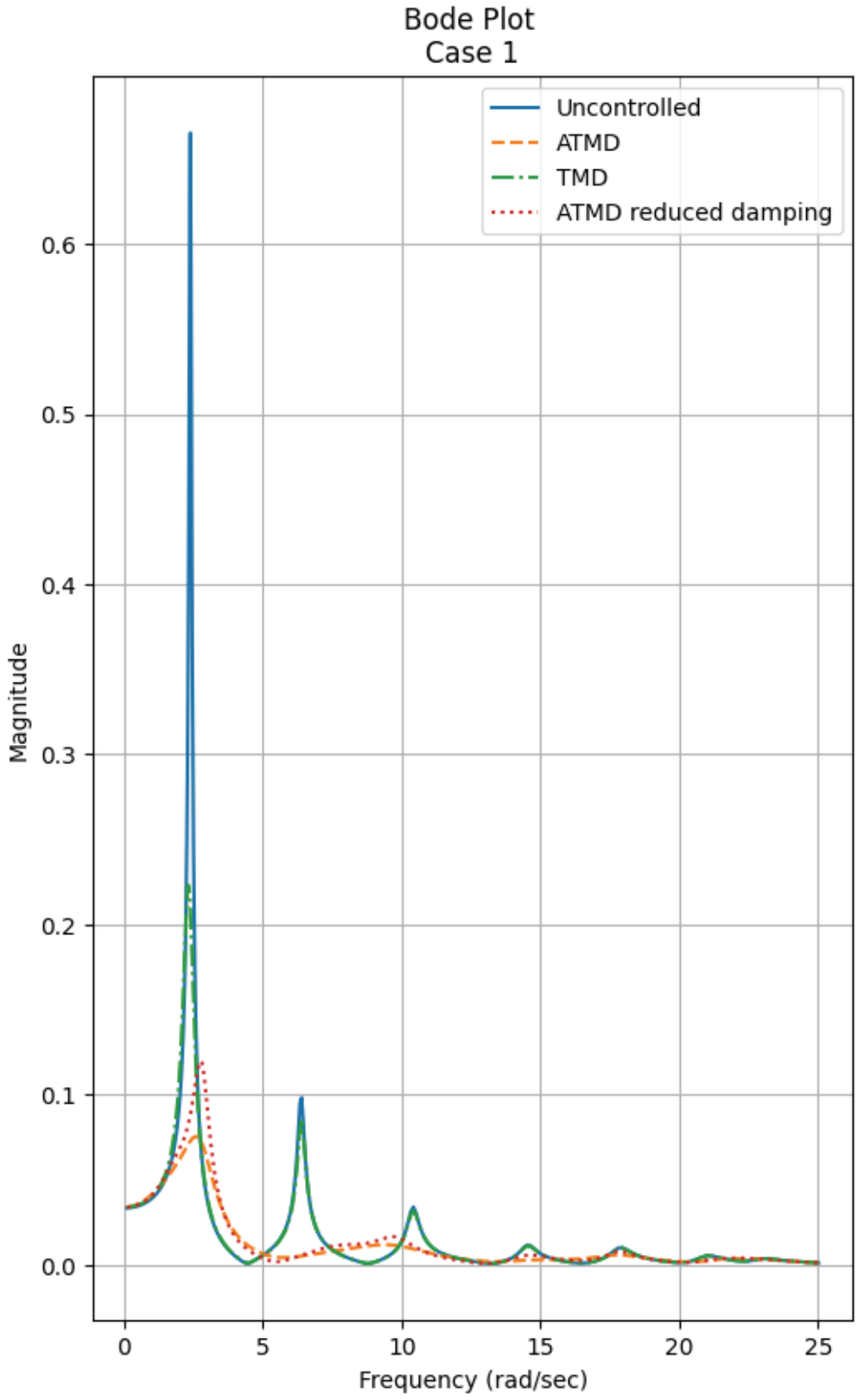

Figure 5.10 Bode plot for different controlled system

The bode plot of the reduced ATMD damping and other models are plotted in Figure 5.10. The difference lies in the first peak in the region of the first mode, and it is not much different. The effect on the response is presented in Figure 5.11, and it is clear that the J5 index changed just slightly. In contrast, other indices indicate a worse performance.

The reduced damping model did not achieve acceptable performance in general, so a combination between LQR-ATMD and the reduced damping model is proposed. The partially reduced model combines two sets of gains values: the first is related to LQR-ATMD, and the second is related to the reduced damping model. A force limit will be used to shift from the first set to the second for n time steps before shifting back to the first set. Suppose the calculated force by (3.21) is higher than the provided limit. In that case, the system will shift to the gains set from reduced damping models for n time steps.

The Partially Reduced model is a semi-linear method. If the force exceeds the specified limit, the force will be recalculated based on different gain values. The recalculated force may be higher than the limit. For example, suppose the limit is 10 kN, and the calculated force is 70. The force recalculation gives 30 kN. The force to be applied is 30 kN which is higher than the limit. In other words, the first force is limited, and the second is not.

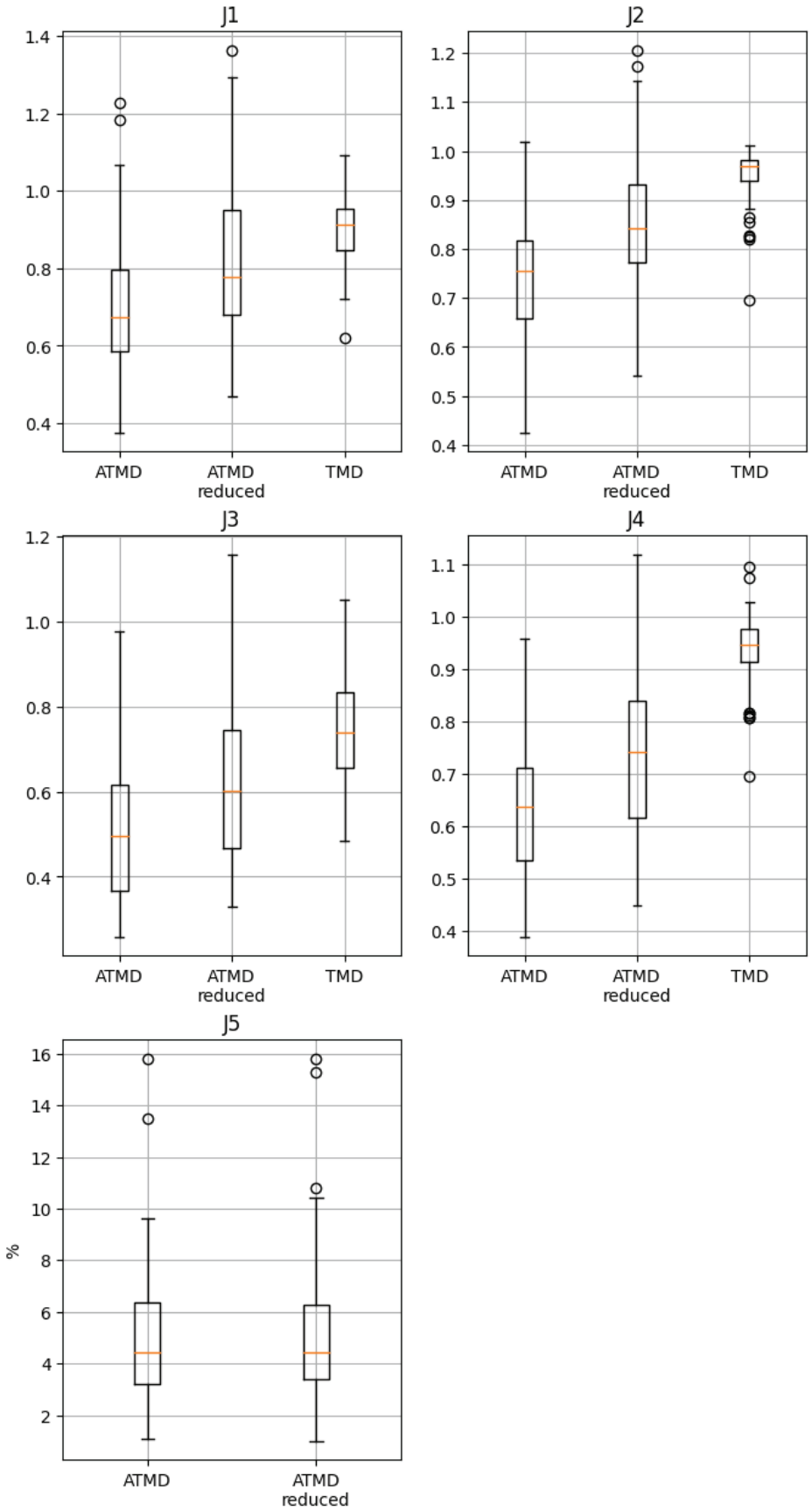

Figure 5.11 Performance indices of LQR-ATMD, reduced ATMD, TMD controlled structure

Figure 5.12 shows the result of the partially reduced damping model (n=10 & limit=245 kN) against other models. The partial model performs better than the original unreduced model, decreasing the demand slightly while keeping the first four indices nearly unchanged.

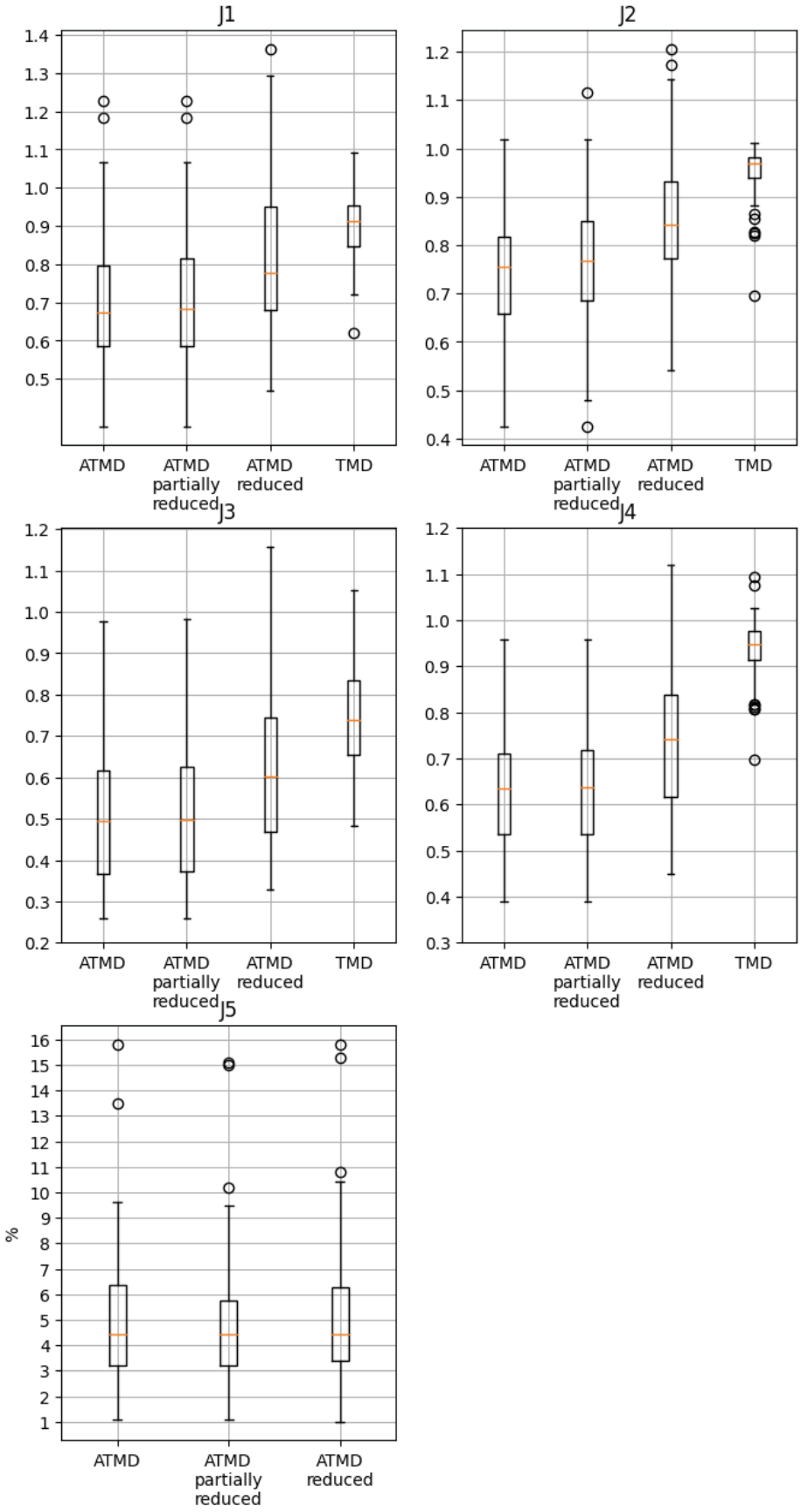

Figure 5.12 Performance indices of LQR-ATMD, reduced ATMD, partially reduced ATMD, TMD controlled structure

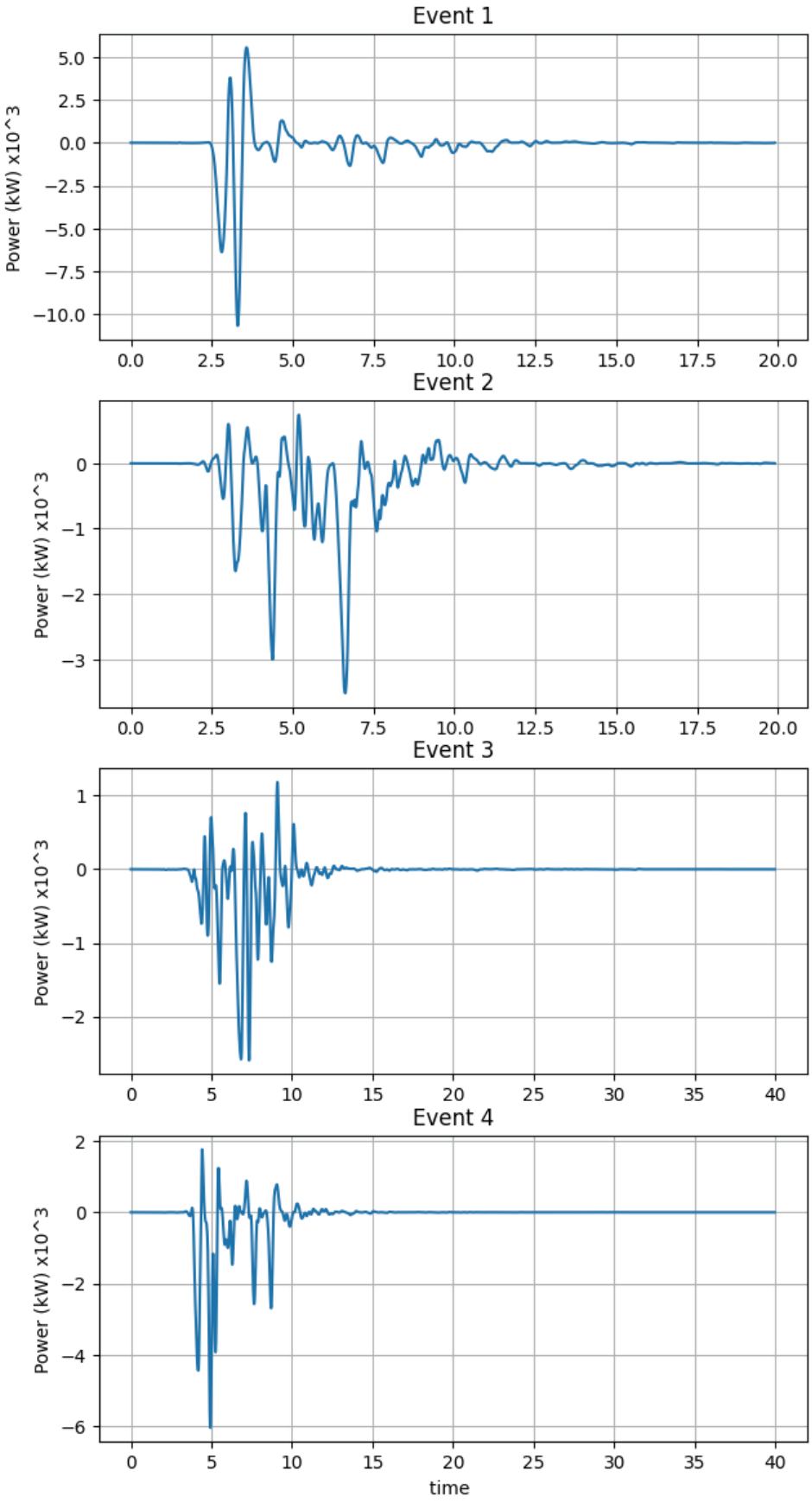

Figure 5.13 Power requirements for several events

5.2. Nonlinear Case

The only difference from the linaer case is the upper limit on the control force during the simulations. As a result, the optimization algorithm obtained a different feedback controller. The optimization result is presented in Table 5.6, and associated drift gains obtained by LQR design are presented in Table 5.7. Table 5.8 introduces the transformed displacement gain values from drift gain values using (3.28). As the system is nonlinear under the force limitation, the characteristics of this system under the given gain values can not be obtained. A way around that, however, is to linearize the system by removing the limit on the force.

The linearized system characteristics against TMD and uncontrolled structure are presented in Figure 5.14. In contrast with case 1 presented in Figure 5.1, there is a change in natural frequencies and modal dampings, and the relation between the frequency and effect of ATMD is not True.

A comparison between ATMD in the linear case and linearized ATMD in the current case is presented in Figure 5.15. The bode plot of the linear case is clearly better than case 2, and that can be returned to the different natural frequencies and modal dampings.

Table 5.6 Nonlinear case optimization variable result

q_{11}	1
q_{10}	1279046.44
q_9	4310468.71
q_8	6184.12004
q_7	25712.6606
q_6	172.459522
q_5	23047.0234
q_4	15627.8109
q_3	180284.54
q_2	80799.563
q_1	115021.004

Table 5.7 Nonlinear case drift-coordinate gain values

$\bar{x}_{11}$	10448.67	$\dot{\bar{x}}_{11}$	44950.78
$\bar{x}_{10}$	-6939171.31	$\dot{\bar{x}}_{10}$	-472825.26
$\bar{x}_{9}$	46304.81	$\dot{\bar{x}}_{9}$	-388677.06
$\bar{x}_{8}$	-3053987.54	$\dot{\bar{x}}_{8}$	-276563.79
$\bar{x}_{7}$	-2032319.15	$\dot{\bar{x}}_{7}$	-50415.48
$\bar{x}_{6}$	-791488.60	$\dot{\bar{x}}_{6}$	62031.40
$\bar{x}_{5}$	-1909911	$\dot{\bar{x}}_{5}$	148261.32
$\bar{x}_{4}$	-1317616.15	$\dot{\bar{x}}_{4}$	268104.95
$\bar{x}_{3}$	86106.59	$\dot{\bar{x}}_{3}$	340494.27
$\bar{x}_{2}$	565367.96	$\dot{\bar{x}}_{2}$	331162.20
$\bar{x}_{1}$	122452.41	$\dot{\bar{x}}_{1}$	292287.34

Table 5.8 Nonlinear case displacement-coordinate gain values

x_{11}	10448.67	$\dot{x}_{11}$	44950.78
x_{10}	-6949619.98	$\dot{x}_{10}$	-517776.05
x_{9}	6985476.12	$\dot{x}_{9}$	84148.19
x_{8}	-3100292.35	$\dot{x}_{8}$	112113.27
x_{7}	1021668.39	$\dot{x}_{7}$	226148.31
x_{6}	1240830.54	$\dot{x}_{6}$	112446.89
x_{5}	-1118422.39	$\dot{x}_{5}$	86229.91
x_{4}	592294.84	$\dot{x}_{4}$	119843.63
x_{3}	1403722.75	$\dot{x}_{3}$	72389.31
x_{2}	479261.36	$\dot{x}_{2}$	-9332.06
x_{1}	-442915.54	$\dot{x}_{1}$	-38874.85

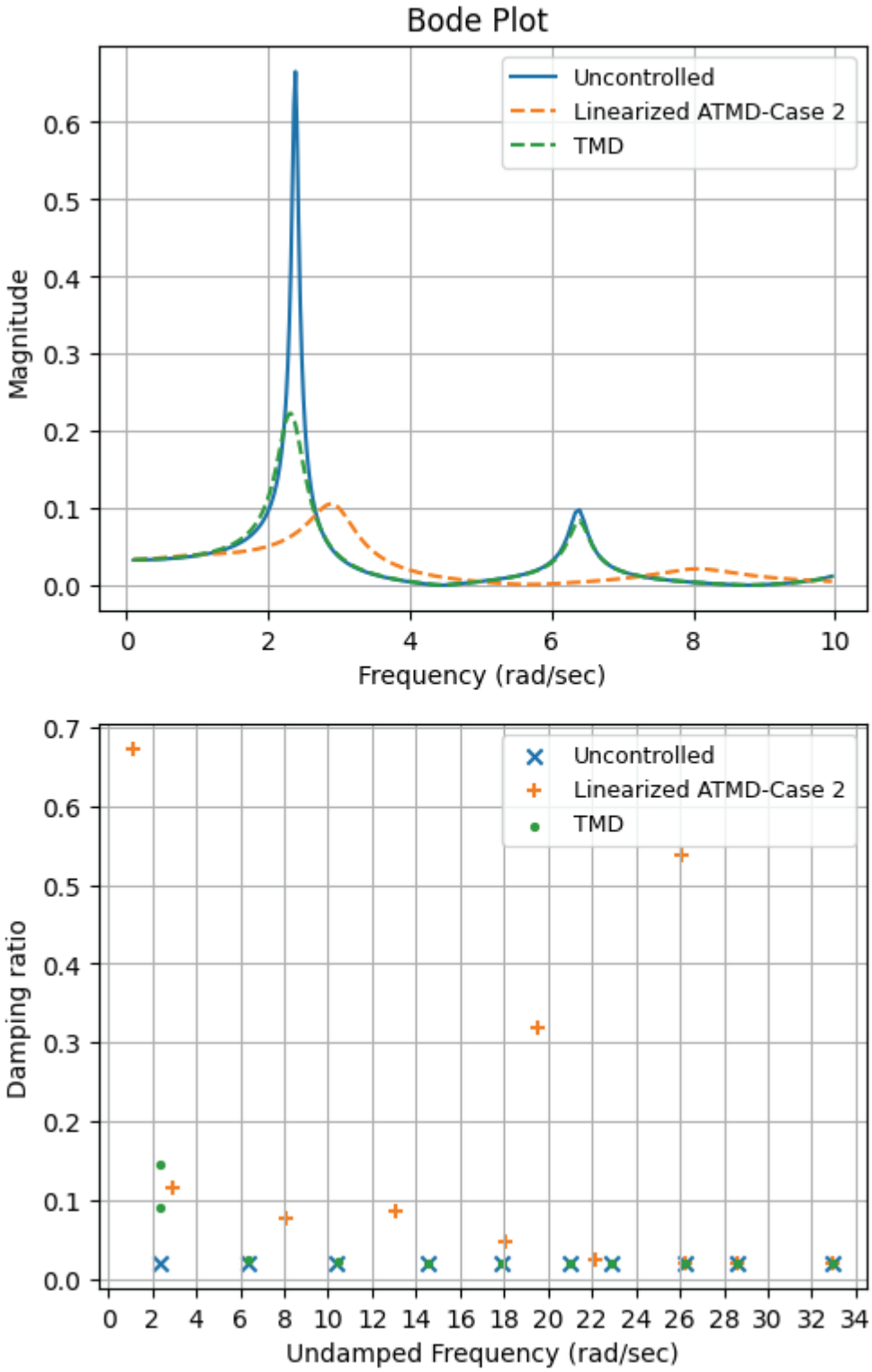

Figure 5.14 Characteristics of linearized ATMD, TMD and uncontrolled structure

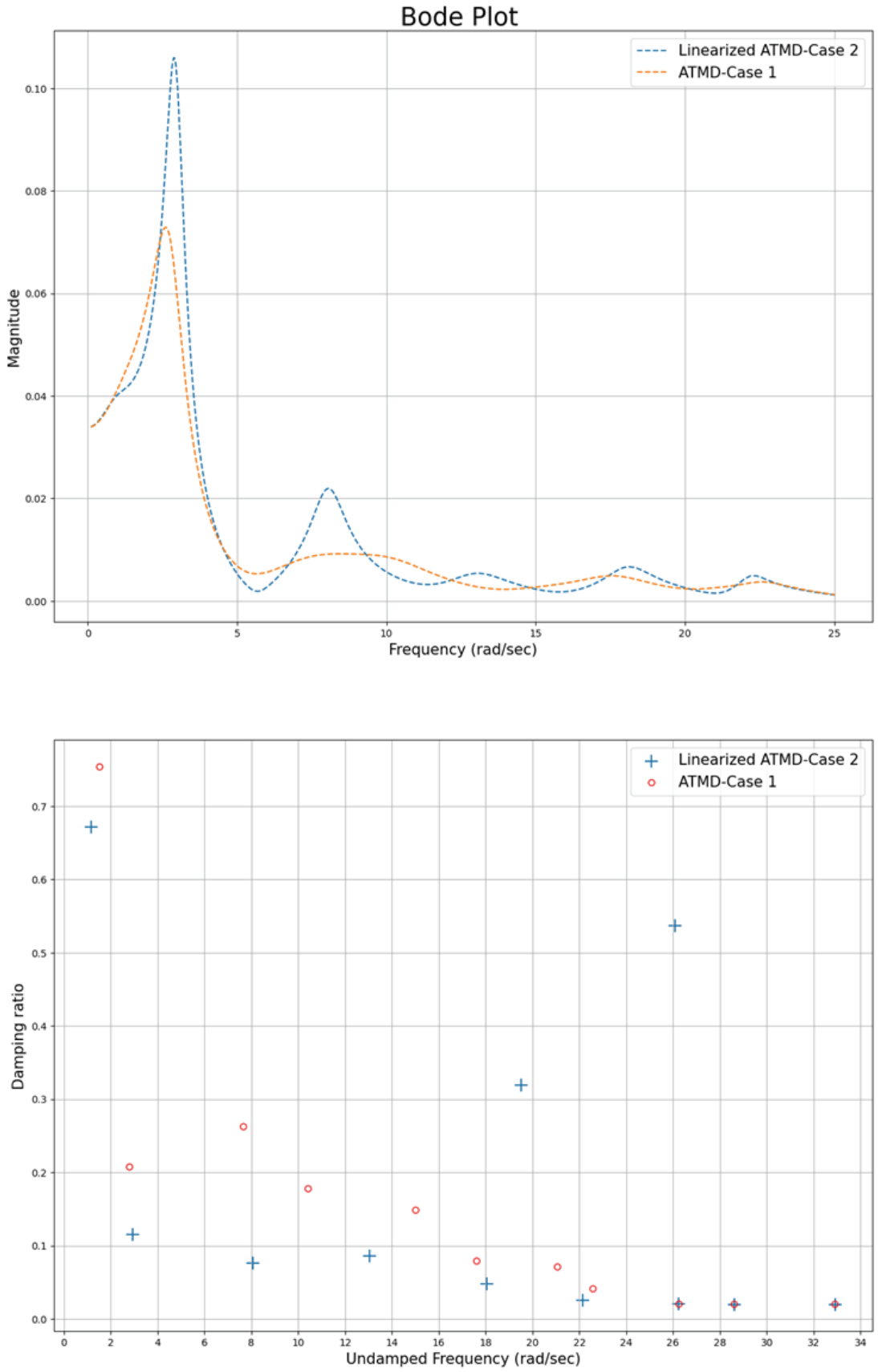

Figure 5.15 Comparison between linear case and nonlinear case characteristics

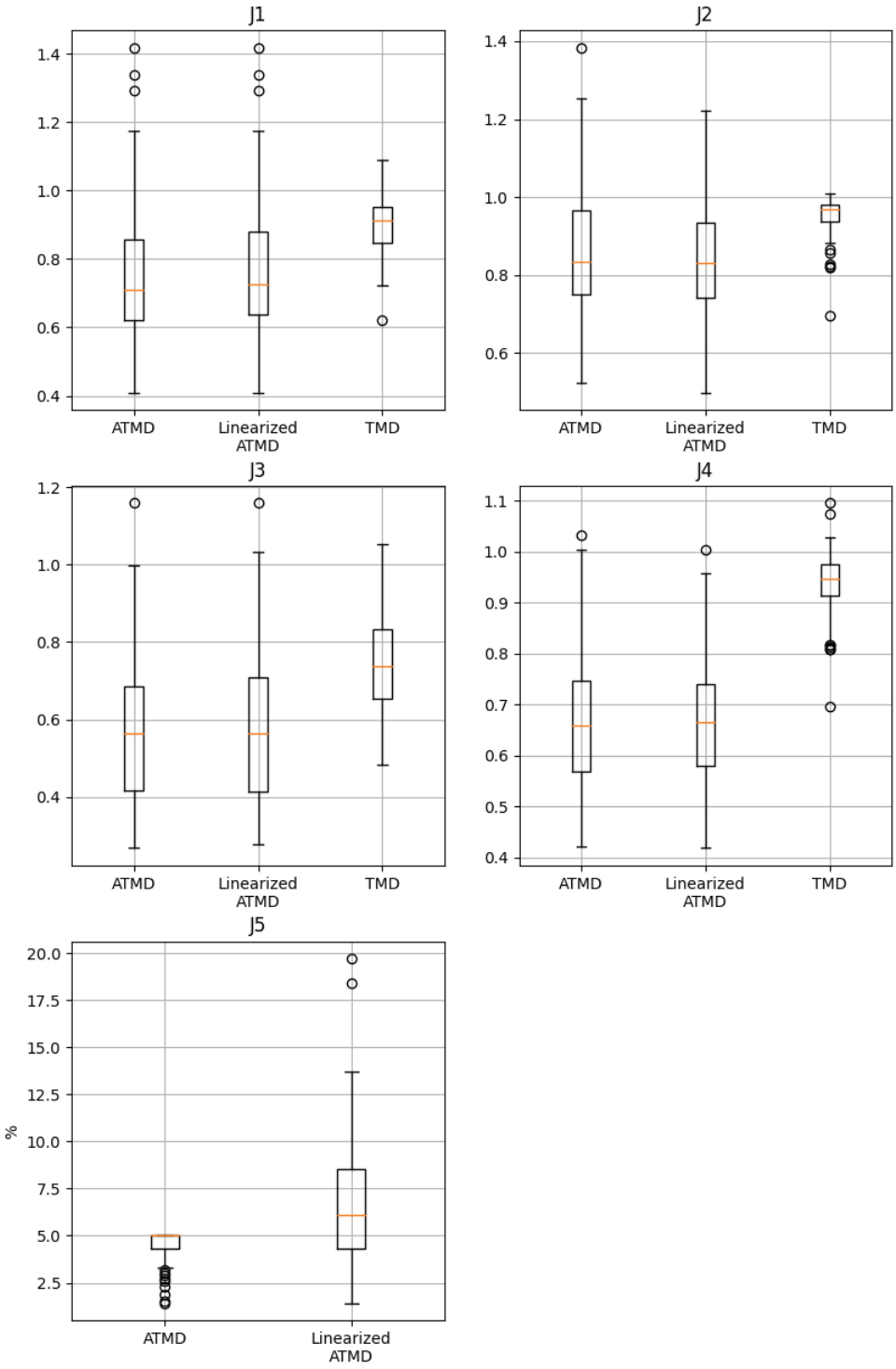

Figure 5.16 Performance indices of ATMD, linearized ATMD and TMD controlled structure

Figure 5.16 presents the performance indices of this case system and TMD. The findings about indices J1 to J4 in Figure 5.2 are also valid for case 2, while J5 differs. The findings indicated that ATMD outperforms the TMD in drift and normalized displacement reduction. However, both are not as efficient in reducing base shear as in reducing drift. It is worth noting that the increment in the base shear force does not occur in the record that has been used in the optimization.

Figure 5.17 presents portions of control forces' time histories for several events. Graphs (a) to (f) shed light on the problems of the limited force design, while graph (g) represents a case where the required force never passes the limit.

The first problem is the saturation. It is normal to have saturation in control algorithms. However, the saturations in graphs are prolonged in time, making it hard to implement. For instance, a massive amount of fluid is needed in a hydraulic actuator system to provide prolonged saturation, which is impractical.

The second problem is a high fluctuation in force between positive and negative maximum force values in a short time. The problem with this issue is that it is impossible to implement.

The third problem is turning the controller into a bang-bang type controller, where the force in that controller has only two values, either positive or negative maximum force.

The second and third problem is presented clearly in Figure 5.18. The second problem is presented in graph (a) and its FFT in graph (b), while the third problem is presented in graph (c) and its FFT in graph (d). Overall, as long as the force is smaller than the specified limit, the control force is applicable and provides a good response. In contrast, if the force reaches the limit, the control force is probably not applicable, and the generated response is not trusted.

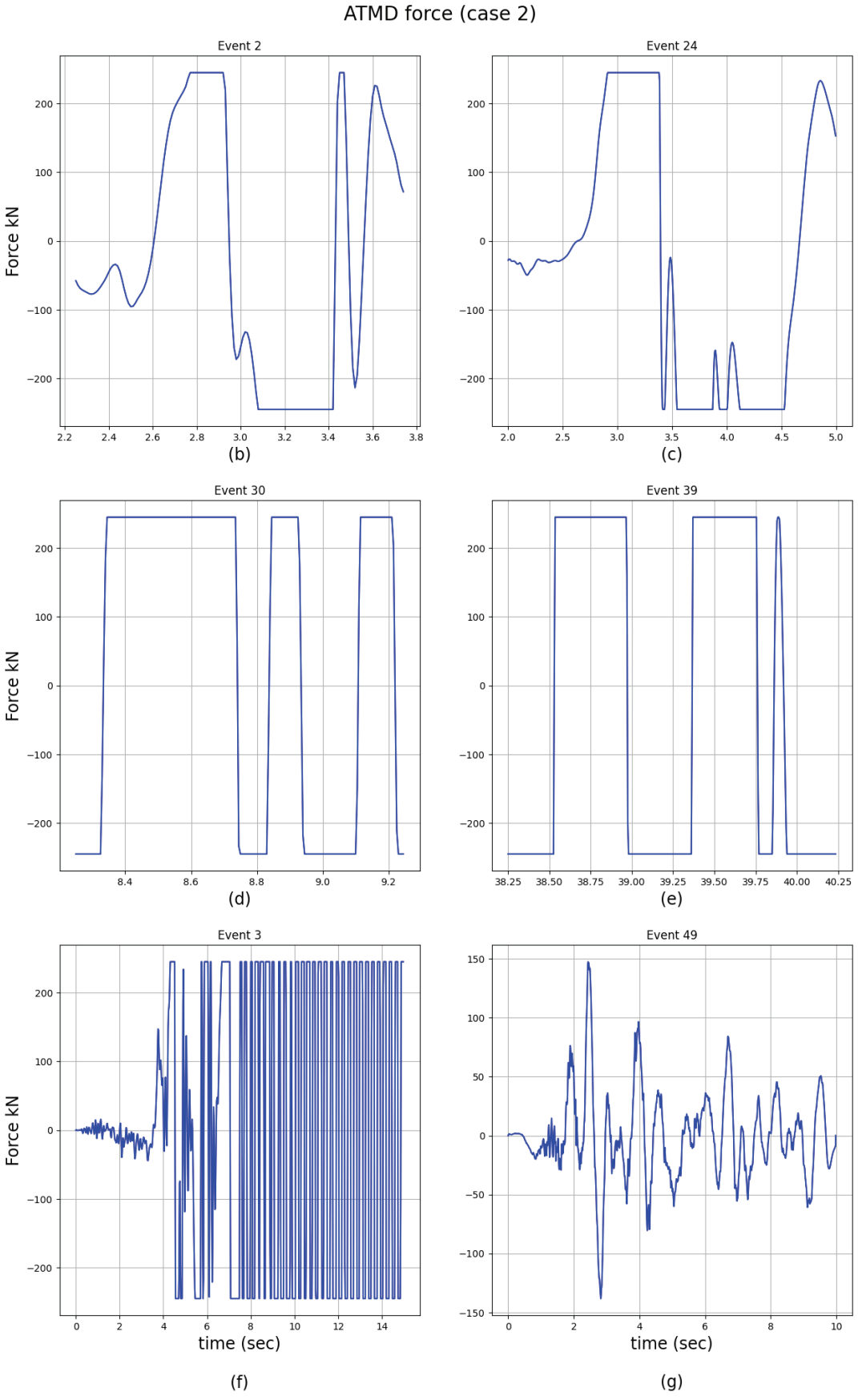

Figure 5.17 ATMD forces for several events

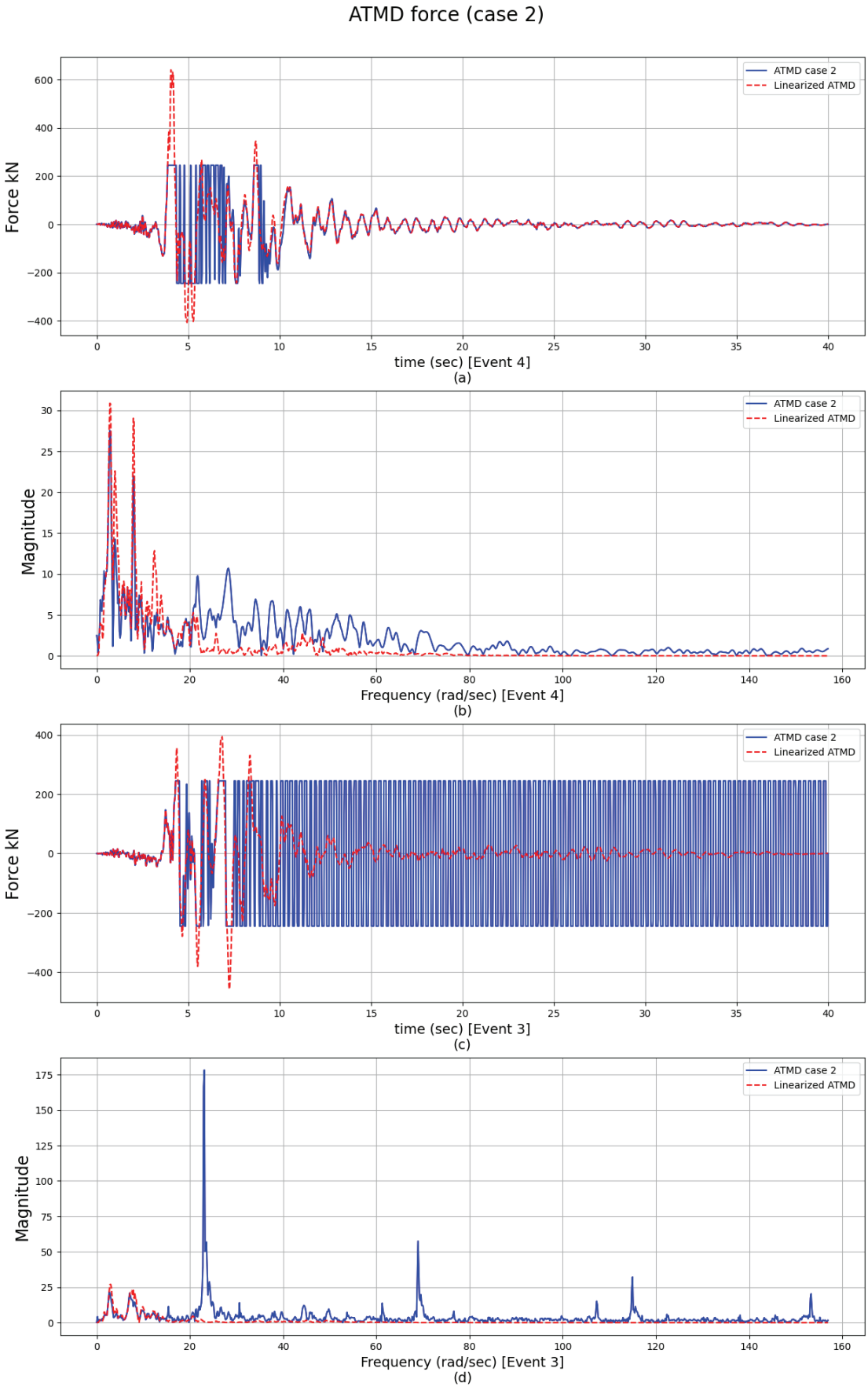

Figure 5.18 Time history and spectrum of the control force for different models

There are additional observations regarding saturation where Figure 5.19 demonstrate it. The first observation is the alignment in the forces after the main shock for both linearized and normal ATMD.

The second observation is clear in graph (e), where the ATMD saturation starts and ends when the linearized ATMD passes the limit with some delay. In graphs (a) to (d), it is clear for the first peak. This observation is not common and not clear as the first one.

Figure 5.20 presents the frequency response magnitude of forces time histories shown in Figure 5.19. There is a noise with a frequency higher than 20 rad/sec, while there is a high-frequency pulse in other cases. A different filter approach has been made to eliminate the problem.

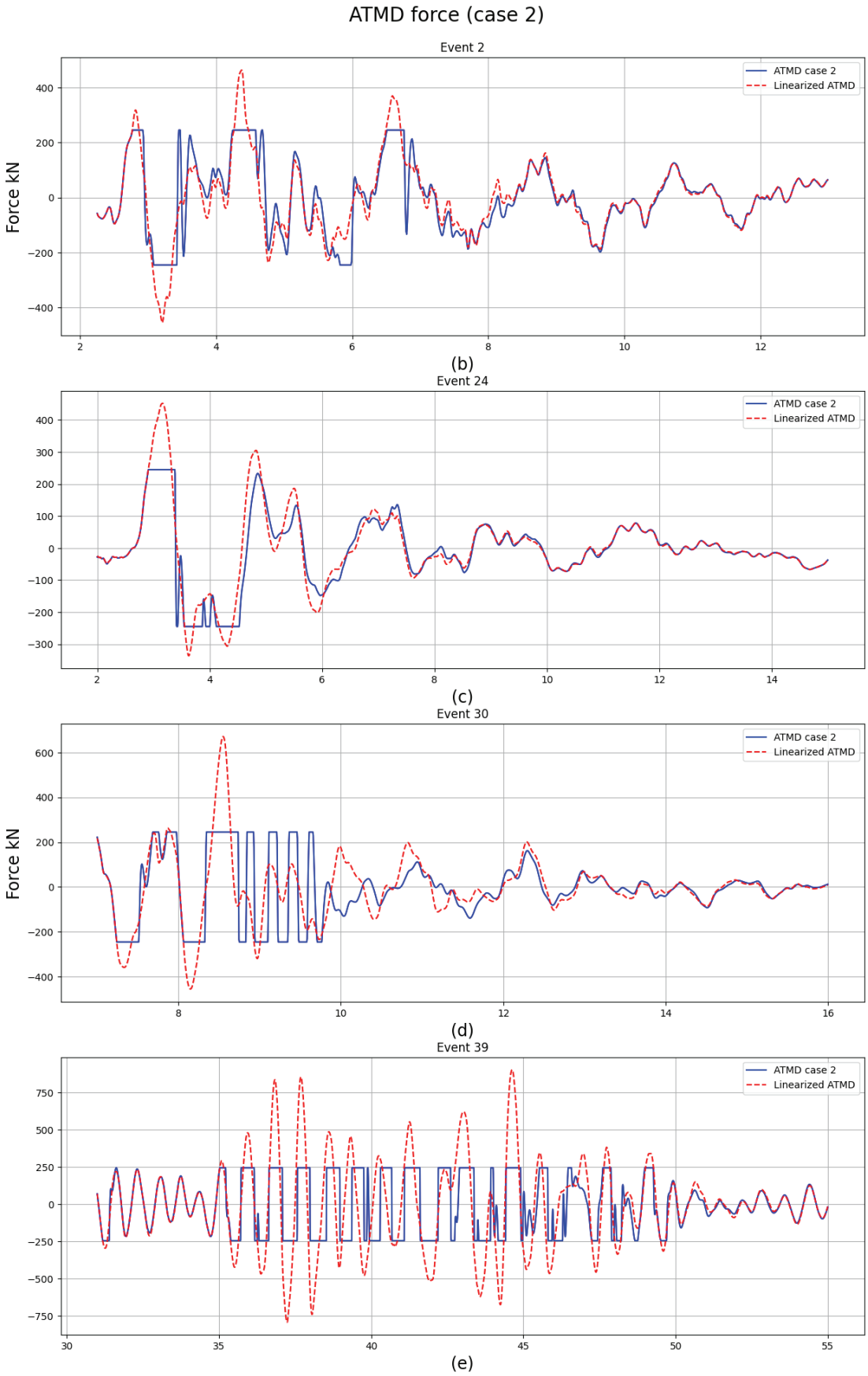

Figure 5.19 Force time histories for linierized ATMD and ATMD of several event

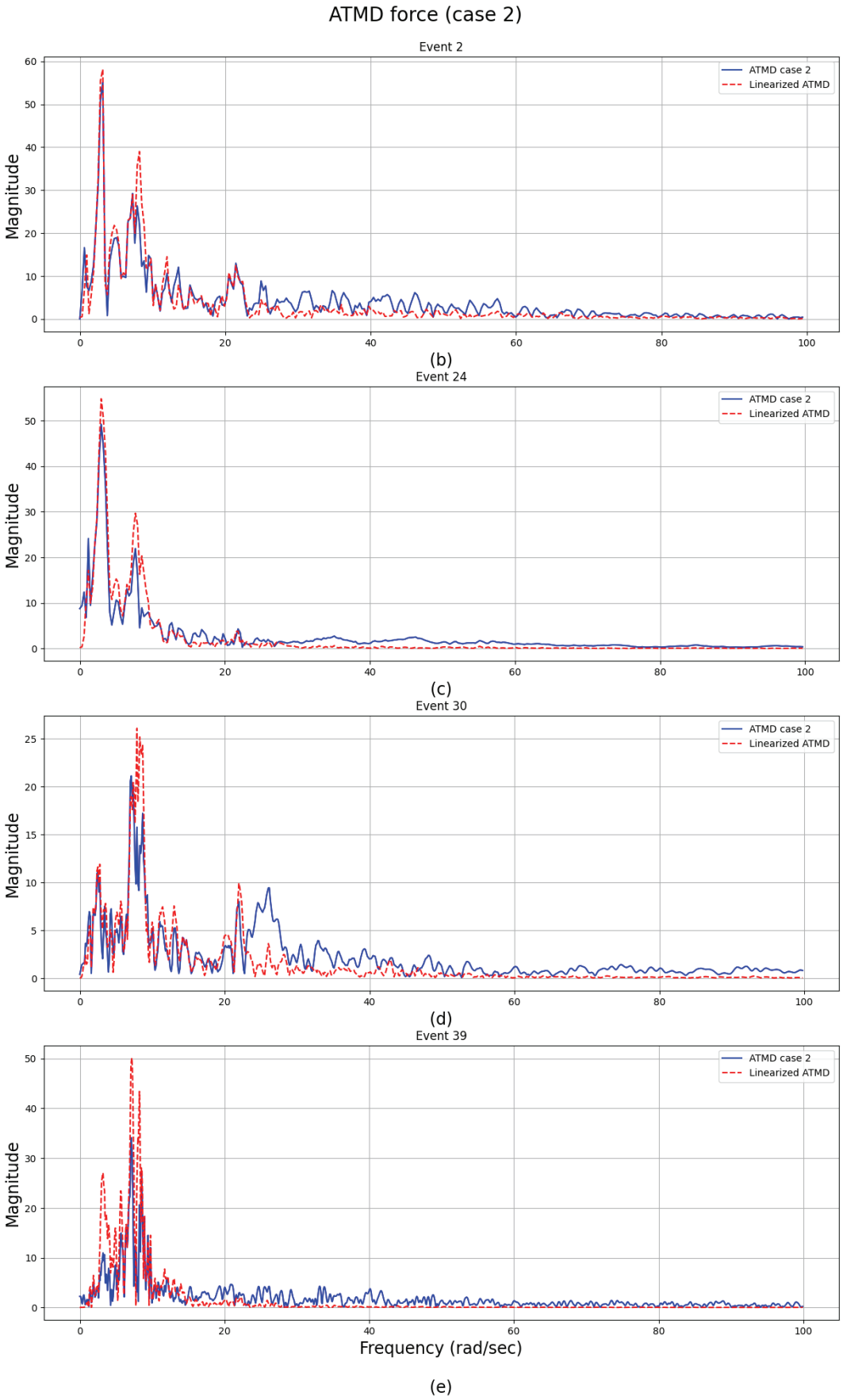

Figure 5.20 FFT of force time histories for several events

A low-pass filter was deployed using four characteristics set presented in Table 5.9, all the cases are FIR-type filters. The filters here are limited input and limited output type unless otherwise indicated. The limited input means that whatever the output of the filter is, it must not exceed the limit force. The limit force must be applied in case of exceedance, not the filter's output. The limited input means the maximum force should be fed into the filter must not exceed the limit force. If the input has a larger magnitude than the limit force, the limit force will be fed to the filter.

Table 5.9 FIR low pass filters characteristics

Case	Stop-band (rad/sec)	Order
#1	20	4
#2	20	25
#3	50	4
#4	50	20

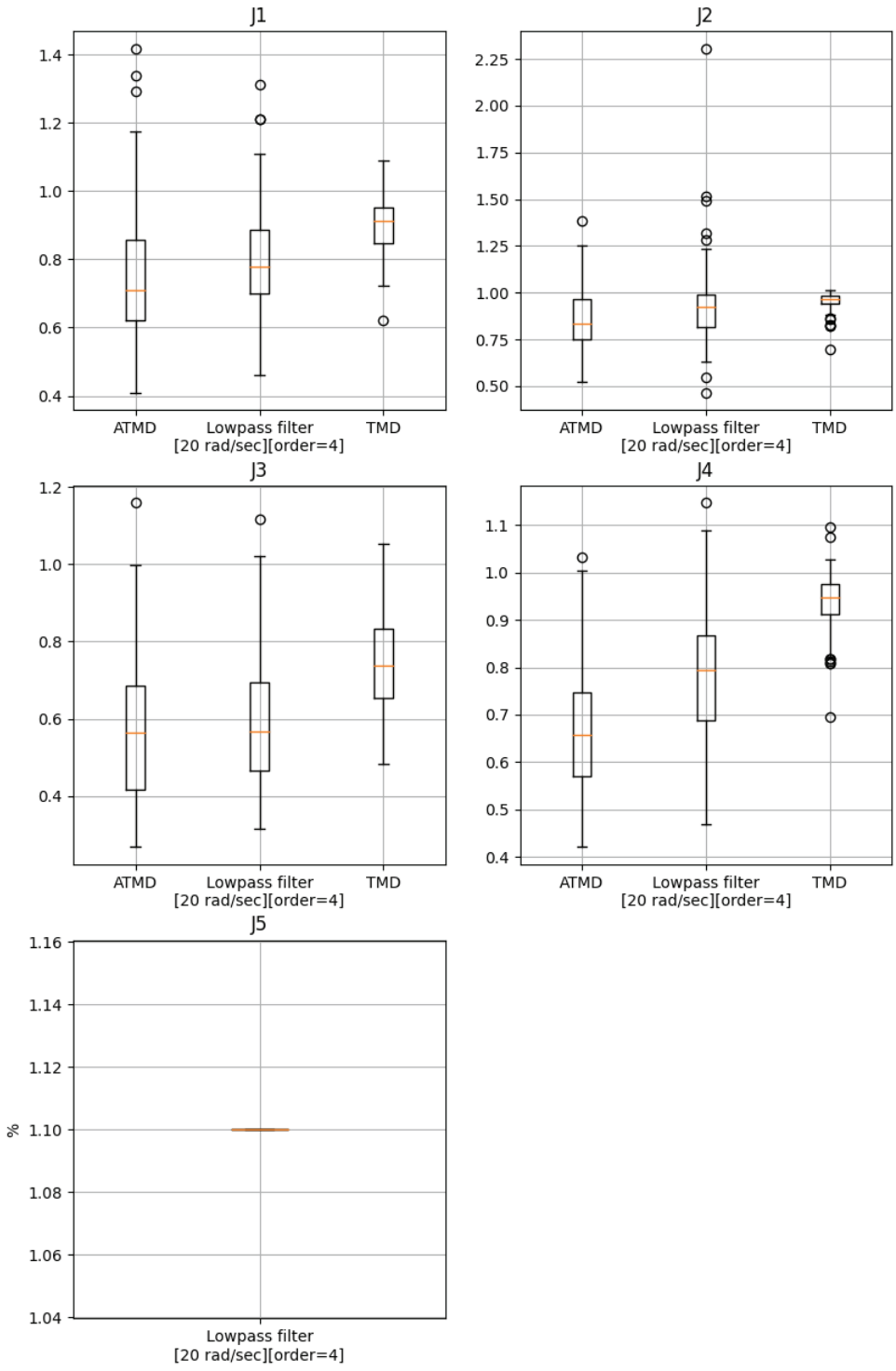

Figure 5.21 Low pass filter case #1 results

The results of the first trial are shown in Figure 5.21.The indices J1 to J4 show good values compared to the original ATMD, with a constant force of 1.1% for all events. However, the force-time histories in Figure 5.22 indicate that the bang bang now is happening at the 1.1% force limit rather than the 5% force limit, which means this filter is worsening the quality of the controller.

The result of removing the limit on the input is presented in Figure 5.23. The difference between a filter with a limit on the input and a filter without a limit on the input is the point at which the bang-bang action starts.

The transfer function of the filter displayed in Figure 5.22 and Figure 5.23 is presented in (5.1)

$$H(z) = 0.01 + 0.09625\, z^{-1} + 0.09625\, z^{-2} + 0.01\, z^{-3} \qquad (5.1)$$

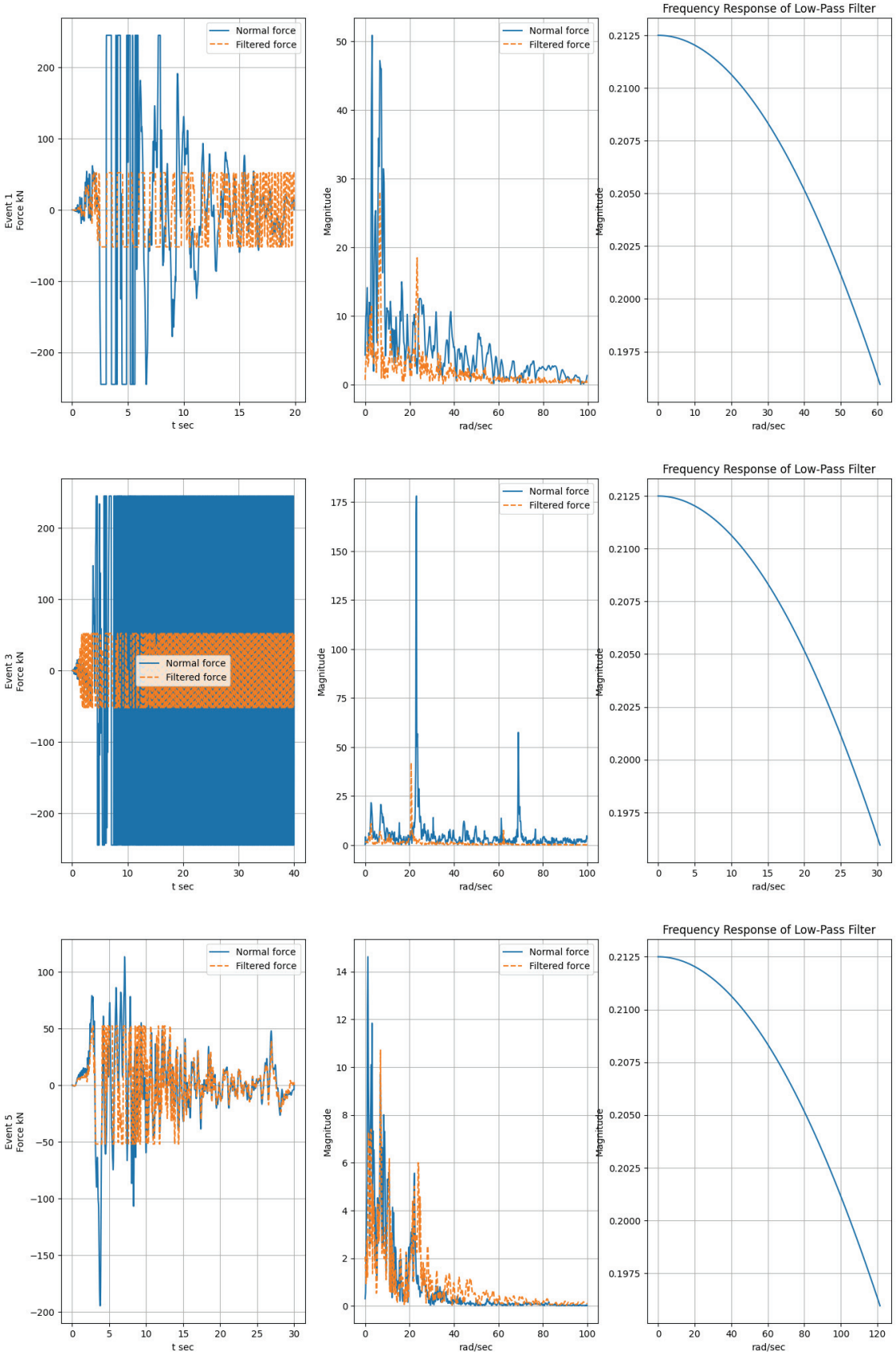

Figure 5.22 Events results under limited input case #1 filter

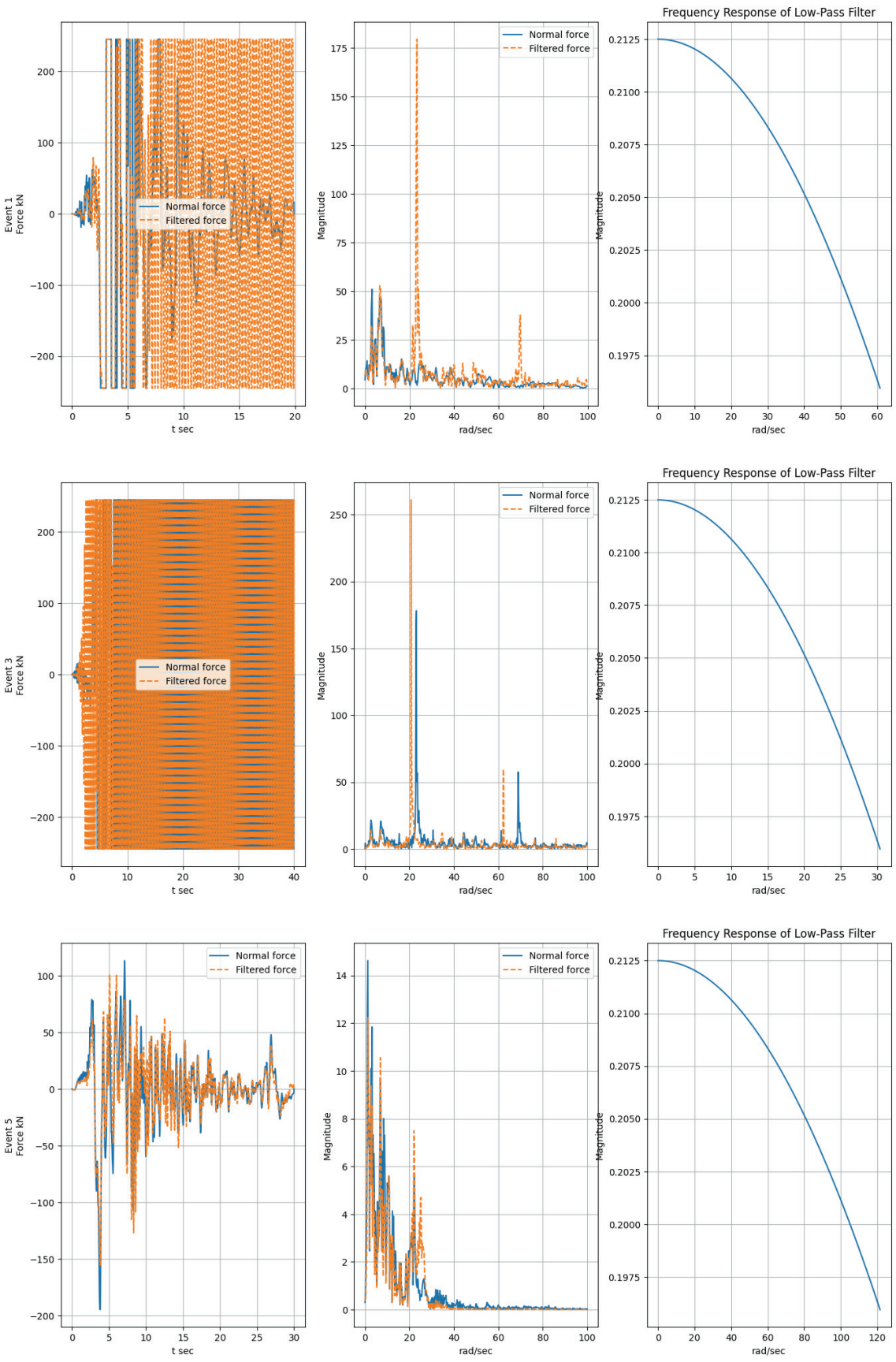

Figure 5.23 Events results under unlimited input case #1 filter

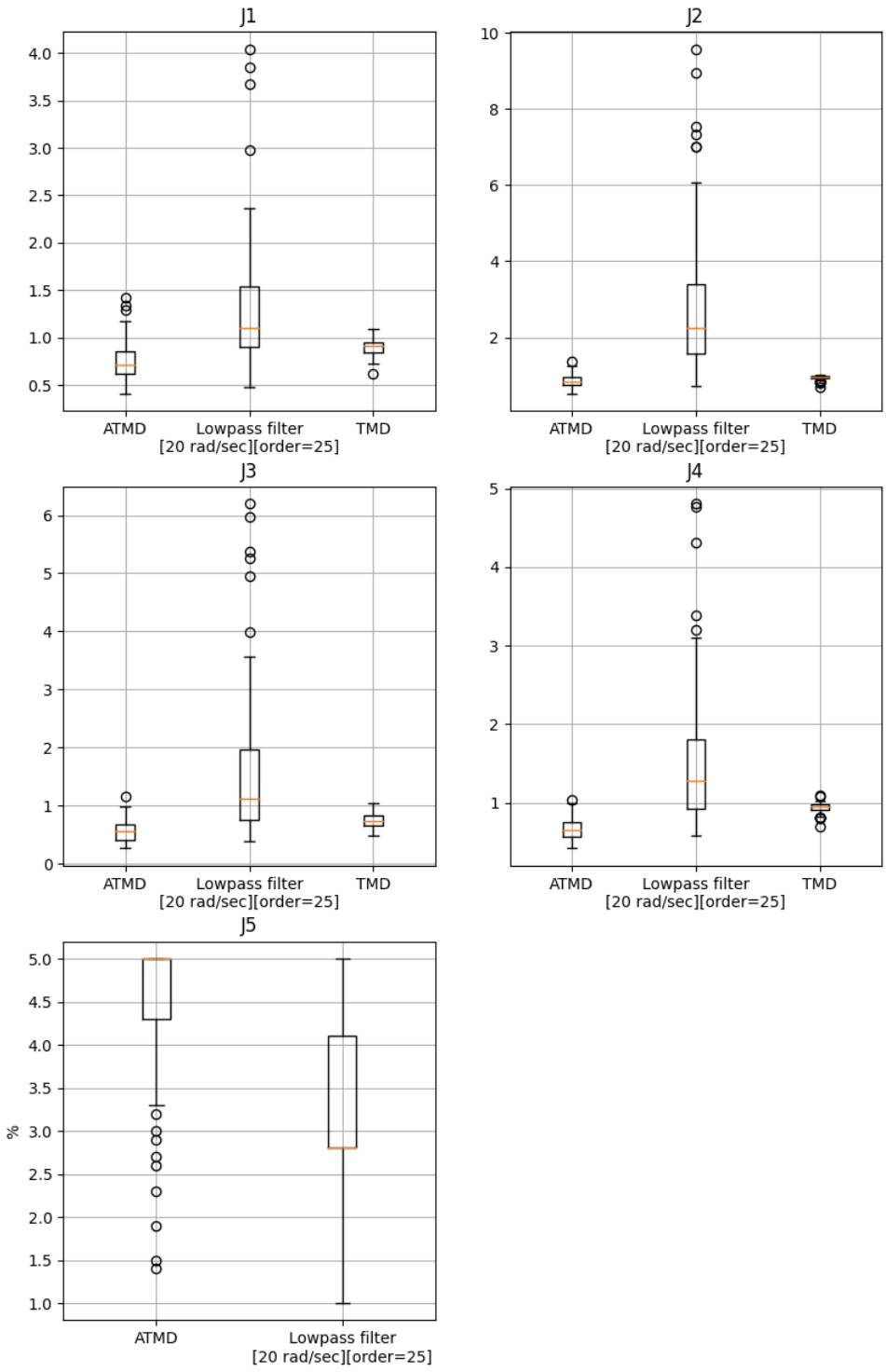

Figure 5.24 Low pass filter case #2 results

The results of the second trial with limited input are shown in Figure 5.24. The indices J1 to J4 show bad values compared to the original ATMD. The force-time histories and associated frequency response for limited and unlimited input are shown in Figure 5.25 and Figure 5.26, respectively, and both graphs indicate that the filters are amplifying the force signal, which causes the bang-bang action. The filter coefficients are presented in Table 5.10.

Table 5.10 Case 2 filter coefficients

Filter coefficient	Event 1	Event 3	Event 16
Z^{0}	0.00044	-0.00187	0.00221
Z^{-1}	0.00124	-0.00288	0.0029
Z^{-2}	0.00298	-0.00449	0.00467
Z^{-3}	0.0063	-0.00581	0.00761
Z^{-4}	0.01169	-0.00484	0.01169
Z^{-5}	0.01931	0.00096	0.01675
Z^{-6}	0.02893	0.0137	0.02247
Z^{-7}	0.0399	0.03404	0.02846
Z^{-8}	0.05128	0.06049	0.03426
Z^{-9}	0.06188	0.08938	0.0394
Z^{-10}	0.07051	0.11563	0.04342
Z^{-11}	0.07616	0.13402	0.04599
Z^{-12}	0.07812	0.14062	0.04688
Z^{-13}	0.07616	0.13402	0.04599
Z^{-14}	0.07051	0.11563	0.04342
Z^{-15}	0.06188	0.08938	0.0394
Z^{-16}	0.05128	0.06049	0.03426
Z^{-17}	0.0399	0.03404	0.02846
Z^{-18}	0.02893	0.0137	0.02247
Z^{-19}	0.01931	0.00096	0.01675
Z^{-20}	0.01169	-0.00484	0.01169
Z^{-21}	0.0063	-0.00581	0.00761
Z^{-22}	0.00298	-0.00449	0.00467
Z^{-23}	0.00124	-0.00288	0.0029
Z^{-24}	0.00044	-0.00187	0.00221

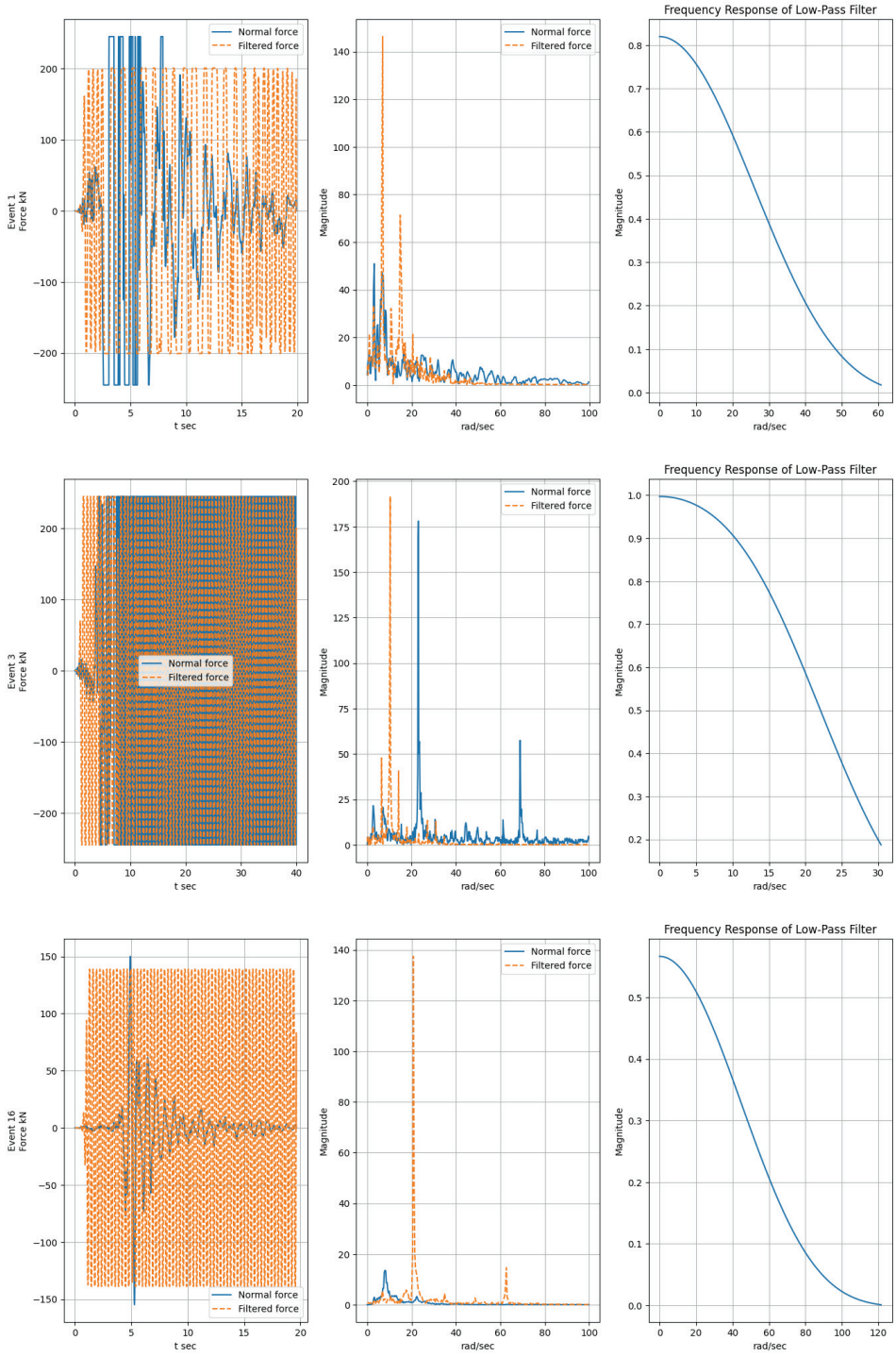

Figure 5.25 Events results under limited input case #2 filter

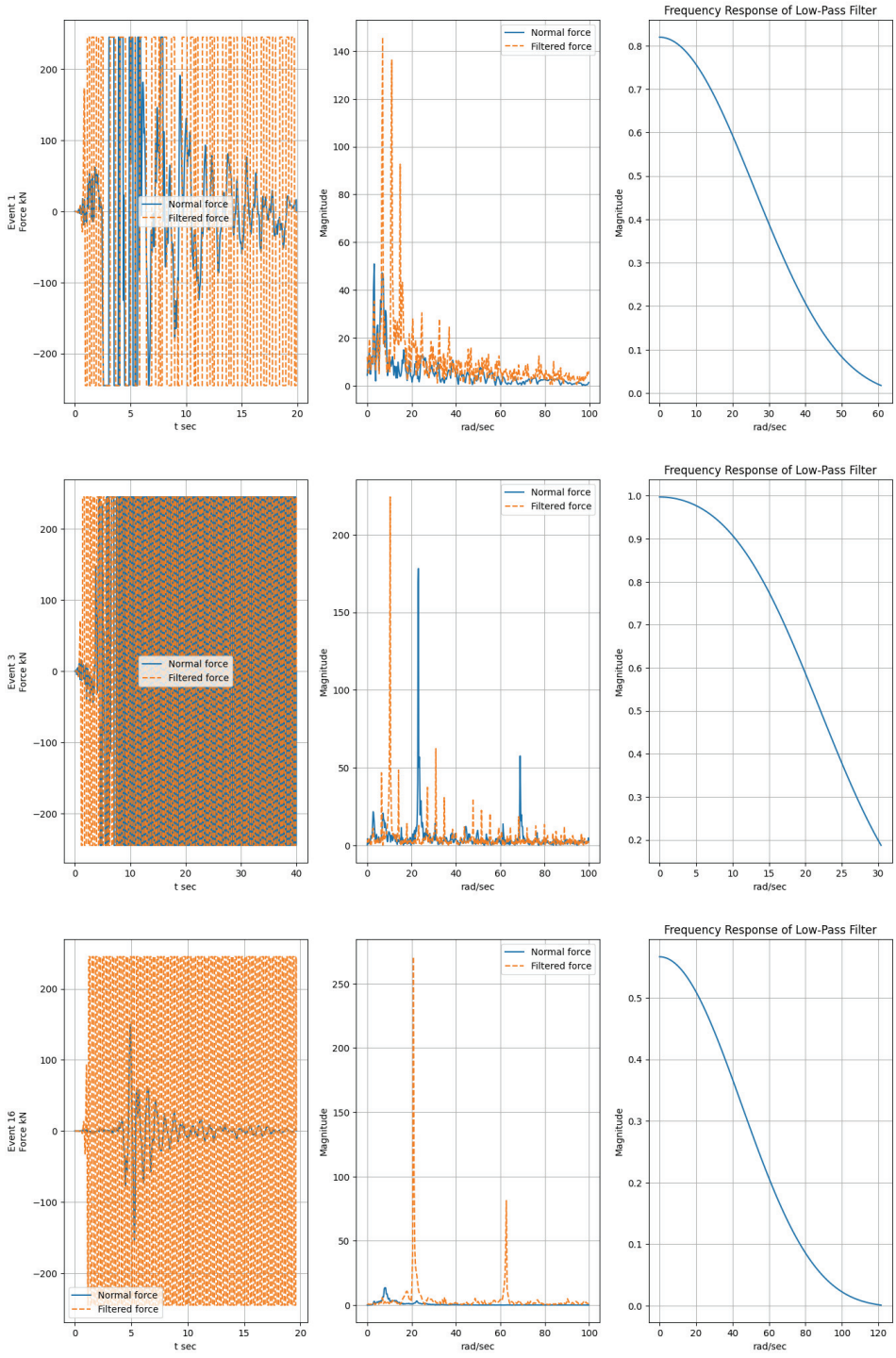

Figure 5.26 Events results under unlimited input case #2 filter

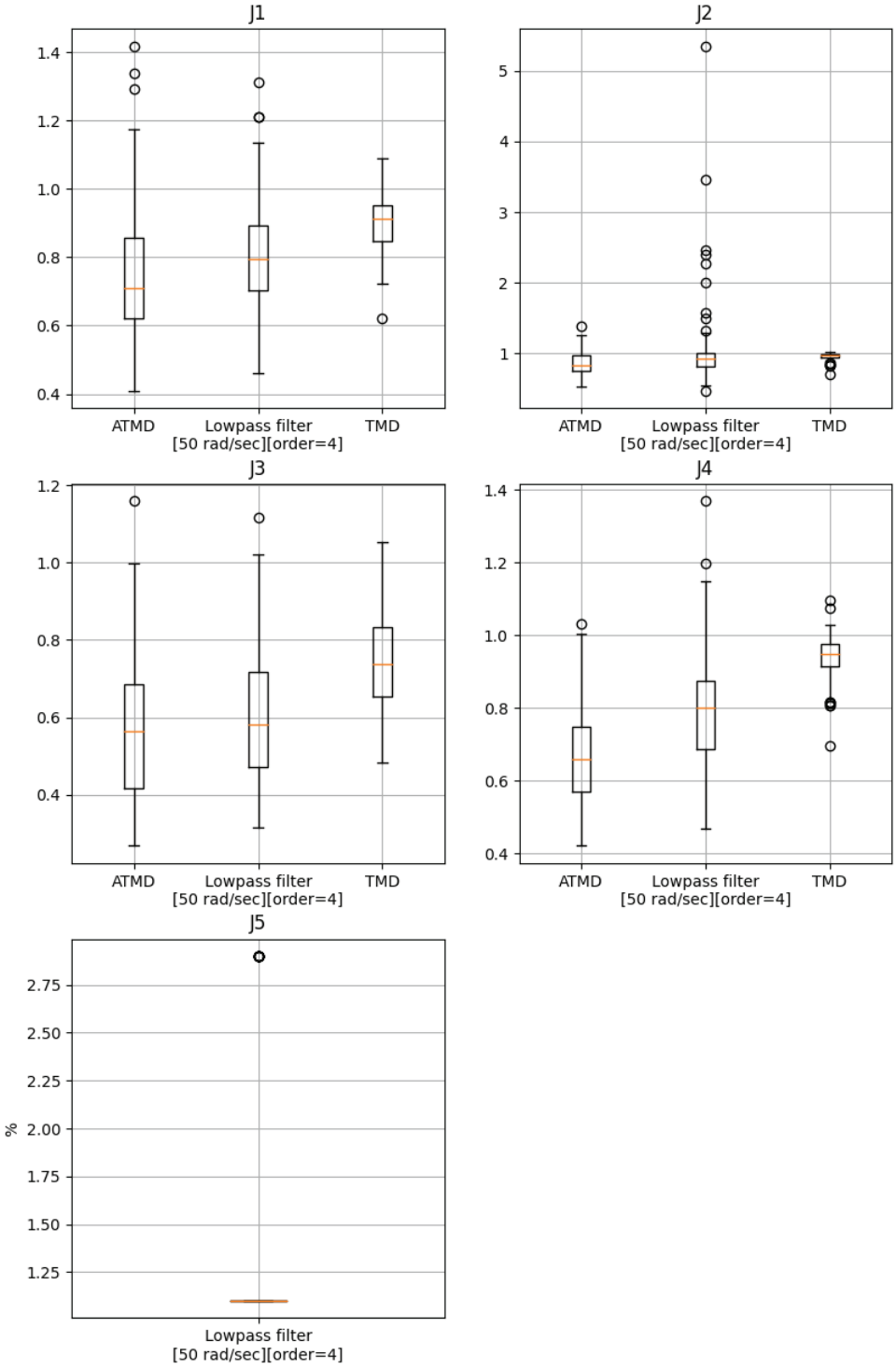

Figure 5.27 Low pass filter case #3 results

The results of the third trial with limited input shown in Figure 5.27 have the same trend as the first case, where the indices J1 to J4 are good, and the required force is lower while the bang-bang action occurs on a lower value than the limit.

Figure 5.28 and Figure 5.29 presents the time histories and corresponding frequency response of limited and unlimited input for the current filters, respectively. There are two differences between the graphs. The first difference lies in the threshold that initiates the bang-bang action, which is lower in the limited input case. The second difference is that the unlimited input amplifies the signal and produces a very high pulse compered to the unfiltered response.

The filters displayed in Figure 5.28 and Figure 5.29 have different sampling frequencies, resulting in different transfer functions. Events 1 and 16 transfer function presented in (5.2) while event 3 transfer function presented in (5.3)

$$H(z) = 0.01 + 0.09625\, z^{-1} + 0.09625\, z^{-2} + 0.01\, z^{-3} \tag{5.2}$$

$$H(z) = 0.0176536 + 0.2740968\, z^{-1} + 0.2740968\, z^{-2} + 0.0176536\, z^{-3} \tag{5.3}$$

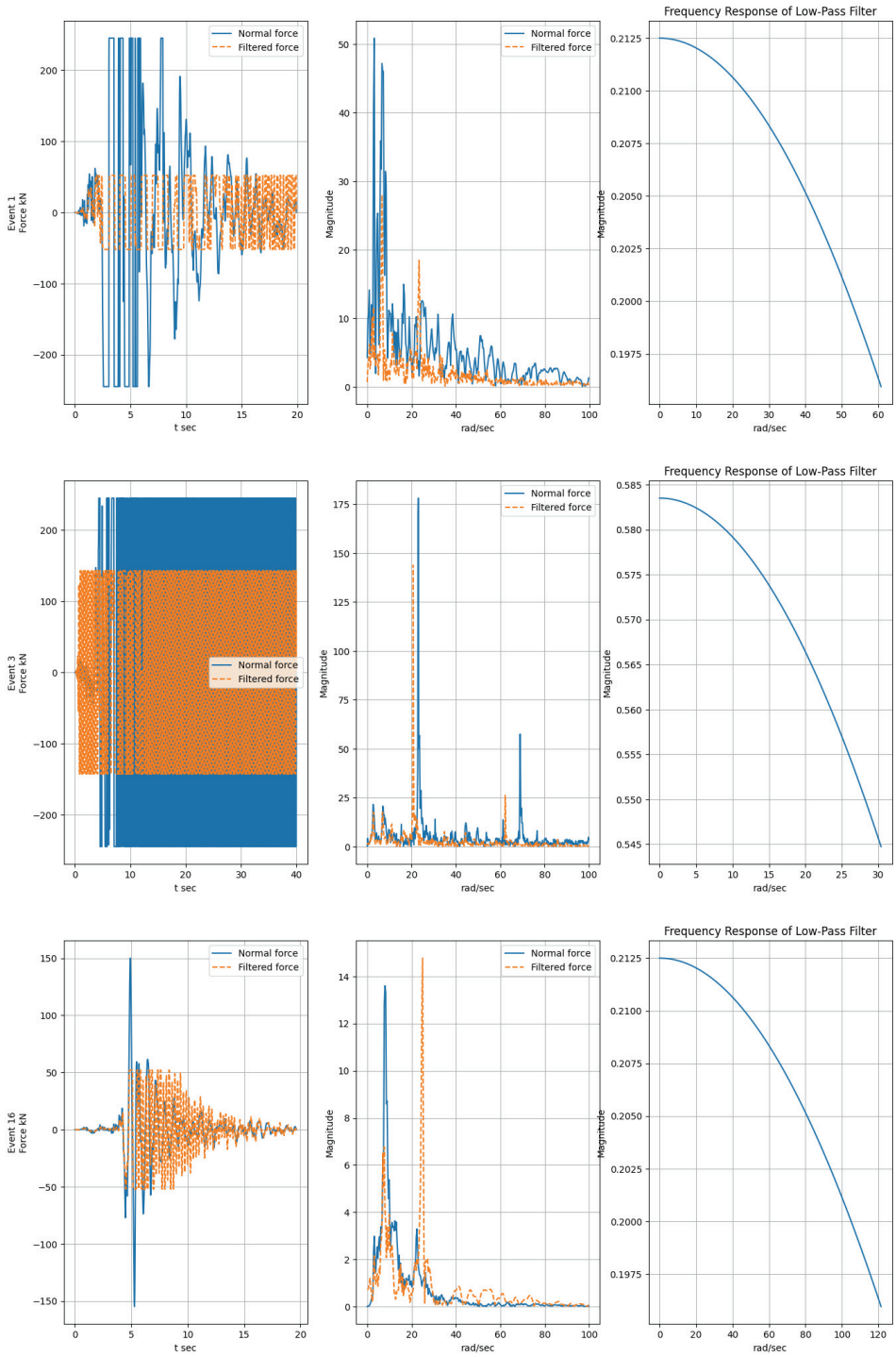

Figure 5.28 Events results under limited input case #3 filter

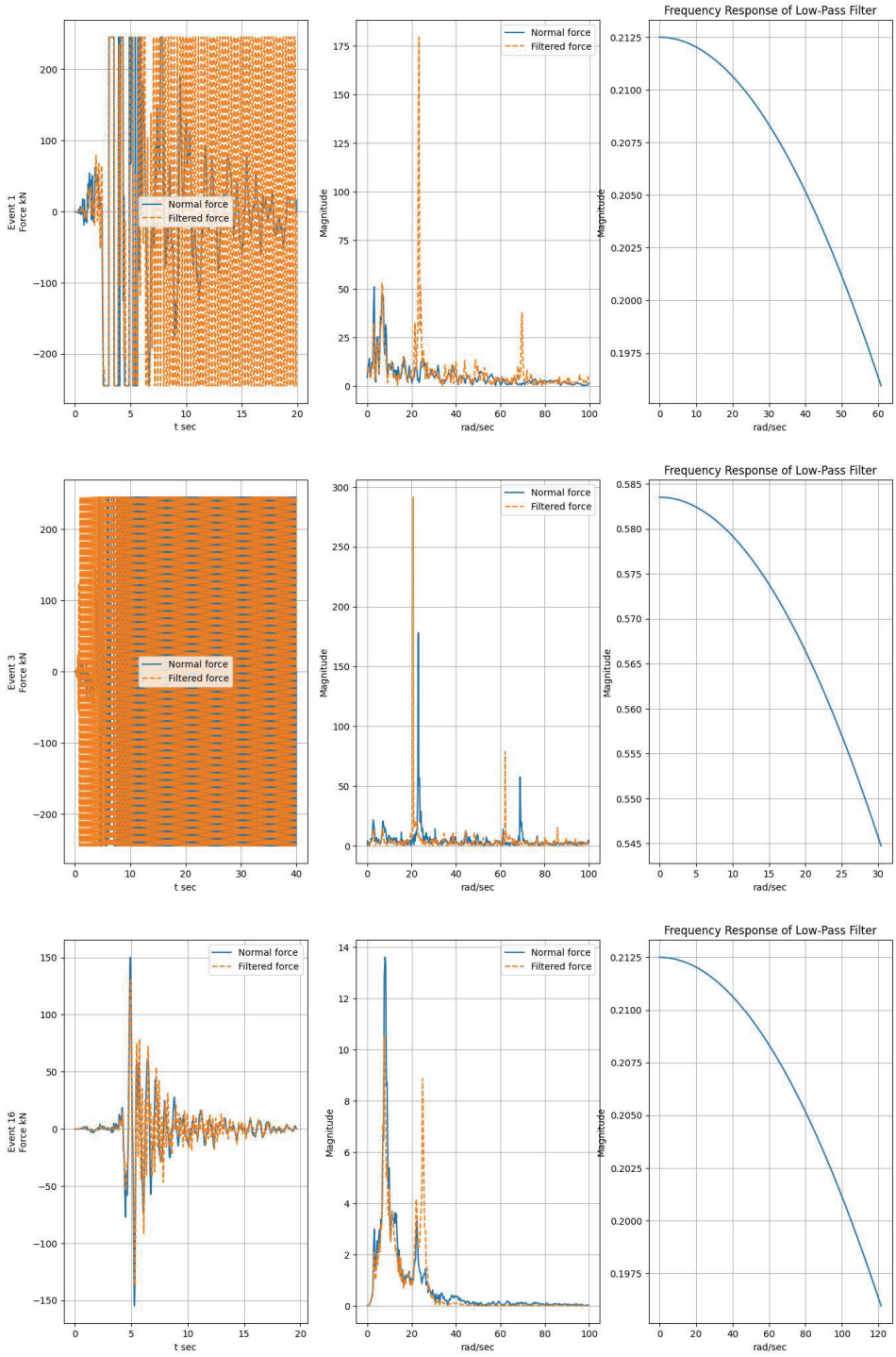

Figure 5.29 Events results under unlimited input case #3 filter

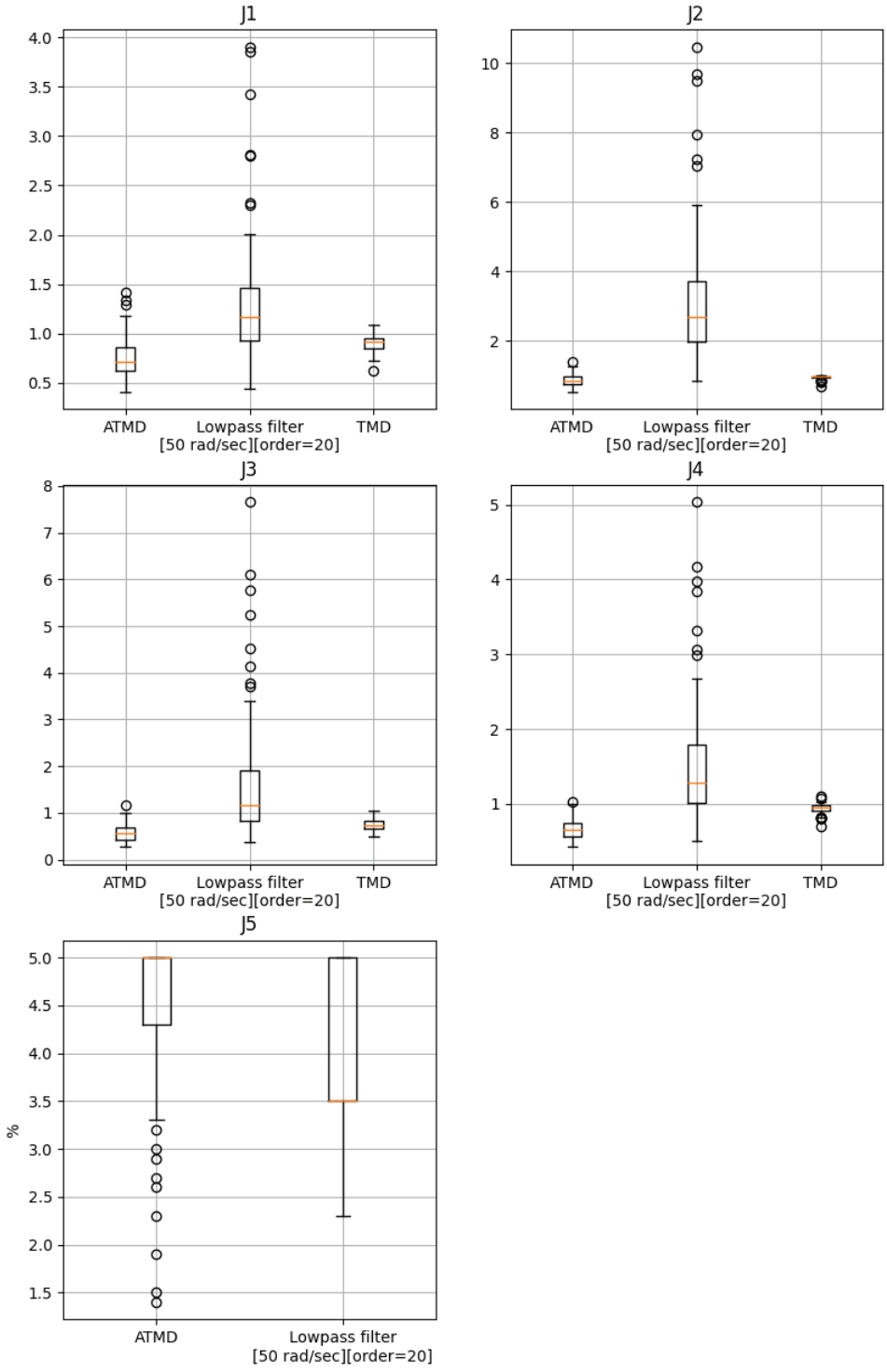

Figure 5.30 Low pass filter case #4 results

The results of the second trial with limited input are shown in Figure 5.30. The indices J1 to J4 show bad values compared to the original ATMD. The force-time histories and associated frequency response for limited and unlimited input are shown in Figure 5.31 and Figure 5.32 two respectively, and both graphs indicate that the filters are amplifying the force signal, which causes the bang-bang action.

Table 5.11 Case 4 filter coefficients

Filter coefficient	Event 1	Event 3	Event 16
Z^{0}	-0.00254	-0.00134	0.00201
Z^{-1}	-0.00402	0.00185	0.00352
Z^{-2}	-0.00606	0.00736	0.00741
Z^{-3}	-0.00517	0.00716	0.01436
Z^{-4}	0.00428	-0.01188	0.02441
Z^{-5}	0.02692	-0.04057	0.03682
Z^{-6}	0.0629	-0.03344	0.05016
Z^{-7}	0.10605	0.05332	0.06259
Z^{-8}	0.1453	0.20027	0.0722
Z^{-9}	0.16875	0.3172	0.07745
Z^{-10}	0.16875	0.3172	0.07745
Z^{-11}	0.1453	0.20027	0.0722
Z^{-12}	0.10605	0.05332	0.06259
Z^{-13}	0.0629	-0.03344	0.05016
Z^{-14}	0.02692	-0.04057	0.03682
Z^{-15}	0.00428	-0.01188	0.02441
Z^{-16}	-0.00517	0.00716	0.01436
Z^{-17}	-0.00606	0.00736	0.00741
Z^{-18}	-0.00402	0.00185	0.00352
Z^{-19}	-0.00254	-0.00134	0.00201

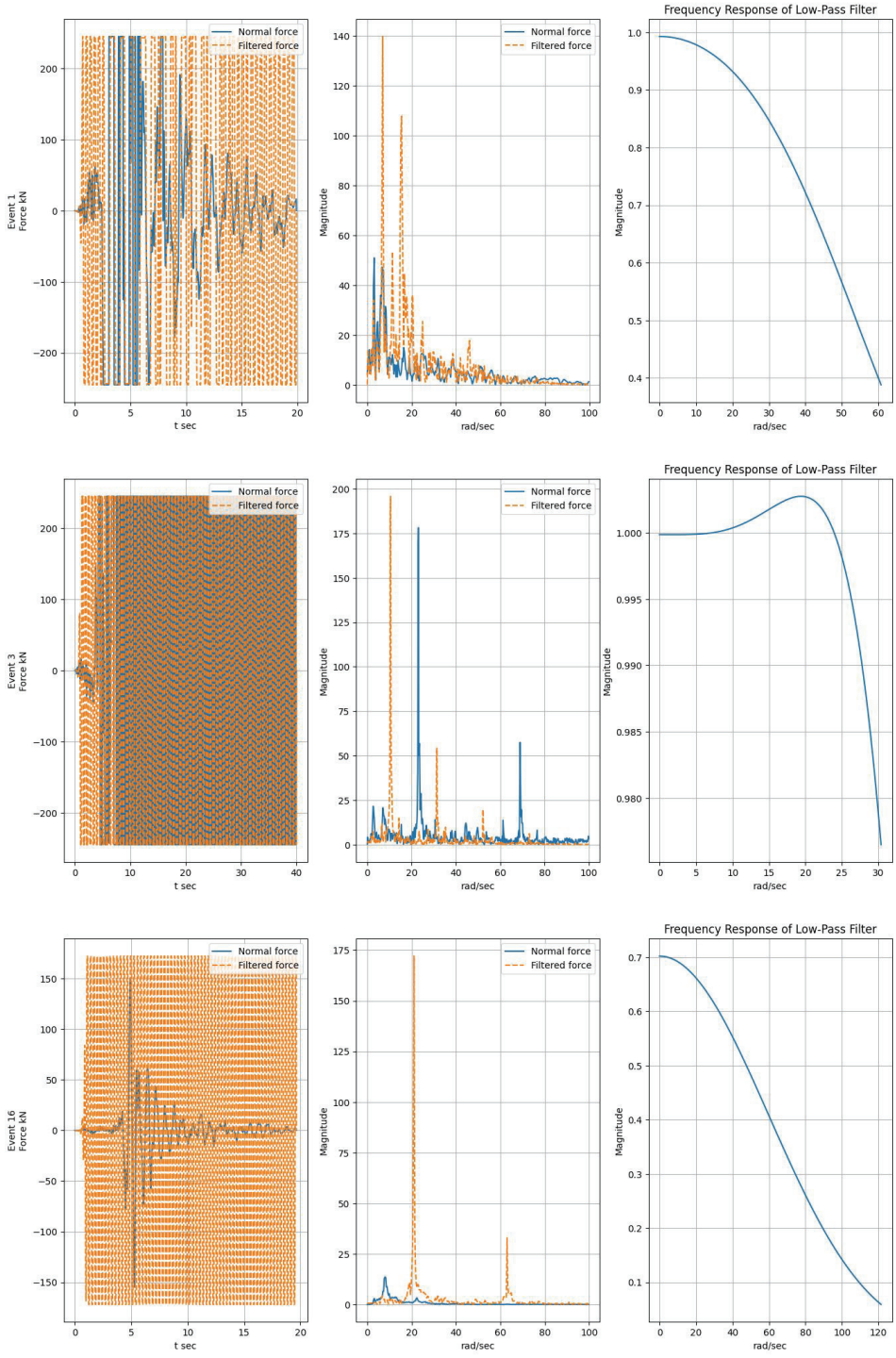

Figure 5.31 Events results under limited input case #4 filter

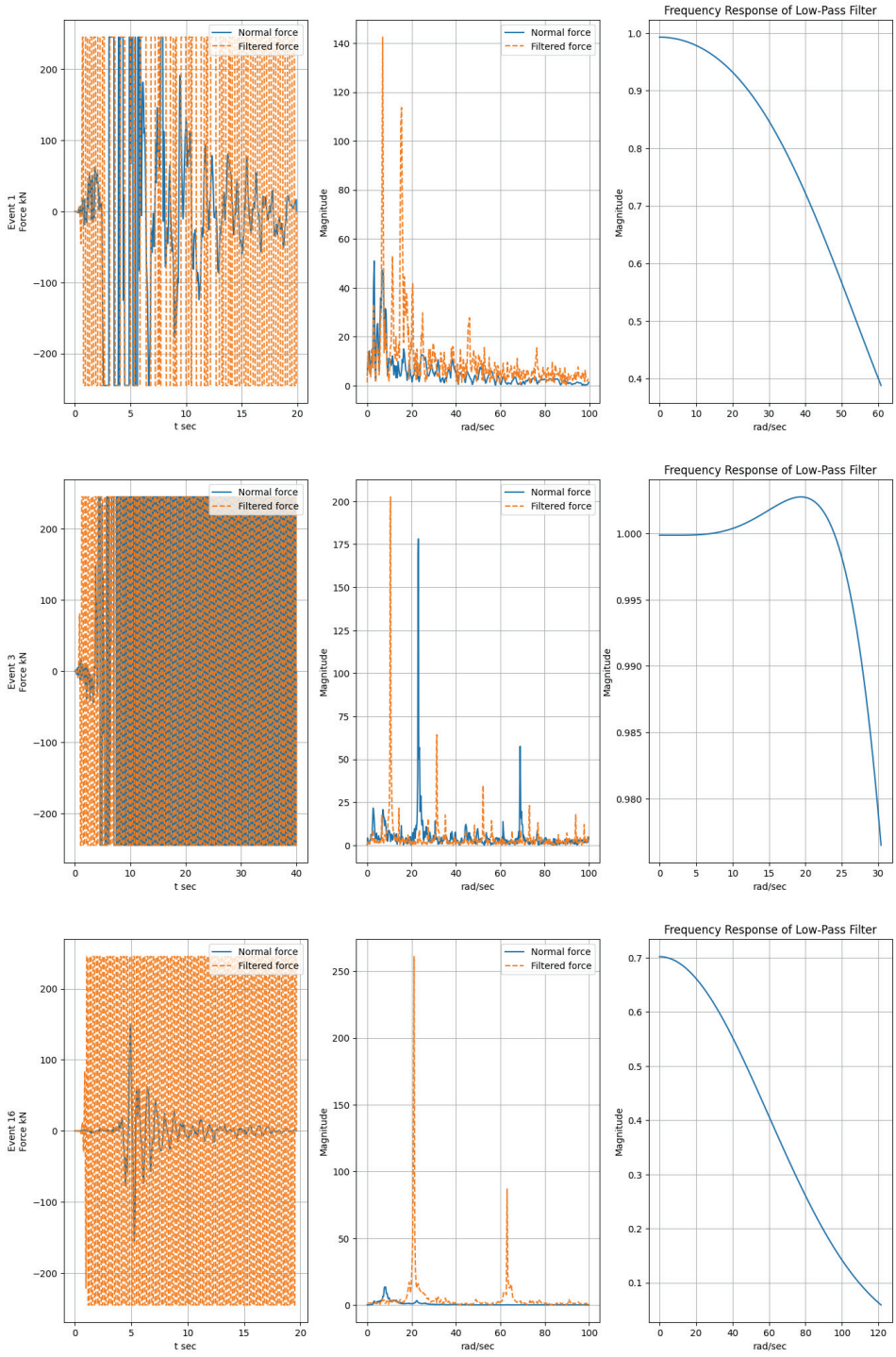

Figure 5.32 Events results under unlimited input case #4 filter

The conclusion of the previous cases is outlined as the following:

- Deploying a filter after the optimization process does not enhance the controller.
- The cutoff frequency and order of the filter affect the bang-bang threshold.
- In the best case, the filter will not affect the force-time history. In contrast, in the worst case, it amplifies the signal and initiates the bang-bang action on a lower threshold.
- The magnitude of the filter and the limitation on the input play a vital role in the amplification of the signal and producing a pulse.

The optimization process was based on completely identifying the original structure characteristics and assuming the structure would stay linear, which can not be true, especially if a severe earthquake occurred. The LQR controller's performance against uncertainties will be assessed by manipulating the system's stiffness matrix. This method was proposed by Kayabekir et al. (KayabekİR et al., 2022). The stiffness matrix will be changed according to (5.4). Noting that TMD mass, damping and stiffness would not change.

$$K_{new}=\left(\frac{100\text{-}E}{100}\right) K \tag{5.4}$$

The results are presented in Figure 5.33, which shows that the controller's performance did not degrade, which means it is robust.

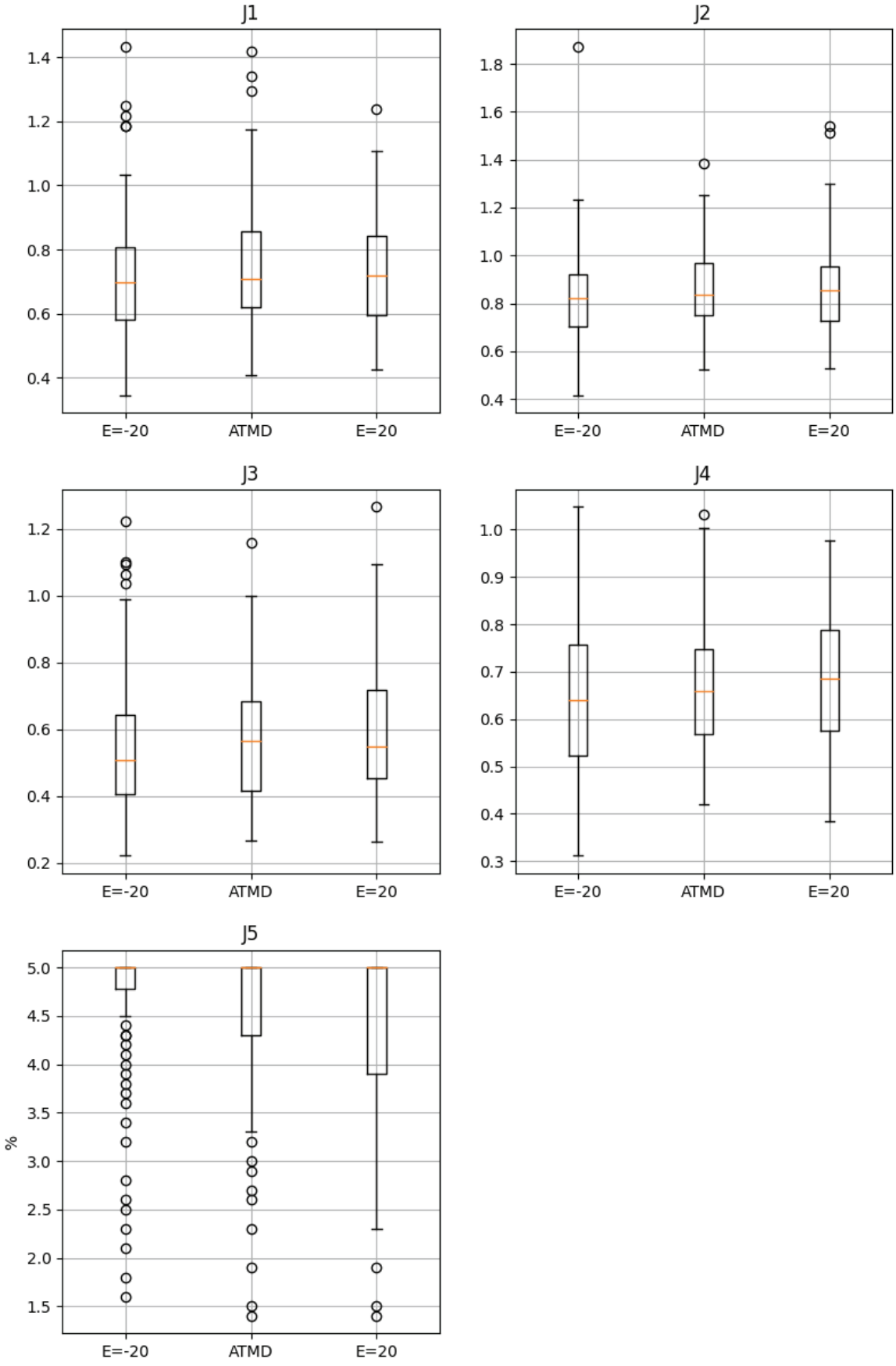

Figure 5.33 Performance indices of ATMD under ±20% uncertinity

The kalman filter's main advantage is decreasing the number of sensors needed to construct the feedback system with maintaining the controller's performance. Figure 5.34 presents the performance index of using the kalman filter. It shows that the kalman filter will not affect the controller's performance. The kalman filter model frequencies are presented in Table 5.12.

Table 5.12 Characteristics of the Kalman filter model

Mode	Natural frequency (rad/sec)
1	2.31
2	2.37
3	6.38
4	10.41
5	14.54
6	17.86
7	20.97
8	22.91
9	26.26
10	28.61
11	32.91

Further investigation of the bang-bang issue has been done to see the effect of the kalman model on the issue. Two samples for force time histories have been displayed in figure to figure. The results show that the kalman model with and without noise follows the same force time history as the original model, which means that the Kalman filter is not the solution. In addition, the figures show that at least one high-magnitude pulse in the spectrum can trigger the bang-bang action regardless of its frequency.

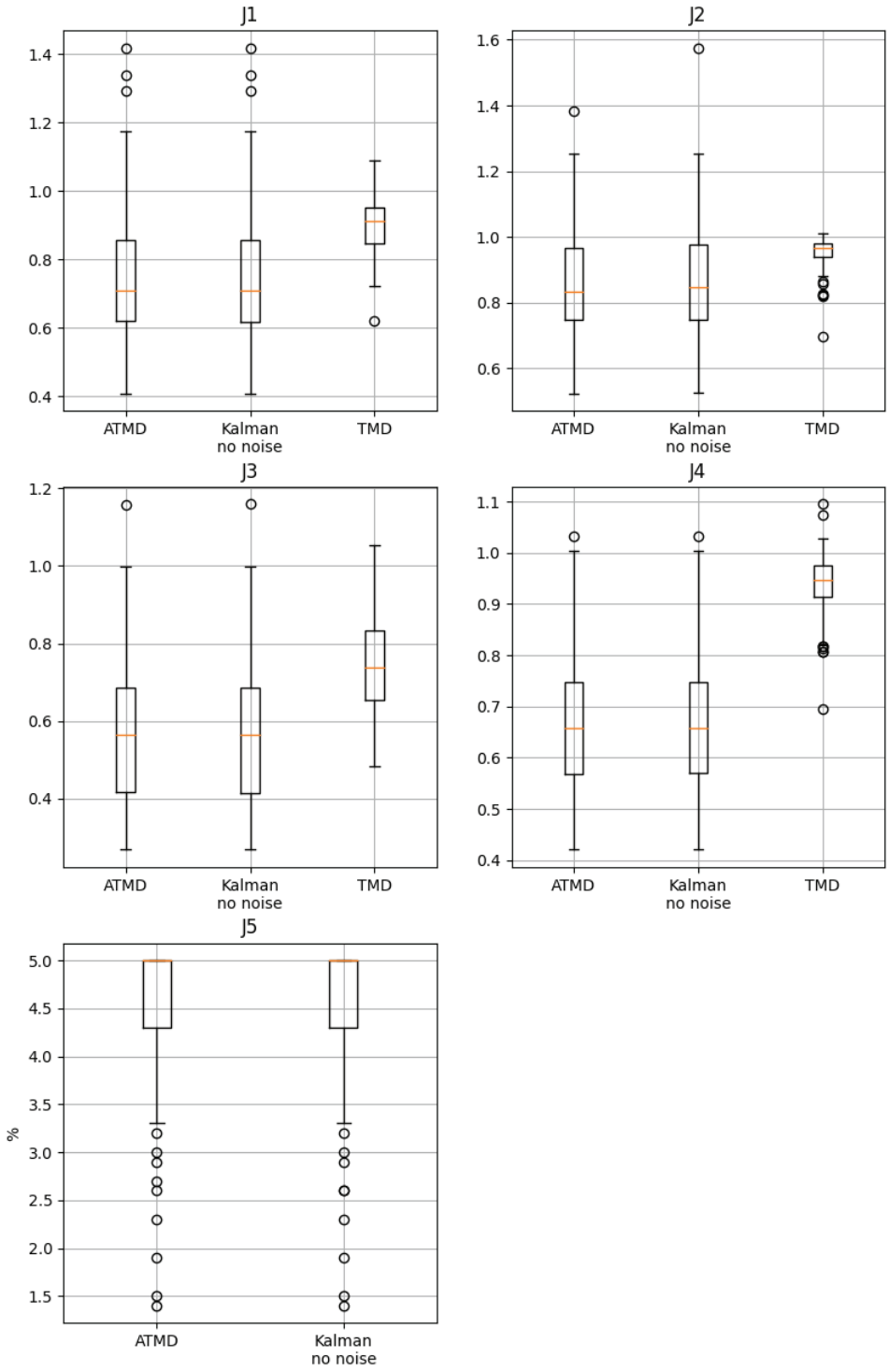

Figure 5.34 Kalman filter performance indices

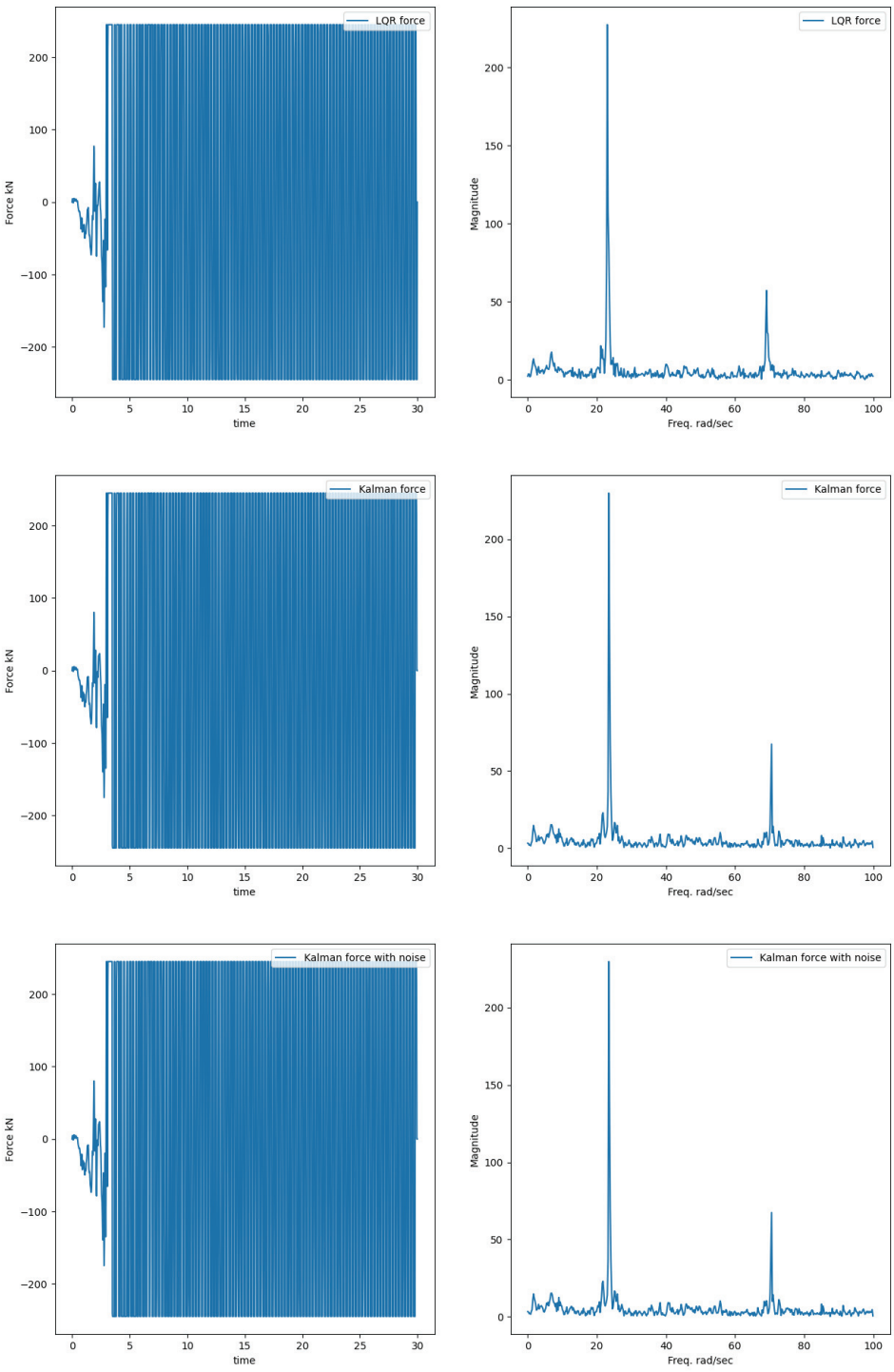

Figure 5.35 Time history and spectrum of active force of different models under the 55th event

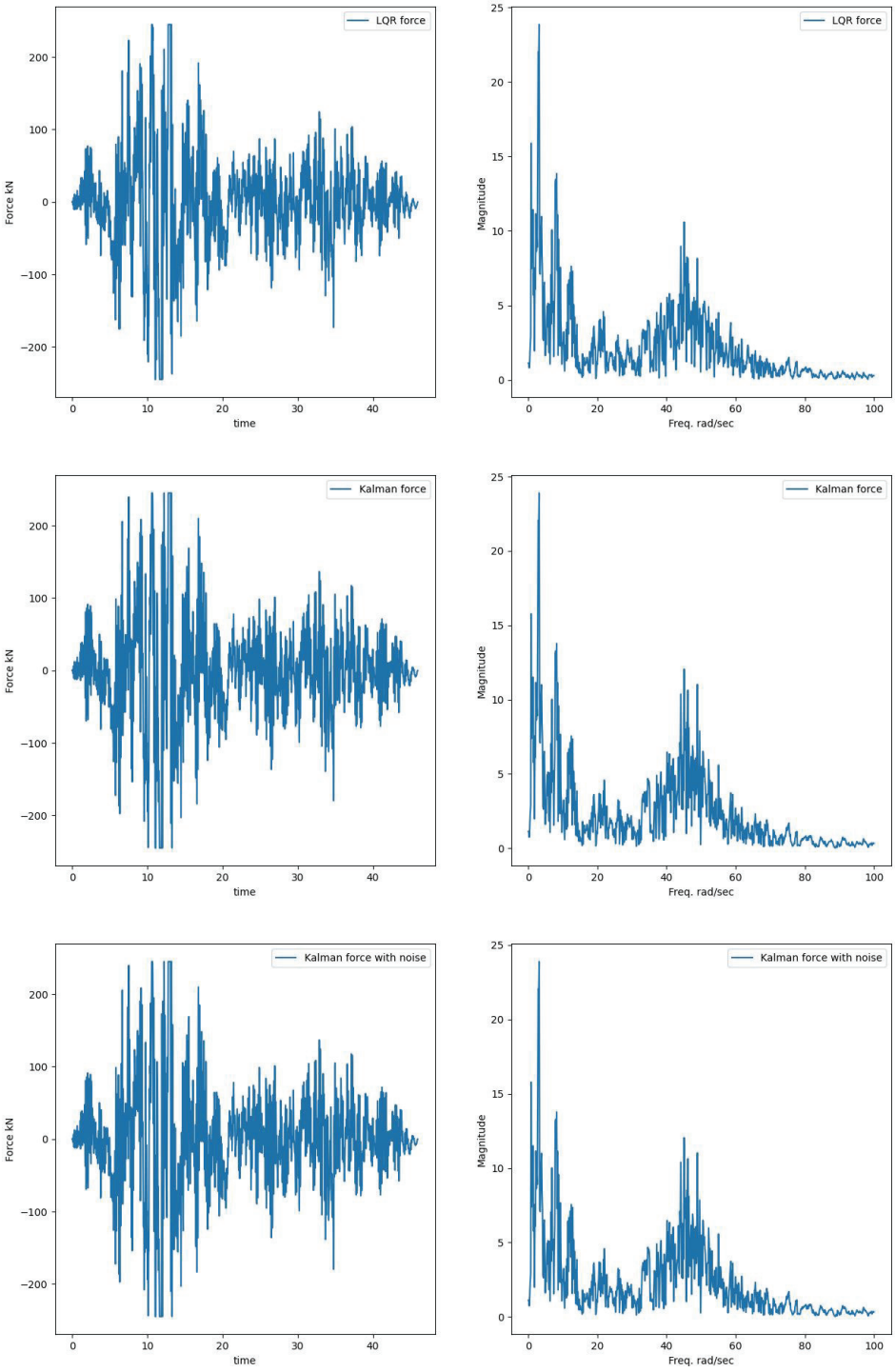

Figure 5.36 Time history and spectrum of active force of different models under the 74th event

CHAPTER 6

CONCLUSION

This thesis studies the influence of the LQR controller type (mention to ATMD) on the structural response and identifies its pros and cons. Two multiobjective problems were formulated in chapter four, in which they have been optimized based on 28 near-field earthquake records with pulse ground motions which are called in this study the optimization records. Five performance indices were used to assess the effectiveness of the derived controller against 96 records comprising of near-field with a pulse, near-field without a pulse, and far-field earthquake records. Each problem utilized an objective function for each story which measures the maximum drift of controlled structure to uncontrolled structure. The first problem is set to optimize unbounded active control force, while in the second problem a lower and an upper bound is considered for the active force.

The first problem results indicated that LQR was able to decrease the drift and RMS indices for all stories under all earthquakes set. However, base shear and acceleration indices were not decreased, and the required active force was high. A linear regression has been carried out to understand if there is a direct relation between active force amount and base shear force. It is concluded that there is no relation between base shear and the active force amount.

Two separate adjustments have been made to the controlled model regarding the high required force. The adjustments aimed to decrease the force by decreasing the damping amount introduced by the LQR gain values.

- The first adjustment is decreasing the damping ratio of the first few modes of the controlled structure and recalculating the gain values using the pole location techniques. The result of this adjustment produces a worse result under higher force demand.

- The second adjustment is changing the LQR gain values to other predefined gain values with a lower damping ratio for a finite time. The results indicated that the response was similar to the output of the original controller but with a slightly lower force demand.

The second problem was formulated in a way that the maximum applicable force is 5% of the structural weight and leaves the algorithm to do the optimization with that limit. The results turned out to be as in the first problem, meaning that it successfully decreased the drift and was also prone to an increment in the base shear. However, the increment only occurs during a few events, and that event does not belong to the 26 earthquakes that we used in the optimization. Increasing the number of optimization records would decrease the possibility of having a high base shear and it would also enhance the controller quality.

The limitation on the active force amount in this problem cause the following issues:

- The first issue is the saturation in the applied force, which means having a constant force for a long time that cannot be delivered in real situations.
- The second issue is shifting into a bang-bang controller, which means the force will shift between the force's upper and lower limits in a one-time step.
- The third issue combines saturation and bang-bang controller issues.

A linearized version of the controller has been used to determine the limitation's effect. Comparison between the active force time history of the current controller and the linearized version pointed to the following observation:

- The active force of both systems will align after the main shook.
- The saturation starts when the linearised system's active force becomes larger than the limit and ends when it becomes smaller than the limit.
- High-magnitude pulses and noise in the frequency spectrum are responsible for the bang-bang action.

The previous issues make the response untrusted because the required force with the current time history can not be applied. Several low-pass FIR filters with different

orders and stopping bands were implemented to overcome the issue. The filters' results indicate that filters can not solve the issues caused by the force limitation and may worsen it by decreasing the threshold where the bang-bang action starts.

The robustness of the controller was assessed by changing the system's stiffness matrix ±20% to consider the yielding effect that may occur during the earthquake and also to account for errors in identifying the system characteristics. The results show a small amount of deterioration the controller's performance in several events.

Kalman filter was used to decrease the number of sensors needed. The performance indices were unchanged. However, the bang-bang action still occurs.

The future work will include the actuator dynamics, and watch if any filter action is needed.

REFERENCES

Bani-Hani, K. A. (2007). Vibration control of wind-induced response of tall buildings with an active tuned mass damper using neural networks. *Structural Control and Health Monitoring*, *14*(1), 83–108. https://doi.org/https://doi.org/10.1002/stc.85

Battaini, M., Casciati, F., & Faravelli, L. (1998). Fuzzy control of structural vibration. An active mass system driven by a fuzzy controller. *Earthquake Engineering & Structural Dynamics*, *27*(11), 1267–1276. https://doi.org/https://doi.org/10.1002/(SICI)1096-9845(1998110)27:11<1267::AID-EQE782>3.0.CO;2-D

Bekdaş, G., & Nigdeli, S. M. (2013). Mass ratio factor for optimum tuned mass damper strategies. *International Journal of Mechanical Sciences*, *71*, 68–84. https://doi.org/https://doi.org/10.1016/j.ijmecsci.2013.03.014

Bray, J. D., & Rodriguez-Marek, A. (2004). Characterization of forward-directivity ground motions in the near-fault region. *Soil Dynamics and Earthquake Engineering*, *24*(11), 815–828. https://doi.org/10.1016/j.soildyn.2004.05.001

Cancellara, D., & De Angelis, F. (2016). Nonlinear dynamic analysis for multi-storey RC structures with hybrid base isolation systems in presence of bi-directional ground motions. *Composite Structures*, *154*, 464–492. https://doi.org/https://doi.org/10.1016/j.compstruct.2016.07.030

Cao, H., Reinhorn, A. M., & Soong, T. T. (1998a). Design of an active mass damper for a tall TV tower in Nanjing, China. *Engineering Structures*, *20*(3), 134–143. https://doi.org/https://doi.org/10.1016/S0141-0296(97)00072-2

Cao, H., Reinhorn, A. M., & Soong, T. T. (1998b). Design of an active mass damper for a tall TV tower in Nanjing, China. *Engineering Structures*, *20*(3), 134–143. https://doi.org/https://doi.org/10.1016/S0141-0296(97)00072-2

Chesné, S., Inquieté, G., Cranga, P., Legrand, F., & Petitjean, B. (2019). Innovative Hybrid Mass Damper for Dual-Loop Controller. *Mechanical Systems and Signal*

Processing, *115*, 514–523. https://doi.org/https://doi.org/10.1016/j.ymssp.2018.06.023

Clemente, P. (2017). Seismic isolation: past, present and the importance of SHM for the future. *Journal of Civil Structural Health Monitoring*, *7*(2), 217–231. https://doi.org/10.1007/s13349-017-0219-6

Deb, K., Pratap, A., Agarwal, S., & Meyarivan, T. (2002). A fast and elitist multiobjective genetic algorithm: NSGA-II. *IEEE Transactions on Evolutionary Computation*, *6*(2), 182–197. https://doi.org/10.1109/4235.996017

El Ouni, M. H., Abdeddaim, M., Elias, S., & Kahla, N. Ben. (2022). Review of Vibration Control Strategies of High-Rise Buildings. *Sensors*, *22*(21). https://doi.org/10.3390/s22218581

Hoang, N., Fujino, Y., & Warnitchai, P. (2008). Optimal tuned mass damper for seismic applications and practical design formulas. *Engineering Structures*, *30*(3), 707–715. https://doi.org/https://doi.org/10.1016/j.engstruct.2007.05.007

Housner, G. W., Bergman, L. A., Caughey, T. K., Chassiakos, A. G., Claus, R. O., Masri, S. F., Skelton, R. E., Soong, T. T., Spencer, B. F., & Yao, J. T. P. (1997a). Structural Control: Past, Present, and Future . *Journal of Engineering Mechanics*, *123*(9), 897–971. https://doi.org/10.1061/(ASCE)0733-9399(1997)123:9(897)

Housner, G. W., Bergman, L. A., Caughey, T. K., Chassiakos, A. G., Claus, R. O., Masri, S. F., Skelton, R. E., Soong, T. T., Spencer, B. F., & Yao, J. T. P. (1997b). Structural Control: Past, Present, and Future . *Journal of Engineering Mechanics*, *123*(9), 897–971. https://doi.org/10.1061/(ASCE)0733-9399(1997)123:9(897)

Huo, L. S., Song, G. B., Li, H. N., & Grigoriadis, K. (2008). H-infinity robust control design of active structural vibration suppression using an active mass damper. *Smart Materials And Structures*, *17*(1). https://doi.org/10.1088/0964-1726/17/01/015021

Kayabek.Ir, A., Bekdacs, G., & N.IGDEL.I, S. I. (2022). The Effect of Structural Rigidity Uncertainties on ATMD Controlled Structures. *WSEAS Transactions on Systems*, *21*.

KayabekİR, A., Bekdaş, G., & NİGDELİ, S. (2022). The Effect of Structural Rigidity Uncertainties on ATMD Controlled Structures. *WSEAS Transactions on Systems*, *21*.

Kayabekir, A., Bekdas, G., Nigdeli, S., & Geem, Z. W. (2020). Optimum Design of PID Controlled Active Tuned Mass Damper via Modified Harmony Search. *Applied Sciences*, *10*, 2976. https://doi.org/10.3390/app10082976

Krenk, S. (2005). Frequency Analysis of the Tuned Mass Damper. *Journal of Applied Mechanics-Transactions of The Asme - J APPL MECH*, *72*. https://doi.org/10.1115/1.2062867

Krenk, S., & Høgsberg, J. (2008). Tuned mass absorbers on damped structures under random load. *Probabilistic Engineering Mechanics*, *23*(4), 408–415. https://doi.org/https://doi.org/10.1016/j.probengmech.2007.04.004

Li, L., Wang, N., & Han, Q. (2019). Adaptive Model Reference Sliding Mode Control of Structural Nonlinear Vibration. *Shock and Vibration*, *2019*, 13. https://doi.org/https://doi.org/10.1155/2019/3612516

Ohtori, Y., Christenson, R. E., Spencer, B. F., & Dyke, S. J. (2004). Benchmark Control Problems for Seismically Excited Nonlinear Buildings. *Journal of Engineering Mechanics*, *130*(4), 366–385. https://doi.org/10.1061/(ASCE)0733-9399(2004)130:4(366)

Sadek, F., Mohraz, B., Taylor, A. W., & Chung, R. M. (1997). a method of estimating the parameters of tuned mass dampers for seismic applications. *Earthquake Engineering & Structural Dynamics*, *26*(6), 617–635. https://doi.org/https://doi.org/10.1002/(SICI)1096-9845(199706)26:6<617::AID-EQE664>3.0.CO;2-Z

Samali, B., & Al-Dawod, M. (2003). Performance of a five-storey benchmark model using an active tuned mass damper and a fuzzy controller. *Engineering Structures*, *25*(13), 1597–1610. https://doi.org/https://doi.org/10.1016/S0141-0296(03)00132-9

Spencer, B. F., & Nagarajaiah, S. (2003a). State of the Art of Structural Control. *Journal of Structural Engineering*, *129*(7), 845–856. https://doi.org/10.1061/(ASCE)0733-9445(2003)129:7(845)

Spencer, B. F., & Nagarajaiah, S. (2003b). State of the Art of Structural Control. *Journal of Structural Engineering*, *129*(7), 845–856. https://doi.org/10.1061/(ASCE)0733-9445(2003)129:7(845)

Symans, M. D., & Constantinou, M. C. (1999). Semi-active control systems for seismic protection of structures: a state-of-the-art review. *Engineering Structures*, *21*(6), 469–487. https://doi.org/https://doi.org/10.1016/S0141-0296(97)00225-3

Tsai, H.-C., & Lin, G.-C. (1993). Optimum tuned-mass dampers for minimizing steady-state response of support-excited and damped systems. *Earthquake Engineering & Structural Dynamics*, *22*(11), 957–973. https://doi.org/https://doi.org/10.1002/eqe.4290221104

Vinodh Kumar, E., & Jerome, J. (2013). Robust LQR Controller Design for Stabilizing and Trajectory Tracking of Inverted Pendulum. *Procedia Engineering*, *64*, 169–178. https://doi.org/10.1016/J.PROENG.2013.09.088

Wang, H., Dong, H., He, L., Shi, Y., & Zhang, Y. (2010). Design and Simulation of LQR Controller with the Linear Inverted Pendulum. *2010 International Conference on Electrical and Control Engineering*, 699–702. https://doi.org/10.1109/iCECE.2010.178

Warburton, G. B. (1982). Optimum absorber parameters for various combinations of response and excitation parameters. *Earthquake Engineering & Structural Dynamics*, *10*(3), 381–401. https://doi.org/https://doi.org/10.1002/eqe.4290100304

Wu, J.-C., & Yang, J. N. (2000). LQG control of lateral–torsional motion of Nanjing TV transmission tower. *Earthquake Engineering & Structural Dynamics*, *29*(8), 1111–1130. https://doi.org/https://doi.org/10.1002/1096-9845(200008)29:8<1111::AID-EQE957>3.0.CO;2-R

Yang, F., Sedaghati, R., & Esmailzadeh, E. (2022). Vibration suppression of structures using tuned mass damper technology: A state-of-the-art review. *Journal of Vibration and Control*, *28*(7–8), 812–836. https://doi.org/10.1177/1077546320984305

Yang, Y. (2012). Analytic LQR design for spacecraft control system based on quaternion model. *Journal of Aerospace Engineering*, *25*(3), 448–453.

You, K.-P., You, J.-Y., & Young-Moon, K. (2014). LQG Control of Along-Wind Response of a Tall Building with an ATMD. *Mathematical Problems in Engineering*, *2014*. https://doi.org/https://doi.org/10.1155/2014/206786

APPENDIX A

EARTHQUAKES DETAILS

Table A.1 Earthquake details

Event Number	Earthquake Name	Recording Station	Componant	Year	Type	PGA (g)
1	Northridge-01,	Rinaldi Receiving Sta.	228	1994	Near field- with pulse	0.87406
2	Northridge-01,	Rinaldi Receiving Sta.	318	1994	Near field- with pulse	0.47235
3	Northridge-01,	Sylmar - Olive View	90	1994	Near field- with pulse	0.60488
4	Northridge-01,	Sylmar - Olive View	360	1994	Near field- with pulse	0.84336
5	Kocaeli Turkey	Izmit	90	1999	Near field- with pulse	0.23017
6	Kocaeli Turkey	Izmit	180	1999	Near field- with pulse	0.16515
7	Chi-Chi Taiwan	TCU065	E	1999	Near field- with pulse	0.78978
8	Chi-Chi Taiwan	TCU065	N	1999	Near field- with pulse	0.57547
9	Chi-Chi Taiwan	TCU102	E	1999	Near field- with pulse	0.30393
10	Chi-Chi Taiwan	TCU102	N	1999	Near field- with pulse	0.17172
11	Duzce Turkey	Duzce	180	1999	Near field- with pulse	0.4043
12	Duzce Turkey	Duzce	270	1999	Near field- with pulse	0.51496
13	Imperial Valley-06	El Centro Array #6	140	1979	Near field- with pulse	0.44729
14	Imperial Valley-06	El Centro Array #6	230	1979	Near field- with pulse	0.44904
15	Imperial Valley-07	El Centro Array #6	140	1979	Near field- with pulse	0.16033
16	Imperial Valley-07	El Centro Array #6	230	1979	Near field- with pulse	0.27437
17	Irpinia Italy-01	Sturno	0	1980	Near field- with pulse	0.22666
18	Irpinia Italy-01	Sturno	270	1980	Near field- with pulse	0.32052
19	Superstition Hills-02	Parachute Test Site	225	1987	Near field- with pulse	0.43182
20	Superstition Hills-02	Parachute Test Site	315	1987	Near field- with pulse	0.38427
21	Loma Prieta	Saratoga - Aloha	0	1989	Near field- with pulse	0.51446
22	Loma Prieta	Saratoga - Aloha	90	1989	Near field- with pulse	0.32623
23	Erzican, Turkey	Erzincan	EW	1992	Near field- with pulse	0.49618
24	Erzican, Turkey	Erzincan	NS	1992	Near field- with pulse	0.38671
25	Cape Mendocino	Petrolia	0	1992	Near field- with pulse	0.59079
26	Cape Mendocino	Petrolia	90	1992	Near field- with pulse	0.66156
27	Landers	Lucerne	260	1992	Near field- with pulse	0.72516
28	Landers	Lucerne	345	1992	Near field- with pulse	0.78876
29	Northridge-01,	LA - Sepulveda VA	270	1994	Near field- without pulse	0.75251

(cont. on next page)

Table A.1 (cont.)

30	Northridge-01,	LA - Sepulveda VA	360	1994	Near field- without pulse	0.93201
31	Northridge-01,	Northridge - Saticoy	90	1994	Near field- without pulse	0.34148
32	Northridge-01,	Northridge - Saticoy	180	1994	Near field- without pulse	0.4593
33	Kocaeli, Turkey	Yarimca	60	1999	Near field- without pulse	0.22675
34	Kocaeli, Turkey	Yarimca	150	1999	Near field- without pulse	0.3218
35	Gazli, USSR	Karakyr	0	1976	Near field- without pulse	0.70171
36	Gazli, USSR	Karakyr	90	1976	Near field- without pulse	0.86395
37	Chi-Chi Taiwan	TCU067	E	1999	Near field- without pulse	0.49896
38	Chi-Chi Taiwan	TCU067	N	1999	Near field- without pulse	0.3192
39	Chi-Chi Taiwan	TCU084	E	1999	Near field- without pulse	1.00889
40	Chi-Chi Taiwan	TCU084	N	1999	Near field- without pulse	0.43112
41	Imperial Valley-06	Bonds Corner	140	1979	Near field- without pulse	0.59872
42	Imperial Valley-06	Bonds Corner	230	1979	Near field- without pulse	0.77692
43	Imperial Valley-06	Chihuahua	12	1979	Near field- without pulse	0.26993
44	Imperial Valley-06	Chihuahua	82	1979	Near field- without pulse	0.25424
45	Denali, Alaska	TAPS Pump Sta. #10	47	2002	Near field- without pulse	0.3326
46	Denali, Alaska	TAPS Pump Sta. #10	317	2002	Near field- without pulse	0.29741
47	Nahanni, Canada	Site 1	10	1985	Near field- without pulse	1.10788
48	Nahanni, Canada	Site 1	280	1985	Near field- without pulse	1.20068
49	Nahanni, Canada	Site 2	240	1985	Near field- without pulse	0.51921
50	Nahanni, Canada	Site 2	330	1985	Near field- without pulse	0.35501
51	Loma Prieta	BRAN	0	1989	Near field- without pulse	0.45636
52	Loma Prieta	BRAN	90	1989	Near field- without pulse	0.50228
53	Loma Prieta	Corralitos	0	1989	Near field- without pulse	0.64473
54	Loma Prieta	Corralitos	90	1989	Near field- without pulse	0.48279
55	Cape Mendocino	Cape Mendocino	0	1992	Near field- without pulse	1.49357
56	Cape Mendocino	Cape Mendocino	90	1992	Near field- without pulse	1.03873
57	Kobe, Japan	Nishi-Akashi	0	1995	Far field	0.48323
58	Kobe, Japan	Nishi-Akashi	90	1995	Far field	0.46432
59	Kobe, Japan	Shin-Osaka	0	1995	Far field	0.225
60	Kobe, Japan	Shin-Osaka	90	1995	Far field	0.23335
61	Kocaeli Turkey	Arcelik	0	1999	Far field	0.21008
62	Kocaeli Turkey	Arcelik	90	1999	Far field	0.1342
63	Kocaeli Turkey	Duzce	180	1999	Far field	0.31191
64	Kocaeli Turkey	Duzce	270	1999	Far field	0.36418
65	Chi-Chi Taiwan	CHY101	E	1999	Far field	0.33966
66	Chi-Chi Taiwan	CHY101	N	1999	Far field	0.39805
67	Friuli, Italy	Tolmezzo	0	1976	Far field	0.35713
68	Friuli, Italy	Tolmezzo	270	1976	Far field	0.31512
69	Chi-Chi Taiwan	TCU045	E	1999	Far field	0.47308

(cont. on next page)

Table A.1 (cont.)

70	Chi-Chi Taiwan	TCU045	N	1999	Far field	0.50682
71	Duzce Turkey	Bolu	0	1999	Far field	0.73925
72	Duzce Turkey	Bolu	90	1999	Far field	0.80568
73	Manjil, Iran	Abbar	L	1990	Far field	0.51456
74	Manjil, Iran	Abbar	T	1990	Far field	0.49687
75	Imperial Valley-06	Delta	62	1979	Far field	0.2357
76	Imperial Valley-06	Delta	52	1979	Far field	0.3497
77	Imperial Valley-06	El Centro Array #11	140	1979	Far field	0.36681
78	Imperial Valley-06	El Centro Array #11	230	1979	Far field	0.37936
79	Hector Mine	Hector	0	1999	Far field	0.26547
80	Hector Mine	Hector	90	1999	Far field	0.32819
81	San Fernando	LA – Hollywood Stor	90	1971	Far field	0.22476
82	San Fernando	LA – Hollywood Stor	180	1971	Far field	0.19493
83	Superstition Hills-02	El Centro Imp. Co.	0	1987	Far field	0.35726
84	Superstition Hills-02	El Centro Imp. Co.	90	1987	Far field	0.25947
85	Superstition Hills-02	Poe Road (temp)	270	1987	Far field	0.47498
86	Superstition Hills-02	Poe Road (temp)	360	1987	Far field	0.28618
87	Loma Prieta	Capitola	0	1989	Far field	0.51113
88	Loma Prieta	Capitola	90	1989	Far field	0.4386
89	Loma Prieta	Gilroy Array #3	0	1989	Far field	0.55912
90	Loma Prieta	Gilroy Array #3	90	1989	Far field	0.36823
91	Landers	Coolwater	LN	1992	Far field	0.28368
92	Landers	Coolwater	TR	1992	Far field	0.4172
93	Landers	Yermo Fire Station	270	1992	Far field	0.24452
94	Landers	Yermo Fire Station	360	1992	Far field	0.15176
95	Northridge-01,	Canyon Country-WLC	0	1994	Far field	0.40361
96	Northridge-01,	Canyon Country-WLC	270	1994	Far field	0.47163

APPENDIX B

LINEAR CASE

Table B.1 Linear case ATMD results

Event	1	2	3	4	5	6	7	8	9	10	11
J1	0.74	0.53	0.67	0.60	0.68	0.90	0.88	0.47	0.44	0.47	0.64
J2	0.74	0.57	0.65	0.77	0.56	0.53	0.59	0.58	0.48	0.43	0.82
J3	0.84	0.37	0.37	0.33	0.34	0.78	0.62	0.42	0.27	0.33	0.64
J4	0.65	0.55	0.53	0.65	0.64	0.59	0.68	0.46	0.45	0.41	0.71
J5(%)	15.8	6.8	6.5	8.7	3.1	1.8	6.8	8.2	6.2	3.8	6.3
Event	12	13	14	15	16	17	18	19	20	21	22
J1	0.90	0.69	0.68	0.96	0.88	0.43	0.48	0.91	0.60	0.78	0.48
J2	0.82	0.63	0.65	0.86	0.98	0.73	0.53	0.78	0.64	0.76	0.61
J3	0.61	0.29	0.30	0.77	0.96	0.32	0.31	0.52	0.38	0.68	0.30
J4	0.66	0.54	0.59	0.80	0.74	0.53	0.42	0.73	0.50	0.76	0.53
J5(%)	7.2	5.2	5.3	1.1	2.2	3.9	4.5	7.7	4.3	4.8	3.2
Event	23	24	25	26	27	28	29	30	31	32	33
J1	0.68	0.79	0.63	0.60	1.05	0.57	0.64	0.70	0.49	0.69	0.65
J2	0.69	0.78	0.82	0.67	0.80	0.72	0.74	0.86	0.78	0.81	0.75
J3	0.34	0.41	0.34	0.36	0.68	0.36	0.48	0.26	0.43	0.51	0.51
J4	0.63	0.66	0.65	0.78	0.85	0.64	0.60	0.64	0.48	0.61	0.65
J5(%)	6.6	7.2	7.7	9.2	5.2	2.8	9.6	7.2	3.2	6.5	3.5
Event	34	35	36	37	38	39	40	41	42	43	44
J1	0.63	0.93	0.79	0.71	0.59	0.80	0.47	0.72	0.87	0.69	0.50
J2	0.68	0.95	0.63	0.67	0.82	0.55	0.51	0.67	0.77	0.77	0.68
J3	0.48	0.98	0.67	0.37	0.39	0.68	0.37	0.55	0.73	0.51	0.50
J4	0.69	0.53	0.62	0.77	0.55	0.53	0.48	0.70	0.60	0.68	0.46
J5(%)	4.1	6.7	6.9	7.3	5.7	13.5	5.2	6.2	5.7	3.1	4.1
Event	45	46	47	48	49	50	51	52	53	54	55
J1	0.55	0.63	0.63	0.55	0.96	0.69	0.63	0.81	0.82	1.05	0.75
J2	0.58	0.82	0.91	0.88	0.79	0.70	0.73	0.62	0.85	0.84	1.02
J3	0.31	0.43	0.64	0.54	0.65	0.75	0.44	0.57	0.62	0.61	0.38
J4	0.49	0.83	0.52	0.45	0.73	0.75	0.62	0.72	0.70	0.81	0.91
J5(%)	7.7	4.4	3	3.2	2.3	2.5	5.9	4.8	4.6	6.6	7.4

(cont. on next page)

Table B.1 (cont.)

Event	56	57	58	59	60	61	62	63	64	65	66
J1	0.60	0.61	0.90	0.72	1.18	0.58	0.73	0.95	0.74	0.59	0.57
J2	0.88	0.76	0.81	0.95	0.98	0.84	0.77	0.80	0.74	0.48	0.62
J3	0.30	0.48	0.53	0.32	0.56	0.43	0.52	0.68	0.55	0.36	0.67
J4	0.65	0.54	0.71	0.72	0.96	0.49	0.73	0.81	0.60	0.54	0.56
J5(%)	3.3	3.8	4.1	3.4	3.8	1.2	1.6	4	5.6	4	7.2
Event	67	68	69	70	71	72	73	74	75	76	77
J1	0.90	0.79	0.70	1.07	0.66	0.55	0.58	0.56	0.52	0.38	0.61
J2	0.68	0.70	0.79	0.70	0.75	0.65	0.76	0.82	0.87	0.58	0.90
J3	0.50	0.78	0.45	0.52	0.35	0.69	0.35	0.34	0.41	0.26	0.37
J4	0.61	0.76	0.68	0.80	0.52	0.55	0.68	0.51	0.53	0.41	0.70
J5(%)	1.9	3.7	5.1	4.5	5	8.6	4.5	4.9	2.5	3.6	3.5
Event	78	79	80	81	82	83	84	85	86	87	88
J1	0.87	0.57	0.74	0.74	0.84	0.92	0.72	0.64	0.67	0.56	0.87
J2	0.87	0.77	0.60	0.78	0.79	0.91	0.73	0.82	0.65	0.68	0.98
J3	0.54	0.50	0.43	0.59	0.53	0.48	0.33	0.41	0.49	0.79	0.67
J4	0.68	0.39	0.57	0.59	0.66	0.71	0.73	0.54	0.65	0.52	0.72
J5(%)	2.4	2.2	3.4	1.9	1.2	3.9	3.1	2.7	2.3	5.7	4.5
Event	89	90	91	92	93	94	95	96			
J1	0.61	0.78	0.67	1.23	0.55	0.52	0.65	0.58			
J2	1.02	0.77	0.66	0.96	0.87	0.75	0.72	0.76			
J3	0.53	0.43	0.93	0.90	0.52	0.38	0.54	0.52			
J4	0.56	0.64	0.57	0.91	0.72	0.51	0.63	0.54			
J5(%)	3.1	3.3	2.2	5.1	4.4	1.8	3.8	6			

Table B.2 TMD results

Event	1	2	3	4	5	6	7	8	9	10	11
J1	0.95	0.82	0.95	0.80	0.95	1.02	0.94	0.89	0.62	0.72	0.99
J2	0.98	0.93	0.94	0.98	0.92	0.89	0.97	0.96	0.70	0.82	1.00
J3	1.01	0.66	0.58	0.59	0.61	0.93	0.87	0.73	0.52	0.58	0.91
J4	0.97	0.92	0.91	0.90	0.82	1.01	0.98	0.86	0.70	0.82	1.01
Event	12	13	14	15	16	17	18	19	20	21	22
J1	0.96	0.80	0.93	1.00	0.96	0.81	0.80	0.94	0.89	0.92	0.82
J2	0.98	0.97	0.93	0.99	1.00	0.94	0.88	0.95	0.93	0.97	0.96
J3	0.82	0.57	0.62	0.93	0.93	0.63	0.60	0.76	0.73	0.82	0.65
J4	0.98	0.95	0.92	1.00	0.98	0.81	0.88	0.94	0.90	0.98	0.83
Event	23	24	25	26	27	28	29	30	31	32	33
J1	0.93	0.87	0.86	0.94	1.03	0.84	0.96	0.91	0.79	0.83	0.98
J2	0.94	0.98	0.98	0.94	0.98	0.93	0.98	0.90	0.96	0.99	0.86
J3	0.70	0.69	0.66	0.63	0.97	0.70	0.77	0.55	0.73	0.71	0.72
J4	0.93	0.95	0.88	0.97	1.03	0.97	0.98	0.90	0.85	0.95	0.98
Event	34	35	36	37	38	39	40	41	42	43	44
J1	1.01	0.99	0.85	0.84	0.79	0.96	0.94	0.93	0.95	0.83	0.87
J2	0.95	0.98	0.95	0.90	0.98	0.99	0.98	0.97	0.98	0.99	0.89
J3	0.83	1.05	0.89	0.58	0.62	0.80	0.67	0.78	0.89	0.79	0.80
J4	1.07	0.99	0.93	0.88	0.81	0.98	0.97	0.90	0.98	0.91	1.01
Event	45	46	47	48	49	50	51	52	53	54	55
J1	0.77	0.93	1.00	0.95	0.99	0.96	0.89	0.95	0.91	0.92	0.97
J2	0.89	0.96	1.00	0.92	0.98	0.99	0.97	0.97	0.99	1.01	1.00
J3	0.61	0.73	1.01	0.87	0.82	0.87	0.79	0.85	0.79	0.90	0.71
J4	0.81	0.95	1.09	0.94	0.96	0.95	0.98	0.97	0.95	1.02	1.00
Event	56	57	58	59	60	61	62	63	64	65	66
J1	0.80	0.85	0.95	0.80	0.91	0.77	0.93	0.88	0.95	0.90	0.91
J2	0.94	0.98	0.97	0.96	0.97	0.94	0.95	0.98	0.97	0.82	0.98
J3	0.60	0.69	0.69	0.59	0.75	0.80	0.80	0.85	0.72	0.69	0.90
J4	0.93	0.92	0.94	0.96	0.97	0.92	0.97	1.00	0.95	0.92	0.91
Event	67	68	69	70	71	72	73	74	75	76	77
J1	0.96	0.89	0.95	1.09	0.90	0.96	0.79	0.86	0.87	0.74	0.83
J2	0.99	0.97	0.99	1.01	0.97	0.99	0.88	0.89	0.90	0.83	0.97
J3	0.76	0.93	0.68	0.77	0.68	0.85	0.59	0.63	0.66	0.48	0.69
J4	0.98	0.99	1.00	1.03	0.97	0.98	0.90	0.82	0.89	0.82	0.90
Event	78	79	80	81	82	83	84	85	86	87	88
J1	0.99	0.88	0.80	0.96	0.96	0.80	0.85	0.89	0.94	0.94	0.92
J2	0.99	0.94	0.93	0.98	0.96	0.97	0.92	0.96	0.86	0.96	0.97
J3	0.82	0.73	0.65	0.84	0.75	0.71	0.53	0.74	0.75	0.85	0.82
J4	0.91	0.97	0.93	0.92	0.97	0.93	0.92	0.88	0.93	0.92	0.97
Event	89	90	91	92	93	94	95	96			
J1	0.88	0.86	1.01	0.93	0.93	0.77	0.91	0.85			
J2	0.98	0.94	0.98	1.01	0.98	0.95	0.97	0.95			
J3	0.93	0.64	0.97	0.98	0.80	0.60	0.74	0.81			
J4	0.95	0.94	0.98	0.98	0.94	0.95	0.96	0.92			

APPENDIX C

NONLINEAR CASE

Table C.1 Nonlinear case ATMD results

Event	1	2	3	4	5	6	7	8	9	10	11
J1	0.89	0.63	0.74	0.64	0.69	0.98	0.90	0.51	0.46	0.50	0.77
J2	0.93	0.75	1.21	0.97	0.52	0.62	0.62	0.79	0.58	0.53	1.12
J3	1.00	0.45	0.47	0.40	0.37	0.89	0.70	0.47	0.30	0.39	0.65
J4	0.75	0.56	0.59	0.69	0.63	0.60	0.65	0.47	0.52	0.42	0.73
J5(%)	5	5	5	5	4	2.3	5	5	5	5	5
Event	12	13	14	15	16	17	18	19	20	21	22
J1	1.00	0.67	0.61	0.94	0.88	0.45	0.50	0.97	0.66	0.98	0.49
J2	0.91	0.90	0.70	0.88	0.86	0.74	0.62	1.02	0.60	0.83	0.65
J3	0.72	0.32	0.28	0.91	1.16	0.35	0.34	0.57	0.40	0.85	0.29
J4	0.69	0.56	0.58	0.83	0.81	0.60	0.44	0.81	0.51	0.79	0.51
J5(%)	5	5	5	1.5	3.2	4.3	5	5	5	5	4.1
Event	23	24	25	26	27	28	29	30	31	32	33
J1	0.72	0.76	0.67	0.72	0.91	0.56	0.61	0.74	0.61	0.85	0.64
J2	0.77	0.89	1.38	0.83	0.97	0.75	0.92	1.04	0.73	1.07	0.97
J3	0.36	0.48	0.36	0.44	0.63	0.34	0.57	0.27	0.51	0.66	0.52
J4	0.57	0.74	0.77	0.78	0.85	0.60	0.72	0.56	0.48	0.74	0.64
J5(%)	5	5	5	5	5	4.2	5	5	4.1	5	5
Event	34	35	36	37	38	39	40	41	42	43	44
J1	0.64	0.78	0.71	0.71	0.56	0.70	0.47	0.74	0.75	0.67	0.67
J2	0.76	0.83	0.82	0.74	1.07	0.86	0.70	1.06	0.66	0.91	0.87
J3	0.46	0.92	0.73	0.44	0.44	0.64	0.44	0.68	0.87	0.62	0.56
J4	0.71	0.49	0.63	0.75	0.66	0.62	0.45	0.86	0.61	0.64	0.58
J5(%)	5	5	5	5	5	5	5	5	5	3.8	5

(cont. on next page)

Table C.1 (cont.)

Event	45	46	47	48	49	50	51	52	53	54	55
J1	0.55	0.67	0.65	0.68	0.91	0.89	0.62	0.79	0.89	1.15	0.74
J2	0.70	0.97	0.87	0.81	0.86	0.87	0.74	0.75	0.89	1.16	1.14
J3	0.35	0.45	0.62	0.57	0.82	0.98	0.50	0.64	0.79	0.68	0.43
J4	0.53	0.93	0.56	0.55	0.83	0.73	0.56	0.85	0.74	1.03	0.90
J5(%)	5	5	4.8	5	3	4.3	5	5	5	5	5
Event	56	57	58	59	60	61	62	63	64	65	66
J1	0.67	0.61	1.07	0.68	1.34	0.54	0.69	1.09	0.97	0.56	0.72
J2	1.00	0.82	0.95	0.82	1.00	1.00	0.75	0.86	0.84	0.63	0.80
J3	0.35	0.61	0.65	0.38	0.67	0.47	0.50	0.76	0.70	0.36	0.73
J4	0.71	0.59	0.78	0.66	0.94	0.51	0.67	0.87	0.67	0.50	0.71
J5(%)	5	5	5	4.1	4.6	1.9	2.6	4.5	5	5	5
Event	67	68	69	70	71	72	73	74	75	76	77
J1	1.17	0.76	0.74	1.29	0.66	0.62	0.72	0.71	0.49	0.41	0.70
J2	0.98	0.80	0.77	0.82	0.72	0.88	0.82	0.95	1.12	0.68	1.00
J3	0.64	0.90	0.51	0.70	0.39	0.83	0.40	0.42	0.49	0.29	0.39
J4	0.73	0.79	0.70	0.85	0.54	0.58	0.67	0.60	0.48	0.45	0.71
J5(%)	3.4	5	5	5	5	5	5	5	4.3	4.6	4.8
Event	78	79	80	81	82	83	84	85	86	87	88
J1	0.83	0.72	0.83	0.68	1.02	1.03	0.77	0.75	0.74	0.59	0.76
J2	0.81	0.78	0.71	0.84	0.84	1.05	0.79	0.91	0.73	0.72	0.98
J3	0.63	0.59	0.50	0.62	0.67	0.56	0.40	0.50	0.61	0.89	0.78
J4	0.66	0.49	0.61	0.65	0.79	0.80	0.70	0.64	0.69	0.54	0.76
J5(%)	4.3	3.4	4.9	2.7	1.4	4.9	4.2	4.2	3.3	5	5
Event	89	90	91	92	93	94	95	96			
J1	0.64	0.89	0.86	1.42	0.60	0.56	0.59	0.58			
J2	1.02	0.93	0.69	1.25	1.05	0.82	0.79	0.77			
J3	0.57	0.55	1.00	1.00	0.58	0.42	0.72	0.62			
J4	0.72	0.70	0.70	1.00	0.79	0.56	0.60	0.61			
J5(%)	4.8	4.3	4.1	5	4.9	2.9	5	5			

Table C.2 Linearized ATMD results

Event	1	2	3	4	5	6	7	8	9	10	11
J1	0.72	0.63	0.73	0.76	0.69	0.98	0.90	0.58	0.45	0.50	0.75
J2	0.83	0.61	0.87	0.83	0.52	0.62	0.72	0.76	0.56	0.53	0.96
J3	1.02	0.46	0.46	0.40	0.37	0.89	0.75	0.49	0.29	0.39	0.65
J4	0.66	0.57	0.62	0.65	0.63	0.60	0.68	0.54	0.52	0.42	0.74
J5(%)	19.7	9.4	9.3	13.1	4	2.3	10.7	10.6	8.3	5.3	10.3
Event	12	13	14	15	16	17	18	19	20	21	22
J1	1.01	0.68	0.66	0.94	0.88	0.45	0.52	1.06	0.66	1.00	0.49
J2	0.91	0.88	0.70	0.88	0.86	0.74	0.50	0.98	0.60	0.84	0.65
J3	0.70	0.33	0.28	0.91	1.16	0.35	0.34	0.64	0.40	0.85	0.29
J4	0.69	0.58	0.58	0.83	0.81	0.60	0.46	0.81	0.51	0.79	0.51
J5(%)	8.7	7.6	7.4	1.5	3.2	4.3	6.6	12.3	5.1	6.2	4.1
Event	23	24	25	26	27	28	29	30	31	32	33
J1	0.79	0.88	0.81	0.71	0.94	0.56	0.72	0.79	0.61	0.87	0.64
J2	0.83	0.94	0.92	0.91	0.85	0.75	0.83	1.03	0.73	1.07	0.96
J3	0.37	0.50	0.40	0.45	0.64	0.34	0.57	0.28	0.51	0.67	0.52
J4	0.60	0.74	0.71	0.79	0.86	0.60	0.66	0.60	0.48	0.73	0.64
J5(%)	9	9.2	10.2	12.6	7.3	4.2	12.9	13.7	4.1	9.6	5.5
Event	34	35	36	37	38	39	40	41	42	43	44
J1	0.64	0.89	0.71	0.85	0.56	1.03	0.50	0.84	0.81	0.67	0.67
J2	0.76	0.84	0.80	0.81	1.06	0.80	0.69	0.96	0.66	0.91	0.88
J3	0.46	0.95	0.73	0.47	0.44	0.86	0.45	0.71	0.91	0.62	0.56
J4	0.71	0.53	0.64	0.81	0.69	0.68	0.46	0.85	0.60	0.64	0.58
J5(%)	6.3	8.5	8.5	9.8	6.9	18.4	7.2	10.1	7.1	3.8	5.5
Event	45	46	47	48	49	50	51	52	53	54	55
J1	0.6094	0.71	0.65	0.68	0.91	0.89	0.61	0.79	0.90	1.15	0.74
J2	0.6426	0.91	0.87	0.81	0.86	0.87	0.70	0.76	0.89	1.08	1.04
J3	0.3611	0.46	0.62	0.57	0.82	0.98	0.50	0.65	0.81	0.77	0.40
J4	0.519	0.95	0.56	0.55	0.83	0.73	0.54	0.85	0.74	0.96	0.90
J5(%)	9.8	6.3	4.8	5.2	3	4.3	6.8	6.2	6.4	9.2	12
Event	56	57	58	59	60	61	62	63	64	65	66
J1	0.67	0.61	1.07	0.68	1.34	0.54	0.69	1.09	0.97	0.54	0.68
J2	1.22	0.80	0.95	0.82	1.00	1.00	0.75	0.86	0.84	0.63	0.74
J3	0.35	0.62	0.65	0.38	0.67	0.47	0.50	0.76	0.71	0.36	0.75
J4	0.71	0.60	0.78	0.66	0.94	0.51	0.67	0.87	0.67	0.48	0.67
J5(%)	6.4	6.1	5.7	4.1	4.6	1.9	2.6	4.5	7.7	6.1	11

(cont. on next page)

Table C.2 (cont.)

Event	67	68	69	70	71	72	73	74	75	76	77
J1	1.17	0.76	0.74	1.29	0.67	0.76	0.72	0.73	0.49	0.41	0.70
J2	0.98	0.80	0.77	0.82	0.69	0.81	0.97	1.02	1.12	0.68	1.00
J3	0.64	0.90	0.51	0.70	0.40	0.85	0.41	0.42	0.49	0.29	0.39
J4	0.73	0.79	0.70	0.85	0.56	0.57	0.67	0.60	0.48	0.45	0.71
J5(%)	3.4	5.4	6.1	5.3	7.3	10.9	7.6	8.4	4.3	4.6	4.8
Event	78	79	80	81	82	83	84	85	86	87	88
J1	0.83	0.72	0.83	0.68	1.02	1.03	0.77	0.75	0.74	0.59	0.76
J2	0.81	0.78	0.71	0.84	0.84	1.05	0.79	0.91	0.73	0.72	0.98
J3	0.63	0.59	0.50	0.62	0.67	0.56	0.40	0.50	0.61	0.89	0.78
J4	0.66	0.49	0.61	0.65	0.79	0.80	0.70	0.64	0.69	0.54	0.76
J5(%)	4.3	3.4	4.9	2.7	1.4	4.9	4.2	4.2	3.3	5.4	5.4
Event	89	90	91	92	93	94	95	96			
J1	0.64	0.89	0.86	1.42	0.60	0.56	0.59	0.62			
J2	1.02	0.93	0.69	1.19	1.05	0.82	0.74	0.77			
J3	0.57	0.55	1.00	1.03	0.58	0.42	0.72	0.63			
J4	0.72	0.70	0.70	1.00	0.79	0.56	0.60	0.61			
J5(%)	4.8	4.3	4.1	7.2	4.9	2.9	5.9	6.4			